INSTITUTO DE PESQUISAS ENERGÉTICAS E NUCLEARES
Autarquia Associada à Universidade de São Paulo

First principles calculations of hyperfine magnetic field in RECd compounds (RE = Ce, Gd and Er) using FP-LAPW ELK code

LEVY SCALISE MACIEL

Dissertação apresentada como parte dos requisitos para obtenção do Grau de Mestre em Ciências na Área de Tecnologia Nuclear - Aplicações

Orientador:
Prof. Dr. Artur Wilson Carbonari

São Paulo
2020

INSTITUTO DE PESQUISAS ENERGÉTICAS E NUCLEARES
Autarquia Associada à Universidade de São Paulo

First principles calculations of hyperfine magnetic field in RECd compounds (RE = Ce, Gd and Er) using FP-LAPW ELK code

Versão Corrigida

Versão Original disponível no IPEN

LEVY SCALISE MACIEL

Dissertação apresentada como parte dos requisitos para obtenção do Grau de Mestre em Ciências na Área de Tecnologia Nuclear - Aplicações

Orientador:
Prof. Dr. **Artur Wilson Carbonari**

São Paulo
2020

Fonte de Financiamento: CNPQ

Como citar:

SCALISE MACIEL, L. ***First principles calculations of hyperfine magnetic field in RECd compounds (RE = Ce, Gd and Er) using FP-LAPW ELK code***. 2020. 145 p. Dissertação (Mestrado em Tecnologia Nuclear), Instituto de Pesquisas Energéticas e Nucleares, IPEN-CNEN/SP, São Paulo. Disponível em: (data de consulta no formato: dd/mm/aaaa)

Ficha catalográfica elaborada pelo Sistema de geração automática da Biblioteca IPEN/USP,
com os dados fornecidos pelo(a) autor(a)

Scalise Maciel, Levy
   First principles calculations of hyperfine magnetic field in RECd compounds (RE = Ce, Gd and Er) using FP-LAPW ELK code / Levy Scalise Maciel; orientador Artur Wilson Carbonari. -- São Paulo, 2020.
   145 p.

   Dissertação (Mestrado) - Programa de Pós-Graduação em Tecnologia Nuclear (Aplicações) -- Instituto de Pesquisas Energéticas e Nucleares, São Paulo, 2020.

   1. elk code. 2. density functional theory. 3. hyperfine parameters. 4. first principles calculations. I. Wilson Carbonari, Artur, orient. II. Título.

To Valentim Scalise and Dolores Morales.

Acknowledgements

I would like to thank everyone who somehow contributed to my journey here. I do not think it will be possible to quote everyone but know that I know who you are. In particular, I would like to thanks:

- Prof. Dr. Artur, for being my advisor, always helping me with patience and disposition and serving as an example of a professional and person.
- Dr. Luciano Fabrício Dias Pereira for being my co-advisor, by friendship, advice and often acting like a father or older brother. I would like to be someone like you "when I grow up".
- Dr. Anastasia Burimova for the friendship, conversations and passion shown by science.
- Vitor Cavalcanti for being a companion and great friend during this journey.
- To the other members of the Hyperfine Interactions Group (you are many and I consider them all), I thank you for becoming my family and making this environment the place I most like to be.
- Professors Rodrigo Sponchiado and Vladimir Pershin for being initial examples and helping me in the initial steps of my academic journey.
- To the members of the group "Satanagens and Diabruras" because madness has no limits.
- To Will, Márcio, Bruna and Thabata; "aqui é aqui, ali é ali e nã nã nã é nã nã nã."
- To all my family.
- To Dolores and Valentim, without you I would be nothing.
- To CNPQ for financial support.
- To the workers of IPEN (ArchAngels) and the University City (University Restaurant, Bus, Libraries), for the great service showed.
- And lastly (because they are the smallest), Ellinha, Selina, Susy, Tomzinho, Nicholas, Eugênio, Genaro and Andreinha, my family of paws.

“Knowledge destroys myths“

Abstract

SCALISE MACIEL, Levy. ***First principles calculations of hyperfine magnetic field in RECd compounds (RE = Ce, Gd, and Er) using FP-LAPW ELK code.*** 2020. 149 p. Dissertação (Mestrado em Tecnologia Nuclear) - Instituto de Pesquisas Energéticas e Nucleares - IPEN-CNEN/SP. São Paulo.

The use of nuclear techniques, mainly Time Differential Perturbed Angular Correlation Spectroscopy (PAC), for the study of materials provides information on the interactions between the energy levels of an atomic nucleus with the electrmagnetic fields surrounding this nucleus, and this type of phenomenon is called Hyperfine Interactions (HI). The information on these interactions is contained in various hyperfine quantities, among which the most important are the Electric Field Gradient (EFG) and the Magnetic Hyperfine Field (MHF).

Given the gigantic scientific capacity of electronic structure calculations based on Density Functional Theory (DFT), they are a great tool for the investigation of HIs either as a purely theoretical study or as an addition to experimental measurements. This work implies calculating the hyperfine magnetic field in the RECd compounds (RE = Ce, Pr, Gd, Nd, Sm, Tb, Dy, Ho, Er, Eu, Tm and Yb) with first principles methods based on the density functional theory using the FP-LAPW ELK code and comparing the outcome to the experimental results, as well as to those obtained with the WIEN2k code.

To achieve this goal, calculations were carried out for the RECd compounds. Firstly, the parameters needed to apply the calculation methodology were optimized, then the calculations were carried out by varying the polarization of spins for each compound in order to investigate their impact on MHF.

After that, the MHF and the density of states (DOS) of all compounds in their various spin polarization configurations were calculated, so that a more thorough analysis of the results became possible.

The work concludes with four appendices, the first is an explanation of the Born-Oppenheimer Approximation used to treat many-body systems, the second contains the proofs of the two main theorems of the DFT, the Hohenberg-Kohn Theorems, the third is a step-by-step tutorial on how to start a calculation with the ELK and the fourth comprises the optimization graphs which haven't got into the main text.

Key-words: elk. dft. hyperfine interactions. frist principles. magnetism. rare-earth compounds.

Resumo

SCALISE MACIEL, Levy. ***Cálculos por primeiros princípios do campo hiperfino magnético em compostos TRCd (TR = Ce, Gd and Er) usando o código FP-LAPW ELK.*** 2020. 149 p. Dissertação (Mestrado em Tecnologia Nuclear) - Instituto de Pesquisas Energéticas e Nucleares - IPEN-CNEN/SP. São Paulo.

O uso de técnicas nucleares, principalmente Espectroscopia de Correlação Angular Diferencial no Tempo (PAC), para o estudo de materiais fornece informações sobre as interações entre os níveis de energia de um núcleo atômico e os potenciais eletrônicos em torno desse núcleo, esse tipo de fenômeno é denominado Interações Hiperfinas (IH). Essas informações estão nas várias quantidades hiperfinas, dentre elas, as mais importantes são o Gradiente de campo elétrico (GCE) e o Campo Hiperfino Magnético (CHM).

Dada a gigantesca capacidade científica de cálculos de estrutura eletrônica com base na Teoria da Densidade Funcional (DFT), eles são uma grande ferramenta na investigação IHs: puramente teóricas, além de medidas experimentais. Este trabalho de mestrado consiste no cálculo do campo hiperfino magnético nos compostos RECd (RE = Ce, Pr, Gd, Nd, Sm, Tb, Dy, Ho, Er, Eu, Tm e Yb) pelos métodos dos primeiros princípios baseados na teoria da densidade funcional, usando o código ELK, comparando os resultados com os resultados experimentais e também resultados obtidos com o código WIEN2k.

Para atingir esse objetivo, foram feitos cálculos nos compostos RECd. Primeiramente, os parâmetros necessários para aplicar a metodologia de cálculo foram otimizados e, em seguida, os cálculos foram realizados variando a polarização dos spins de cada composto para investigar seu impacto em seu CHM.

Depois disso, o campo hiperfino magnético e a densidade de estado (DOS) de todos os compostos em suas várias configurações de polarização foram calculados para ter uma maior possibilidade de analisar os resultados.

O trabalho termina com quatro apêndices, o primeiro é uma explicação sobre a aproximação de Born-Oppenheimer, usada para tratar sistemas de muitos corpos, o segundo contém as provas dos dois principais teoremas da DFT, os Teoremas de Hohenberg-Kohn, o terceiro é um tutorial passo à passo sobre como iniciar um cálculo no ELK e o quarto são os gráficos de otimização que não entraram no texto principal.

Palavras-chaves: elk. dft. interações hiperfinas. primeiros princípios. magnetismo. com-

postos terra-rara.

List of Figures

List of Tables

List of abbreviations and acronyms

AMF	Around the Mean Field
APW	Augmented Planes Waves
Ce	Cerium element
Cd	Cadmium element
DFT	Density Functional Theory
DOS	Density of States
Dy	Dysprosium element
EFG	Electric Field Gradient
ELK	Electrons in k-space
Er	Erbium element
Eu	Europium element
FLL	Fully Localized Limit
FP	Full Potential
Gd	Gadolinium element
GGA	Generalized Gradient Approximation
Ha	Hartree
HI	Hyperfine Interactions
HMI	Hyperfine Magnetic Interaction
Ho	Homium element
IPEN	Institute for Energetic and Nuclear Research (abbreviation in portuguese)
KS	Kohn-Sham
La	Lanthanum element
LAPW	Linearized Augmented Plane Waves

LDA	Local Density Approximation
MFA	Mean Field Approximation
MHF	Magnetic Hyperfine Field
MT	Muffin-tin
Nd	Neodymium element
OPM	Orbital Polarization Method
PAC	Time Differential Angular Correlation Spectroscopy
PBE96	Perdew-Burke-Ernzerhof 1996 Functional
Pr	Praseodymium element
PW	Plane Waves
RE	Rare-Earth
RKKY	Ruderman-Kittel-Kasuya-Yosida model
SIC	Self Interaction Correction
Sm	Samaryum element
sp	Spin polarized
so	Spin polarized + spin orbit coupling
Tb	Terbium element
Tm	Tulium element
WIEN2k	Wien code 2000
Yb	Ytterbium element

Contents

Introduction

Condensed matter is one of the most dynamic areas of research from all physics, looking at past 100, 50 or even 15 years one may see a fast-changing field. But there is one thing known since the first day: the behavior of solids is governed by the well-known equations of quantum mechanics. In principle, solving these equations, all properties of solids can be predicted. However, it is easier said than done, and in practice this turns out to be a hard numerical task, so that only idealized cases, or those with a lot of approximations can be approached. The importance of this problem dictated the development of more efficient theoretical methods. Together with the advent of faster and cheaper hardware, it has begun to change this situation. Indeed, today it is possible to predict many properties of materials in real situations.

But even with the success of the theoretical methods, physics is an experimental science, and there is a continuous necessity to explain experimental results. One of such findings that require an additional theoretical study is the behavior of the magnetic hyperfine field (MHF) in RECd (RE = Rare-Earth) type compounds. These compounds are important as they help our society in the transition to a clean-tech-driven economy [1]. They are used in electric car motors, lithium ion batteries, computer hard drives, solar panels, and wind turbines. Just to cite one example, the use of these magnetic materials in electric motors in hybrid and electric vehicles allows increasing their efficiency and redcing their weight down to only a half of the weight of a traditional ferrite motor. A Toyota Prius hybrid motor, for example, uses 1kg of Neodymium, and a Mercedes S400 uses 0.5kg [1].

These experimental results were obtained by the Hyperfine Interaction Group at Nuclear and Energy Research Institute (IPEN) [2], using the Time Differential Perturbed Angular Correlation γ-γ spectroscopy (PAC). This technique provides information about interactions between energy levels of the nucleus with the potentials (electric and magnetic) in their surroundings (this phenomenon is called Hyperfine Interactions (HI) [3]) and raises a discussion about the possible the source of magnetism in these compounds. Since one of the quantities obtained from HI is the value of the Magnetic Hyperfine Field (MHF), the presence of this field at atomic nuclei is desirable for providing information on the source of magnetism from a local perspective.

Besides MHF there are a lot of other quantities which could be extracted from HI, and the most important and responsible for the perturbation of energetic levels of the nuclei are (already cited) Magnetic Hyperfine Field [3, 4] and the Electric Field Gradient (EFG) [3, 5]. Thus, this work aims to contribute to the explanation of the magnetic

behavior of RECd type compounds.

Together with this experimental technique, many theories were developed to understand the properties of these materials, the Density Functional Theory (DFT) [6, 7, 8] being one of those approaches frequently used for band structure calculations in solids. It has proven itself a good tool to study HI in a purely theoretical way [9, 10], or in complement to the experimental results [11, 12, 13, 2].

With the advent of accessible (from the financial aspect) and more powerful computers, the creation and implementation of many numerical simulation codes allowing to perform studies based on this theoretical approach became possible. One of those is to be discussed in this work. Namely,

- the FP-LAPW ELK Code [14] is an open source and free code of collective development, originated from the EXCITING Code due to the effort of the scientific community. It is approximately 8 years old, its philosophy prioritizes user-friendliness. The code allows calculations with applied magnetic fields, time dependent DFT and many others options. This work aims to test its functionalities and check the viability of its major use by the group of Hyperfine Interactions in the future.

ELK is an *all electron* code, meaning that it considers all electrons of the atom, not just those of the valence shell. Codes that only consider valence shell electrons are known as *pseudopotential* codes, because they treat the electrons closest to the nucleus as a part of the "core" formed by the nucleus plus these electrons (thus commonly called core electrons), leaving the valence electrons subject to the potential created by this core.

Simulations performed using DFT-based computational codes are called calculations by first principles, meaning that there is no need for experimental parameters as initial inputs for their realization, starting only from theory and obtaining values for the physical quantities of interest.

Of all hyperfine quantities, the EFG is very well predicted by computational codes based on DFT. The EFG calculation methodology that has been developed by Blaha *et al.* [7, 15] is implemented today in various computational codes (including the ELK Code) and has demonstrated great results to determine EFG values for different systems (magnetic or non-magnetic metals, dielectric or semiconductor oxides, etc) [5, 9, 10].

On the other hand, the calculation of the Magnetic Hyperfine Field using electronic structure simulations by first principles are still a challenge to the scientific community. DFT has certain limitations in its formulation that degrade the MHF estimate [16, 17, 18], regardless of which component of the MHF is predominant in a given atom. We can cite the case of the Rare Earths that have MHF defined essentially by its orbital component (orbital hyperfine field), and the predicted values for the orbital angular momentum (of the

atomic shells not fully filled) smaller than those observed [16]. With a goal to overcome this limitation, specific methodologies have been developed and tested [16, 17]. What is observed is that these methodologies are directed to specific systems having no character of global applicability. These results, in a search for numerical agreement between theory and experiments, do not provide a fundamental understanding of the limitations of DFT and how those can be overcome. Therefore, there is a huge space for MHF study with first principles: whether it is about getting closer to the experimental results, or the development of methodology and/or simulation protocol using different all electron codes (the codes that, in contrast to pseudopotential methods, take all electrons into consideration when solving the Kohn-Sham equation [8]).

That said, the study of MHF in the cerium and cadmium atoms is an excellent laboratory to probe the limits of DFT and specific calculation methodologies, as well as the limitations of the codes themselves. The MHF of these atoms may originate from different effects and Cd is a diamagnetic atom, so it only feels the molecular field of the host matrix. This type of MHF is refered to as *transferred field*. Hence, the fact that DFT predicts values smaller than the angular orbital moment (L_z) will not be a problem because Cd has all its shells completely filled leading to a zero contribution to MHF. On the other hand, Ce (inserted into a magnetic matrix) also receives the transferred MHF, but also has the possibility of having its own contribution to MHF, caused by core polarization. This, in turn, depends on some parameters, as the value of L_z and the relocation of the single $4f$ electron of Ce (if it is fully not located the MHF itself will be zero but will increase as its electron becomes more localized). A theoretical determination of the MHF of a magnetic atom is, therefore, more challenging.

Thus, this work consists of the calculation of the hyperfine field of RECd (RE = Ce, Pr, Gd, Nd, Sm, Tb, Dy, Ho, Er, Eu, Tm and Yb) by first-principle methods based on the density functional theory using the ELK FP-LAPW code and implies a comparison of the results with the calculations already performed by the group using the code WIEN2k and with the experimental results [2, 13].

1 Theoretical Aspects

"The underlying physics laws necessary for a large part of physics and the whole of chemistry are thus completely known, and the difficulty is only that the exact applications of the laws lead to equations much too complicated to be soluble."

Paul Dirac[19]

1.1 Many - Body Quantum Mechanics

One of the problems of quantum mechanics that allow analytical solution is the hydrogen atom, where the Hamiltonian is given by

$$\hat{H}_{H.A} = -\frac{\hbar^2}{2\mu}\nabla^2 - \frac{e^2}{4\pi\epsilon_o r^2} \tag{1.1}$$

where μ is the reduced mass given by $\mu = m_e M/(m_e + M)$, the first term is the kinetic energy of the electron and the second term is the Coulomb potential between the nucleus and the electron. This is only the first element in the periodic table and the world around us is not composed only of hydrogen atoms, therefore we must search for a description of the other elements of the periodic table.

At first, we could consider a solid being composed of various atoms (independently of the species of the element), arranged in a regular geometrical structure[1], and these atoms interact with their neighbor nuclei and electrons, the electrons interact among themselves. As we try, like we did in the hydrogen atom, to write a Hamiltonian to describe this system, we get:

$$\hat{H} = -\frac{\hbar^2}{2}\sum_i^N \frac{\nabla^2_{\vec{R}_i}}{M_i} - \frac{\hbar^2}{2}\sum_i^N \frac{\nabla^2_{\vec{r}_i}}{m_e} - \frac{1}{4\pi\epsilon_0}\sum_{i,j}^N \frac{e^2 Z_i}{|\vec{R}_i - \vec{r_j}|} + \frac{1}{8\pi\epsilon_0}\sum_{i\neq j}^N \frac{e^2}{|\vec{r_i} - \vec{r_j}|} + \\ + \frac{1}{8\pi\epsilon_0}\sum_{i\neq j}^N \frac{e^2 Z_i Z_j}{|\vec{R}_i - \vec{R}_j|} \tag{1.2}$$

[1] Assuming that it is not an amorphous solid.

where $\vec{R_i}$ is the position of i-th nucleus with mass M_i, $\vec{r_i}$ are the electron's positions, and m_e is the mass of electron. The first two terms are the operators of kinetic energy of the nuclei and electrons respectively. The last three terms describe the Coulomb interactions between electrons and nuclei, electrons and electrons and nuclei and nuclei, we are initially neglecting the degree of freedom of spin that would be an additional difficulty at this stage. Solving the Schrödinger's equation in an analytical way for this Hamiltonian is not possible, and approximations are required. The approximations which will be applied are discussed in the Appendix A.

1.2 Density Functional Theory

The Density Functional Theory imples of the change of mathematical formalism which aims to get around the difficulty in solving the Schrödinger's equation for a many-body system. For this, the DFT treats the problem making use of an energy functional written as a function of the electronic density, that depends on three variables only. We will first discuss the case without spin. After that, we include spin.

1.2.1 DFT without Spin

The DFT's base are two theorems proposed in 1964 by Hohenberg and Kohn [20][2]:

Theorem 1. *The external potential $v_{ext}(\vec{r})$ that acts in a system of interacting particles is determined uniquely by the electronic density of the fundamental state, $\rho_0(\vec{r})$, up tp a constant.*

Theorem 2. *A universal functional could be defined for the energy $E[\rho(\vec{r})]$ in terms of the electronic density $\rho(\vec{r})$ and, for a given external potential $v_{ext}(\vec{r})$, this functional has a global minimum at the exact density of the ground state $\rho_0(\vec{r})$.*

In these theorems, the external potential is the coulomb interaction between the nucleus and the electron.

1.2.1.1 The Kohn-Sham Equations

After the formulation of these theorems, Kohn and Sham [21] treated a system of interacting electrons through a system of non-interacting electrons with the choice of an appropriate potential, thus simplifying the problem.

From the theorems of Hohenberg-Kohn, one can write the energy functional like:

$$E[\rho(\vec{r})] = \int v_{ext}(\vec{r})\rho(\vec{r})d^3r + \frac{1}{2}\int\int \frac{\rho(\vec{r})\rho(\vec{r}\,')}{|\vec{r}-\vec{r}\,'|}d^3r d^3r' + G[\rho(\vec{r})] \tag{1.3}$$

[2] The proofs of all theorems cited in this dissertation may be found in the Appendix B.

where the first term is associated with the external potential, the second term is due the electron-electron interaction and the third term is a universal functional expressed by:

$$G[\rho(\vec{r})] = T_0[\rho(\vec{r})] + E_{xc}[\rho(\vec{r})] \tag{1.4}$$

Being $T_0[\rho(\vec{r})]$ the kinetic energy of a non-interacting system of electrons, with density $\rho(\vec{r})$ and $E_{xc}[\rho(\vec{r})]$ being the exchange and correlation energy of a interacting system with the same density $\rho(\vec{r})$.

The constrained condition is that the total charge has to be fixed, therefore:

$$\int \rho(\vec{r}) d^3r = N \tag{1.5}$$

Applying the variational theorem to the functional (1.3), together with the constrained condition (1.5), we obtain:

$$\delta \left[E[\rho(\vec{r})] - \lambda \left(\int \rho(\vec{r}) d^3r - N \right) \right] = 0 \tag{1.6}$$

with λ being the Lagrange's multiplier. Re-writing the expression above, we have:

$$\int \delta\rho(\vec{r}) \left[\frac{\delta T_0[\rho(\vec{r})]}{\delta\rho(\vec{r})} + v_{ext}(\vec{r}) + \int \frac{\rho(\vec{r})}{|\vec{r} - \vec{r}'|} d^3r' + v_{xc}(\vec{r}) - \lambda \right] d^3r = 0 \tag{1.7}$$

The term $v_{xc}(\vec{r})$ is called exchange-correlation potential, given by:

$$v_{xc}(\vec{r}) = \frac{\delta E_{xc}[\rho(\vec{r})]}{\delta\rho(\vec{r})} \tag{1.8}$$

Given the functional of kinetic energy:

$$T_0[\rho(\vec{r})] = -\frac{\hbar^2}{2m_e} \sum_i^p \int \psi_i^*(\vec{r}) \nabla^2 \psi_i(\vec{r}) d^3r \tag{1.9}$$

remember that ψ_i is the KS orbital in the position i, it is tempting to treat these states as proper electronic particle states; but beware, these are fictitious states. Given the electronic density:

$$\rho(\vec{r}) = \sum_i^p \psi_i^*(\vec{r}) \psi_i(\vec{r}) \tag{1.10}$$

We could find the solution to the equation (1.7), under the conditions of the expressions (1.5) and (1.10), solving the Schrödinger's equation for one particle:

$$\left[-\frac{\hbar^2}{2m_e} \nabla^2 + v_{ks}[\rho(\vec{r})] \right] \psi_i(\vec{r}) = \epsilon_i \psi_i(\vec{r}), \;\; i = 1, 2, 3, ..., p \tag{1.11}$$

The terms in parentheses represent the Hamiltonian $\hat{h}_{ks}$ of Kohn-Sham, while $v_{ks}[\rho(\vec{r})]$ is the effective potential written as:

$$v_{ks}[\rho(\vec{r})] = \int \frac{\rho(\vec{r}')}{|\vec{r} - \vec{r}'|} d^3r' + v_{ext}(\vec{r}) + v_{xc}[\rho(\vec{r})] \tag{1.12}$$

The equations (1.11) are called Kohn-Sham's equations and can be solved in a self-consistent way, in the sense that firstly the potential $v_{ks}[\rho(\vec{r})]$ is calculated from a initial electronic density and after used to find the eigenfunctions $\psi_i(\vec{r})$, which will produce a new density by means of (1.10), repeating the cycle. The process is made until a desired minimum difference is reached between the two consecutives densities, as shown in the Figure 1.

1.2.2 DFT with Spin

In the Density Functional Theory with Spin Polarization (spin-DFT) there are two key variables, the electronic charge densities of spins "up" and "down". In this case the total density is written as:

$$\rho(\vec{r}) = \rho_{\uparrow}(\vec{r}) + \rho_{\downarrow}(\vec{r}) = \sum_{\chi=\uparrow,\downarrow} \chi_{\sigma} \tag{1.13}$$

The Kohn-Sham equations generalized to account spin becomes [22]:

$$\sum_{\chi} \left[\left(-\frac{\hbar^2}{2m_e} \nabla^2 + v_H(\vec{r}) + v_0(\vec{r}) \right) \delta_{\chi,\chi'} + v_{xc}^{\chi,\chi'}(\vec{r}) \right] \psi_i^{\chi}(\vec{r}) = \epsilon_i \psi_i^{\chi'}(\vec{r}) \tag{1.14}$$

where $\psi_i^{\chi}(\vec{r})$ is the χ component of the KS orbital with spin, χ and χ' are indices that run over spin, $\{\uparrow, \downarrow\}$.

The goal of a spin-DFT is to solve the Eq. (1.14) self consistently. It is important to note that, although the spin-orbit interaction has not been discussed yet, it can be included along with other relativistic effects as a perturbation (see Singh and Nordstrom [8], for example).

Also the spin-DFT becomes important when there is the need to simulate systems with external magnetic field application (thus causing the Zeeman effect) or in the case where the polarization spin occurs naturally, that is, low temperature magnetic systems.

Virtually all spin-DFT comes directly from the theoretical construction of DFT, which, in most cases, just attach the spin "Up" and "Down" indexes to the terms, as well as making a sum over them when you want to represent a term as functional of the total charge density. This allows for a theoretical presentation of DFT instead of spin-DFT,

without neglecting significant information[3] and gaining in simplicity, even when the studied system has spin polarization.

The Total Energy Functional (1.3) can be written as follows:

$$E = E[\rho_\uparrow, \rho_\downarrow] \tag{1.15}$$

Obviously, the KS orbitals and eigenvalues are also modified. So, solving each of the KS equations is self-consistent, it turns out that the densities are:

$$\rho_\sigma \sum_{occupied} \psi^*_{i,\sigma}(\vec{r})\psi_{i,\sigma}(\vec{r}) \tag{1.16}$$

Finally, using equation (1.13) we find the electronic density of the ground state.

1.3 Exchange-Correlation Functional Approximations

The method described in the last section gives origin to the exchange and correlation functional, showing a difficulty in principle, since there is no exact functional, not even a way to determine it with precision. Face this situation, it took some approximations for the term $E_{xc}[\rho(\vec{r})]$, with the LDA (Local Density Approximation) and the GGA (Generalized Gradient Approximation).

1.3.1 LDA Approximation

In the LDA, we consider that a point $\vec{r}$, where the density of a system of electrons is equal to the density of a homogeneous electron gas, whose variation is soft in the neighbourhood of $\vec{r}$. Therefore, the exchange-correlation functional is re-written in the following way:

$$E_{xc}[\rho(\vec{r})] = \int \rho(\vec{r})\epsilon^h_{xc}[\rho(\vec{r})]d^3r \tag{1.17}$$

where $\epsilon^h_{xc}[\rho(\vec{r})]$ is the energy functional of exchange and correlation by electron in a homogeneous gas with density $\rho(\vec{r})$.

[3] Here it is important to note that in spin-DFT there is not a single correspondence between the density of spins and the external potential. This is also true for the current density method (current-DFT). Another point in spin-DFT that distinguishes it from DFT, is that certain functionals are not assembled by the simple introduction of the spin index in their formulas, such as the exchange functional E_x.

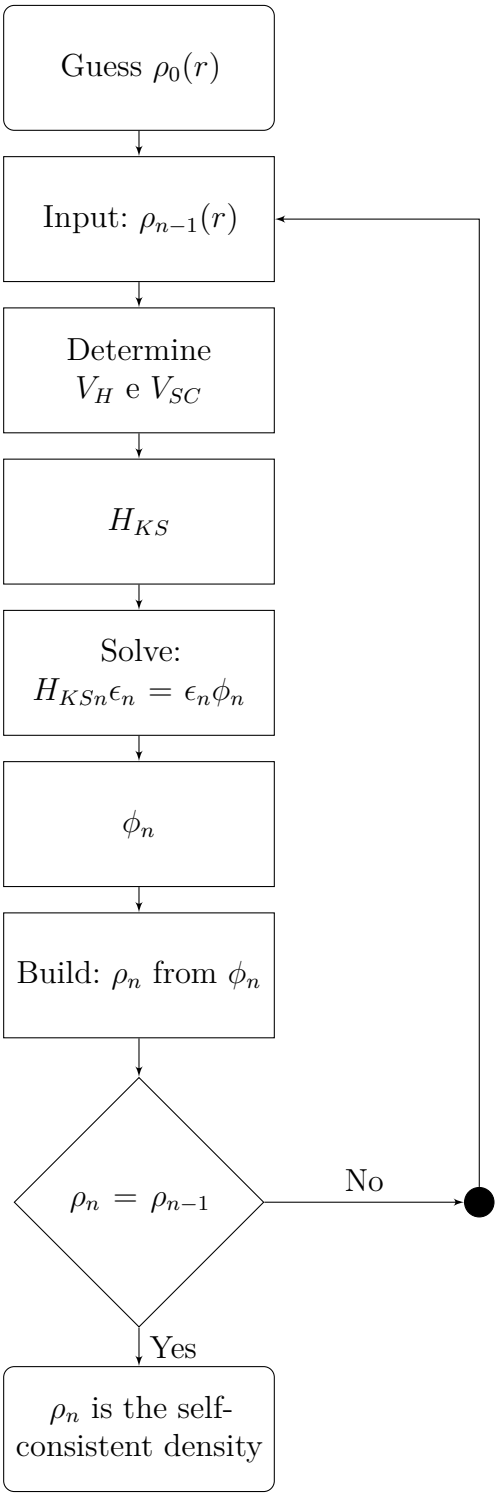

Figure 1 – Flow chart for an iteration in the self-consistent cycle to solve the Kohn Sham equations. Source: the Author.

In this approximation, the functional $\epsilon_{xc}^{h}[\rho(\vec{r})]$ could be written like the addition between the exchange term $\epsilon_{xc}[\rho(\vec{r})]$ and the correlation term $\epsilon_{cor}[\rho(\vec{r})]$ separately, as

follows:

$$\epsilon_{xc}^{h}[\rho(\vec{r})] = \epsilon_{xc}[\rho(\vec{r})] + \epsilon_{cor}[\rho(\vec{r})] \tag{1.18}$$

from where we obtain:

$$E_{xc}[\rho(\vec{r})] \approx E_{xc}^{LDA}[\rho(\vec{r})] = \int \rho(\vec{r}) \left[\epsilon_{xc}[\rho(\vec{r})] + \epsilon_{cor}[\rho(\vec{r})]\right] d^3r \tag{1.19}$$

the application of LDA in atomic and molecular systems has results reasonably precise, except in the cases where an electronic distribution highly inhomogeneous is treated.

1.3.2 GGA Approximation

When we deal with multi electronics real systems, in most cases, its more convenient to use the GGA, since the density is not always homogeneous. Therefore, like second approximation, its used a exchange and correlation functional which now depends on a gradient of the electronic density under the form:

$$E_{xc}^{GGA}[\rho(\vec{r})] \approx \int f(\rho(\vec{r}), \nabla\rho(\vec{r}))d^3r \tag{1.20}$$

From a mathematical point of view, this approximation is reasonably good because it allows us to know the behavior of the functional in a point and in your neighbourhood still that the function is not so smooth.

1.3.3 Remarks about LDA and GGA Approximations

The LDA approximation is generally not accurate enough to magnetism and strong correlated systems. Also, there are many examples where the LDA places the molecular conformations or crystalline phases of the bulk in a qualitatively wrong energetic order [23].

The GGA approximations have overcome these deficiencies to a considerable extent[23, 24, 25], giving for example a more realistic description of the energy barriers in dissociative hydrogen absorption on a metallic and semiconductor surface[26]. The functional GGA depends on the local density as well as the spatial variation of the density. Computationally they are simple to use as well as the LDA. On the other hand it is becoming clear that such functional GGA are still quite limited to provide not only a considerable improvement over the LDA, but also the desired accuracy in general.

1.4 APW method

Proposed by Slater in 1937 [27], the APW (Augmented Planes Waves) method consists of considering a spherical region around the nuclei of atoms, known as the muffin-tin (MT) sphere, and within this sphere, functions that describe the potential in this sphere are adopted. In the more remote regions, called interstitial regions, the potential is almost constant and other basic functions are adopted. Thus, the system is divided into two regions: near the nuclei (region I) and away from the nuclei (region II) shown in Figure 2.

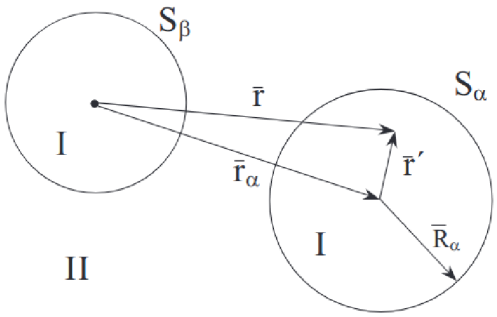

Figure 2 – Division of the unit cell into muffin tin regions (I) and interstitial region (II), for a case of two atoms. Source: [28]

In region I the base functions used are obtained from spherical waves and have the form:

$$\psi_I(E) = \sum_{l,m} A_{l,m} u_l(r', E) Y_m^l(\hat{r}') \tag{1.21}$$

where $u_l(r', E)$ is a radial function of the spherical region, E is an energy parameter which is included explicitly in the dependence of E in the radial functions and $Y_m^l(\hat{r}')$ are the spherical harmonics.

For region II, with almost constant potential, the functions should behave more smoothly in the interstitial region, hence plane waves are used as base functions as follows:

$$\psi_{II}(\vec{K} + \vec{G}, \vec{r}) = V^{-1/2} e^{i(\vec{K}+\vec{G})\cdot\vec{r}} \tag{1.22}$$

Where V is the unit cell volume, $\vec{K}$ are wave vectors in the first Brillouin zone and $\vec{G}$ represents the reciprocal lattice translation vectors.

The term $A_{l,m}$ of Eq.1.21 is the variational term that must guarantee the continuity of the base functions on the spherical surface (i.e. when $\vec{r}' = \vec{R}$), and has the following

form:

$$A_{l,m} = \frac{4\pi i^l e^{i(\vec{K}+\vec{G})\cdot\vec{r}}}{V^{1/2} u_l(\vec{r'} = \vec{R}, E)} j_l(|\vec{K}+\vec{G}|R) Y_m^{l*}(\vec{K}+\vec{G}) \tag{1.23}$$

This expression is obtained by an expansion in base functions from the origin of a unit cell atom, where j_l is the function of the Bessel spherical form that has order l.

For each fixed point $\vec{K}$, the energy eigenvalue E_n is calculated by diagonalizing the secular equation, however, this must be done for all bands since the energy values differ in each region. The APW method presents impossibilities in this case because it considers a set of eigenfunctions inside and outside the MT sphere, depending on E_n arbitrary choice in such a way that nullifies the determinant and finally finds the energy value sought, and how this procedure should be done. For each $\vec{K}$ point, this takes a lot of time and computational resources, making the process unfeasible.

1.5 LAPW Method

In an attempt to improve APW, other methods have emerged to correct or simplify the treatment of the base function in order to obtain corresponding energy values faster and more efficiently. Then came a method widely used today in investigations of structures and bands in matter, the LAPW (Linearized Augmented Plane Waves), in 1975 by the works of Andersen [29]. LAPW deals differently with the radial equation $u_l(r', E)$ of Eq. (1.22) by obtaining a linear shape for it, since an APW problem was to treat nonlinear functions of the MT sphere eigenfunction set, which made the process unfeasible even for a few particles. The proposed solution in LAPW is to expand Taylor's radial series function around an energy value E_0, thus obtaining the expression:

$$u_l(r', E) = u_l(r', E_0) + \underbrace{(E - E_0)}_{B_{l,m}} \dot{u}_l(r', E_0) + ... \tag{1.24}$$

Only the first two terms of the expansion are taken into account. Substituting this linear function in equation (1.22):

$$\psi_l(E) = \sum_{l,m} A_{l,m}[u_l(r', E_{1,l}) + B_{l,m}\dot{u}_l(r', E_{1,l})] Y_m^l(\hat{r'}) \tag{1.25}$$

In this way LAPW can calculate, through numerical method applications, all possible energy values starting from a possible generic amount E_0, this method is widely used and the results are totally in agreement with experimental results.

1.6 LAPW+lo

Assigning *lo* (local orbitals) to the LAPW method is to specifically treat a unit cell α atom, in which case all functions are valid within the MT sphere of this atom and zero in both the interstitial region, as in the MT spheres of all the other atoms in the system. This method seeks greater precision of results by applying a new base function into the MT sphere, where this term is added to the base functions used in LAPW.

$$\psi_{lo}^{\alpha}(E) = \sum_{l,m}[A_{lm}^{\alpha,lo}u_l(r', E_{1,l}) + B_{lm}^{\alpha,lo}\dot{u}_l(r', E_{1,l}) + C_{lm}^{\alpha,lo}u_l(r', E_{2,l})]Y_m^l(\hat{r}') \tag{1.26}$$

The term $C_{lm}^{\alpha,lo}u_l(r', E_{2,l})$ is a function of energy $E_{2,l}$, other than $E_{1,l}$, which represents a specific state (such as the valence state of an atom). This way, it is possible to determine well-defined energy values, since the application of local orbitals guarantees the relaxation of linearization energy $E_{1,l}$ by introducing the radial term dependent on $E_{2,l}$, making the base functions dependent on two different linearization energies. Thus, the accuracy of the results is increased, however, there are no changes in convergence.

1.7 Orbital Polarization in DFT

Because the systems studied here are composed of rare earths, there is a strong local Coulomb repulsion in the $4f$ electrons of these ions, so a method is needed to represent this repulsion. The most popular and efficient among the several existing methods is the LDA+U method. This method is called the Orbital Polarization Method (OPM), developed with the combination of Hubbard's Hamiltonian and simple DFT.

There are several variants of this method, Mean Field Approximation (MFA) [30], Fully Localized Limit (FLL) [31] and Around the Mean Field (AMF) [32]. The idea behind all these variants is to separate electrons into two subsystems: the moving electrons, which can be described using an orbital potential of an independent electron (LDA) and the more localized electrons (d or f) where the Coulomb interaction must be taken into account by an extra term. In other words, a new purely orbital potential is introduced in the KS (1.11) equation, which is a function of the occupation number of each sub-level of a given layer, being it d or f.

Therefore, in DFT+U the total energy is now written as $E = E_0 + E_{DFT+U}$, where E_0 is the energy obtained with the simple DFT and E_{DFT+U} corresponds to the extra term.

In this work we use the method developed by Anisimov [31] called Self-Interaction Correction (SIC), to implement in the total energy the dependence with n_σ, that represents

the occupation of a given sub-level with spin σ. We write the correction energy as:

$$E_{DFT+U^{SIC}} = E_{ee} - E_{dc} \tag{1.27}$$

where,

$$E_{ee} = \langle l, m, \sigma | W | l, m, \sigma \rangle \, , \text{ com } W = \frac{1}{2} \sum_{i \neq j}^{N} \frac{1}{|\vec{r}_i - \vec{r}_j|} \tag{1.28}$$

in which, E_{ee} is the explicit average value of the Coulomb repulsion operator[4] in the state determined by l, m nd σ (where l is the angular momentum of the shell, $m = 2l + 1$ and σ represents the spin "up" or "down"), E_{dc} is the double counting term[5].

Now using the parameters of correlation U (also known as a Coulomb repulsion parameter) and exchange J, we have

$$E_{ee} = \frac{U}{2} N^2 - \frac{J}{2} \sum_{\sigma} N_{\sigma}^2 - \frac{U - J}{2} \sum_{m,\sigma} n_{m,\sigma}^2$$

$$E_{dc} = \frac{U}{2} N(N-1) - \frac{J}{2} \sum_{\sigma} N_{\sigma}(N_{\sigma} - 1) \tag{1.29}$$

$$N_{\sigma} = \sum_{m} n_{m,\sigma} \text{ and } N = \sum_{\sigma = \uparrow, \downarrow} N_{\sigma}$$

where N_{σ} and N are the numbers of electrons with spin σ and total respectively. Therefore, after replacing Eq. (1.29) in Eq. (1.28), are obtained

$$E_{DFT+U^{SIC}} = \frac{U - J}{2} (N - \sigma_{m,\sigma} n_{m,\sigma}^2 \tag{1.30}$$

this is the correction energy obtained by the SIC method, as the potential is a functional derivative of energy, we have

$$v_{m,\sigma} = \frac{\partial E_{DFT+U^{SIC}}}{\partial n_{m,\sigma}} = \frac{U - J}{2} (1 - 2n_{m,\sigma}^2) \tag{1.31}$$

[4] We use here the mean electric field approximation to treat the electron-electron interaction in a spherical atom.

[5] This name is used because this contribution already appears in simple DFT, so its need to be subtracted from $E_{DFT+U^{SIC}}$

Now with the potential $v_{m,\sigma}$ determined, we apply it in the KS equation already considering the sum on the eigenvalues only of the occupied states instead of the unknown kinetic energy of a simple particle, thus we obtain the total energy in the DFT+U^{SIC}:

$$E = E_0 + \frac{U - J}{2} \sum_{m,\sigma} n_{m,\sigma}^2 \tag{1.32}$$

According to Rollman [33], when performing this OPM approach in sub-orbitals filled in certain shells, the energy is reduced by $\frac{1}{2}(U - J)$, the sub-orbitals of this same shell that are above the Fermi level have their energy increased by the same amount, This causes a greater localization of the sub-orbitals. In literature, the term $(U - J)$ its known as V_{eff} and named as an effective Hubbard parameter.

The total energy (1.32) no longer has mathematical accuracy, because parameters U and J are not universal (the W operator depends on each case), their optimized values being specific to each problem. These values are included in the equation (1.32) in an ad-hoc manner, being adjustable "by hand" during the calculation.

This implies that the lowest energy found does not always correspond to the physical reality of the compound under study. Therefore, it is not possible to compare the total energy in the DFT+U with the total energy obtained by the simple DFT since the first is no longer a variational quantity.

In this work during the calculation of MHF in the Cecd compound, we applied $DFT + U$ to Ce and Cd ions.

1.8 Spin-Orbit Coupling

When dealing with heavy atoms (rare earth for example) and magnetism in calculations of electronic structure, one has to take into account relativistic effects. The speed of the electrons approaches the speed of light (c) as the atomic number increases.

When considering such effect, the Dirac's hamiltonian is used, where three new terms that do not exist in the Schrödinger's equation appear. These new terms are: spin-orbit coupling, mass correction and Darwin's correction. When using the complete Dirac equation, the calculation becomes completely relativistic but one can also ignore the spin-orbit coupling which leads to a scalar relativistic approach. This can be done because the spin-orbit interaction is twice as low as the energy levels, so depending on the calculation, it can be ignored.

In fully filled electronic states (which are those within the muffin-tin sphere) it is possible to perform a completely relativistic calculation. Valence states and local orbitals use the scalar relativistic approach.

The spin-orbit coupling causes the LAPW's base functions to be joined, mixing them in spin up and down functions, resulting in a non-diagonal matrix. In order to solve this problem, the $n \times n$ matrix of base functions (required at each k-point) are transformed into a new $2n \times 2n$ matrix.

This increase in the matrix size, increases the computational time of calculation, to circumvent this problem the second variational method is used. In this method, two hamiltonians are assembled, one for each spin and them are diagonalized independently, each with its own LAPW's base, as the spin-orbit coupling is small, a limited number of states is chosen, much smaller than the total number of occupied states, where the spin-orbit coupling will be considered. This done, a new equation is constructed, being formed by the scalar relativistic hamiltonian and a perturbative hamiltonian that represents the spin-orbit coupling. The self-states of this new hamiltonian are expanded in a new LAPW base, this base is assembled by mixing the normal base functions of the LAPW and some lower energy scalar relativistic orbitals (which are incomplete Dirac's hamiltonian eigenfunctions) of both spins.

As the number N of forming orbitals of the new LAPW's base is smaller than the number n of the initial LAPW's base functions and with the N functions being eigenstates of the scalar relativistic hamiltonian, there is a computational economy, because any diagonal eigenvalues are not generated by the disturbance of the spin-orbit coupling.

1.9 Hyperfine Interactions

Hyperfine interactions are electrical and magnetic interactions between the nuclear and electron spin. The energies of those interactions are very small compared to the energy levels of the nucleus itself, but the separation of energy levels can still be observed. Hyperfine interactions can increase energy levels or lift your degenerescence.

The hyperfine magnetic interaction (HMI) occurs when (mainly) the magnetic dipole moment of a nucleus is subjected to magnetic induction at the site of the same nucleus. The latter is generated by the movement and spin of the electrons of that nucleus itself and also of the electronic structure of the solid where it is inserted. This well-located field, felt by the nucleus, is named the hyperfine magnetic field (HMF). Thus, the hyperfine field may be a good instrument to grasp the characteristic of electrons in a certain region of the solid.

The electrical hyperfine interaction occurs especially between the electrical quadrupole moment of the nucleus and the electric field gradient of the electronic charges close to that nucleus. In our work, this interaction will be neglected because our system has cubic symmetry, which will "cancel" this interaction term.

1.9.1 Magnetic Hyperfine Field

The hyperfine magnetic field (HMF) is the magnetic field produced by the electronic charge distribution that surrounds the nucleus. The magnetic field in the nucleus has many terms: the demagnetization term and the Lorentz term, which are the result of the interaction with neighboring and distant atoms, and the Fermi contact term, the dipolar spin term and the orbital term, which are due to the electrons in the region occupied by the atom of that nucleus. The first two contributions to the HMF are generally very small compared to the other terms and will not be considered hereinafter. Thus, we can write the total HMF as the sum of its three largest contributions:

$$B_{tot} = B_f + B_{dip} + B_{orb} \tag{1.33}$$

Now, let's look briefly at each of these terms.

1.9.1.1 The Fermi Contact Term

Fermi's contact contribution is produced by the polarization of electrons at the position of the nucleus:

$$B_f = -\frac{2\mu_B\mu_0}{3}(|\psi_{e,\uparrow}(\vec{r_0}|^2 - |\psi_{e,\downarrow}(\vec{r_0})|^2) \tag{1.34}$$

where μ_B is the Bohr's magneton, μ_0 is the vacuum permeability and ψ_e is the electronic wavefunction.

When performing a non-relativistic treatment, only the electrons of the s shell will have a non-zero probability of being found in the nucleus position. When switching to a relativistic approach, the electrons of the $p_{1/2}$ shells will also have a nonzero probability of being found in the nucleus position, but with a lower probability than those of the s shell. This polarization occurs because of unpaired electrons in the d and f orbitals. The s orbitals with opposite spin will be different from the others resulting in a spin unbalance at the nucleus position, a mechanism known as *exchange polarization*. Because of this exchange polarization, the electrons with spin up of the s shell and the electrons with spin down of the same shell will interact in different ways with the electrons with spin up of the d shell for example.

1.9.1.2 The dipolar term

The dipolar contribution comes from the interaction between the magnetic moment of the spin and the nucleus. It has the following expression:

$$\vec{B}_{dip} = -\frac{\mu_0}{4\pi}\frac{\vec{\mu}_s - 3(\vec{\mu}_s \cdot \vec{e}_r)\vec{e}_r}{r^3} \tag{1.35}$$

where μ_s is the magnetic moment of the electron and r is its distance from the nucleus. This contribution can be understood as being generated by the intrinsic magnetic moment of the electrons. In a more pictorial way, considering the electron as a magnet, the magnetic field generated by these magnets represents the dipolar contribution. This contribution vanishes in a cubic distribution or in a semi-filled shell.

1.9.1.3 The orbital term

Thinking in a classical way, the orbital contribution to MHF is the magnetic field in the nucleus generated by the electron currents orbiting the nucleus.

The orbital contribution that corresponds to a given layer is:

$$\vec{B}_{orb} = -\frac{2\mu_B\mu_0}{4\pi}\left\langle\frac{1}{r^3}\right\rangle\vec{L} \tag{1.36}$$

(assuming the LS is valid). Where $<\frac{1}{r^3}>$ is the average over all electrons in the shell. We can see that if $L = 0$ the orbital contribution becomes zero. We have $L = 0$ in the case of a shell completely filled or half filled, but also in situations where the orbital moment is quenched. This quenching phenomenon of the orbital moment occurs in cases of incomplete d shells and is due to the influence of a large crystalline field in the d electrons. As in the case of dipole contribution, the orbital field is zero when the electronic cloud has cubic symmetry or greater. The orbital contribution becomes large in the case of lanthanides, where the crystalline field is a small effect and an atomic-type orbital moment is large and overlapping.

2 RECd Compounds

2.1 Rare Earth Elements

The rare earth elements (RE) began to be discovered in the 19th century, but it was only after the discovery of nuclear fission that the interest in the properties of these elements really boosted research on them. These elements are distinguished from all other elements of the periodic table by the presence of partially filled $4f$ and $5f$ orbitals. While the other elements share many of their chemical properties in columns, the RE are arranged in rows according to their physical characteristics and are divided into two subgroups: lanthanides and actinides.

2.1.1 Lanthanides

Lanthanides are soft metals with silver color and partially filled $4f$ orbitals, the elements belonging to this group are: Lanthanum (La), Cerium (Ce), Praseodymium (Pr), Neodymium (Nd), Promethium (Pm), Samarium (Sm) , Europium (Eu), Gadolinium (Gd), Terbium (Te), Dysprosium (Dy), Holmium (Ho), Erbium (Er), Thulium (Tm), Ytterbium (Yb) and Lutetium (Lu). Of these, lanthanum is the only exception that if it has no electron f it still shows physical properties that are characteristic of the entire series. In lanthanum, the $5d$ orbital is occupied before $4f$, this fact also happens with cerium. Cerium in turn has the peculiar characteristic of having a single $4f$ electron together with a filled $5d$ state.

The f orbitals have an energy comparable to that of the outermost $6s$ and $5d$ electrons, and are strongly located around the core, so they shield the $6s$ and $5d$ states of the nucleus. As the orbitals are filled throughout the series, the screening of the external electrons becomes more important, leading to a decrease in the atomic volume along the series, this phenomenon is called *lanthanide contraction*[1].

2.2 RECd Intermetallic Compounds

The compounds studied in this work are equiatomic and of the RECd type and thus crystallize in $CsCl$ type structures [34, 35]. The difference in the valence of the non-rare earth component of the compound is responsible for a wide range of the concentration of the conduction electrons.

[1] Even though we have mentioned actinides and lanthanum in this introduction, they will not be the target of the research reported here.

This concentration of the conduction electrons causes changes in magnetic phases to be observed depending on the number of conduction electrons of the compound [35]. A model that has been relatively successful in explaining this phenomenon is the RKKY (Ruderman-Kittel-Kasuya-Yosida) model [36]. In the RKKY model, the $4f - 4f$ indirect coupling is mediated by the s-conduction electron which is polarized spin by exchange with the $4f$ electrons.

Another model for the same phenomenon is the Campbell's model [37]. In the Campbell model, the indirect coupling occurs by intra-atomic exchange $4f - 5d$ and interatomic exchange $5d - 5d$ between the $5d$ electrons that have spin polarization with the neighboring RE atoms. As the $5d$ electrons are more strongly located than the s electrons, the hyperfine field can be expected to be mostly determined by the number N and the R_{NN} distance of the closest RE neighbors. Something in common between the two models is that the spin polarization leads, through the Fermi contact term in the nucleus-electron interaction, to the hyperfine magnetic B_{hf} field in the nuclei of non-rare earth atoms.

But the functioning of this coupling is not yet clear, requiring further studies, together with the electronic structure and optical properties that also lack consensus in their explanations [38].

Dominant as they are with respect to magnetism, $4f$ electrons do not significantly influence chemical bonds between atoms in solids and throughout the series the chemical properties of rare earths are similar [39, 13]. However, each rare earth element has a different number of electrons $4f$ and this difference will directly affect the magnetic moments of these electrons [13].

Thus, there are small differences in crystallographic properties in the RECd compounds for different RE, but large differences in magnetic properties, facilitating the separation of the magnetic parameters from other parameters common to the solid state.

2.3 RECd Magnetism

With respect to the magnetism of RECd compounds, several investigations, both theoretical and experimental, have already been carried out. Here, the report shows what has been raised in the literature about the studied compounds, emphasizing that this review is not exhausted in the area, but only used to understand the state of the art in which the field of study is found and subsequently help in the interpretation of the data that will be reported here.

In a paper from 1974, using the Faraday method for magnetics measures, Buschow [35] reported that the compounds: CeCd, PrCd, NdCd, SmCd, GdCd, TbCd, DyCd, HoCd and ErCd crystallizes in the CsCl structure, results corroborated by Fuji et al. [34] for

CeCd and NdCd, Cavalcante et al. [13] for RECd with RE = Ce, Pr, Nd, Sm, Gd, Tb, Dy, Ho and Er and Ryan et al [40] for YbCd. Highlighting the fact that another experimentals techniques was used by these other authors, Cavalcante et al. used Perturbed Angular Correlation (PAC), Fuji et al. used Neutron Diffraction and Ryan et al. used Mössbauer Spectroscopy.

Regarding magnetic properties, Buschow [35] reports that all compounds are ferromagnetic, Fuji et al. relates that CeCd has a phase transition from ferromagnetic to paramagnetic in $T_c = 16.5K$. For PrCd, Fuji et al. reports a structure transition in $T = 125K$, and a transition from antiferromagnetic to paramagnetic in $T = 40K$ Cavalcante et al. agree with this, in the paper [13] also reports that PrCd is a antiferromagnetic compound. For NdCd Fuji et al. does not report any structural instability.

For GdCd, NdCd and SmCd Cavalcante et al. reports two magnetic transitions, one with $T \approx 35K$ and another $T \approx 80K$. Buschow made some comments that SmCd is diamagnetic in low temperatures and become paramagnetic in $T \approx 110K$, but contest these findings arguing that the compounds is ferromagnetic and a repopulation of the energy levels could lead to another results [35]. Cavalcante et al. agree with Buschow regarding SmCd and DyCd, in respect with the last one, Cavalcante et al. also observe two phase transitions, a first order at $40K$ and a second order at $79K$. The author also reports that TbCd shows a magnetic structure change at $67.5K$ and ErCd is a paramagnetic compound at $T = 4K$.

Ryan et al. [40], using Mösbauer spectroscopy determined that YbCd has a diamagnetic behavior. This study reports many variations of the compound Yb_xCd_y, our interest is focused when $x = y = 1$. The authors argue that because the Yb is an spherical ion with closed $4f$ shell, there is no magnetic moment nor local contribution to the electric field gradient in the nucleus.

The other compounds which are not reported here is due an lack of papers describing them in the RECd configurations, but only with others configurations.

3 Methodology and Optimization of LAPW's parameters

3.1 LAPW's parameters Optimization

As already mentioned in the previous chapter, RECd compounds have the CsCl structure type shown in Figure 3, this structure has the space group $Pm3m$[1]. We built this unit cell for each compound with experimental values taken from [35][2], [40][3], [41][4] and [42][5] shown in Table. 1.

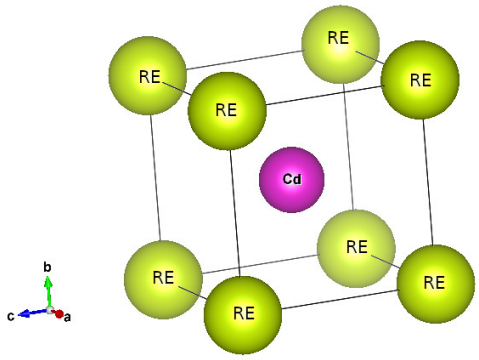

Figure 3 – Unitary cell of CsCl-structure. Source: Created by the author using the software VESTA.

Before any calculation it is necessary to optimize some parameters of the compounds, hence the results are of greater reliability, we show here the optimization procedure for three compounds: CeCd, GdCd and ErCd. The procedure will be the same for the rest of the series and their respectives graphs are on Appendix D, we followed the process described by Cottenier at [28].

The two parameters that we have optimized are the $R_{mt}K_{max}$ and k-points numbers. The $R_{mt}K_{max}$ parameter defines the base functions that will be used in the LAPW method, it is formed by the radius of the smallest MT sphere multiplied by the largest reciprocal lattice wave vector.

In choosing the size of the muffin-tin sphere R_{mt} one has to consider a few important criteria. Small R_{mt} makes the calculations more expensive (more plane waves a needed), but more accurate (plane waves are better basis functions). Large R_{mt} saves computer time,

[1] For more information about how unit cells are created in ELK please see the Appendix C
[2] Values for CeCd, DyCd, ErCd, EuCd, GdCd, HoCd, NdCd, PrCd, SmCd and TbCd
[3] Values for YbCd.
[4] Values for TmCd.
[5] Values for PmCd.

Table 1 – Table with experimental values of lattice parameters and volume for each compound. Source: [35, 40, 41, 42]

Compound	Lattice Parameter (Å)	Volume (Å^3)
CeCd	3.855	57.289
PrCd	3.827	56.050
NdCd	3.819	55.699
PmCd	3.799	54.829
SmCd	3.779	53.967
EuCd	3.955	61.864
GdCd	3.731	51.936
TbCd	3.723	51.603
DyCd	3.716	51.313
HoCd	3.701	50.694
ErCd	3.681	49.876
TmCd	3.665	49.229
YbCd	3.808	55.219

but the calculations lose accuracy. Moreover, the size of the muffin-tin radii of different atoms should not be too different (within 20%) and usually they have values between 1.5 a.u and 3.0 a.u. For the compounds here studied the radius of MT spheres are: 2.8 a.u. and 2.6 a.u. , respectively for RE and Cd, we do not choose these values, they are default in the ELK for more information about how these values are obtained please read the [28]. This implies that in the relation $R_{mt}K_{max}$ there were changes only in the K_{max} term (as is the default) between one calculation and another.

Thus, for the product $R_{mt}K_{max}$, the K_{max} term varied from 4 to 9 in the simulations of the thirteen compounds, in steps of 0.5 in 0.5. For all these calculations we use a $4\times4\times4$ k-point mesh, the ELK code has a feature of automatic determination of the k-point mesh, we made a calculation without any spin property and used this feature, so the code determined this value for the k-point mesh and we use this as our initial *ansatz* during the optimization. This process was done in the thirteen compounds but as already said we will show here only three compounds for exemplify the optimization procedure, with spin polarization and no spin-orbit coupling and after with spin polarization and also spin-orbit coupling. After determining these radius sizes such that their spheres enclosed all the considered core charges (establishing -3.0 Ha as separation energy), we kept their values always constant, both in the optimization process and in any of the following calculations. We then use the ideal value of $R_{mt}K_{max}$ to arrive at the optimized number of k-points. During all the process of optimization and in the rest of the calculations we used the approximation for the exchange-correlation functional the PBE96 [43], which is a Generalized Gradient Approximation (GGA) developed by Perdew et al. and a relative difference in the total energy for convergence of $\leq 10^{-6}$.

The number of k-points from the first Brillouin zone has to be limited as well

because the diagonalization of the Hamiltonian has to be repeated for each k vector. The number of points needed so that the first Brillouin zone is densely enough sampled has to be tested for each case (as the basis set size). The larger the cell, the fewer k points needed (because the volume of the cell in the reciprocal space is smaller). So, we used the optimized $R_{mt}K_{max}$ equal to 8.0 and thus made several simulations with the k-points ranging from $2 \times 2 \times 2$ to $25 \times 25 \times 25$ mesh in $1 \times 1 \times 1$ steps (where each number represents the number of k-points in x, y and z directions respectively).

Therefore, after performing these calculations by varying the two parameters, the graphs shown in Figures 4, 5, 6, 7, 8 and 9 were made. The displayed curves are functions of the parameters $R_{mt}K_{max}$ or k-points, representing the variation of the total crystalline cell energy (ΔE). The graphs have titles that specify the characteristics of their respective simulations, in which the titles are composed by the following acronyms: sp, so; which correspond respectively to the calculations with: spin polarized only and spin-orbit coupling (with spin polarization already included), variation of $R_{mt}K_{max}$ and k-points.

We determined the optimal values of these two parameters visually, observing the saturation of all curves, choosing the optimized numbers not at the beginning of the saturation of the curve, but in the region where they are already on a horizontal line.

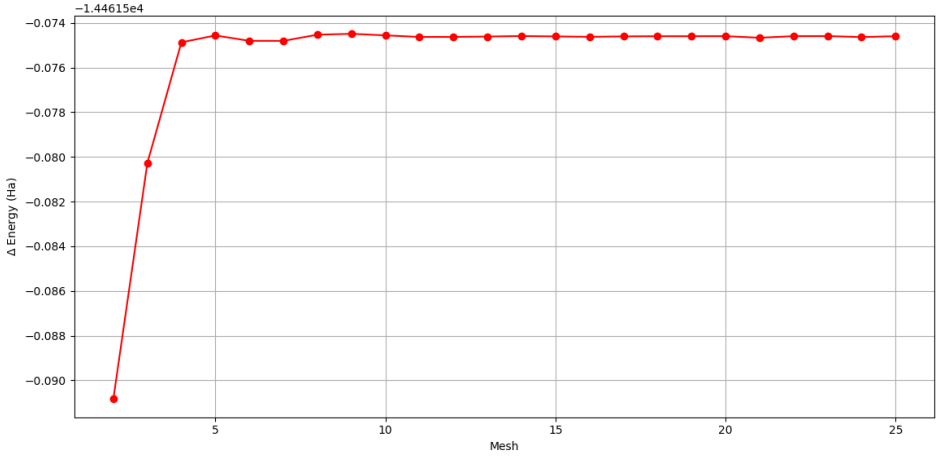

(a) CeCd with sp

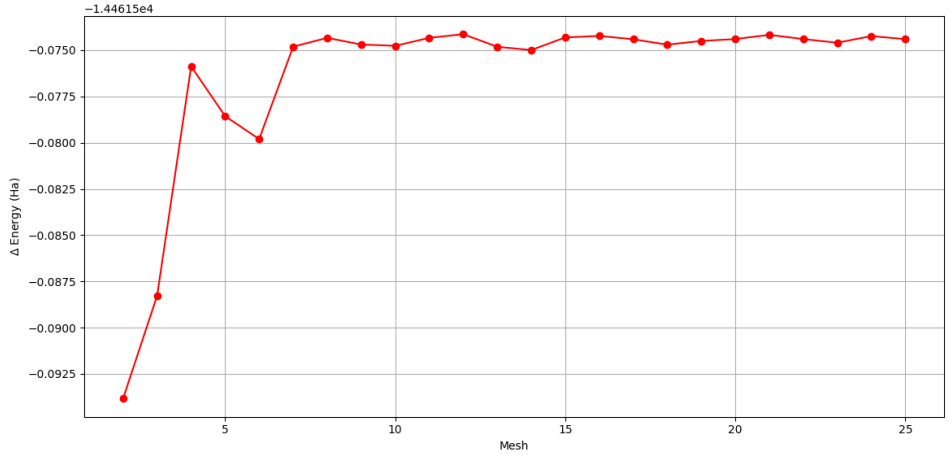

(b) CeCd with so

Figure 4 – k-points variations in function of energies differences of CeCd with spin polarization (sp) and spin polarization plus spin orbit (so), the x-axis represents points in x, y and z direction. Source: the Author.

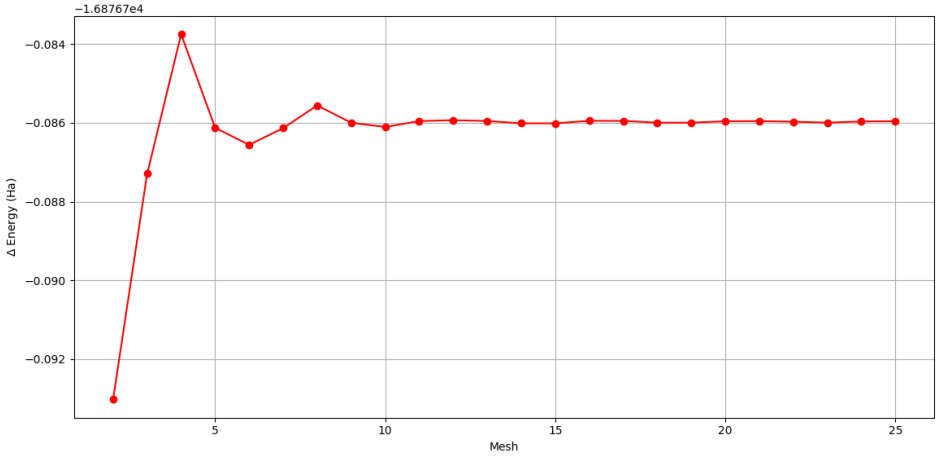

(a) GdCd with sp

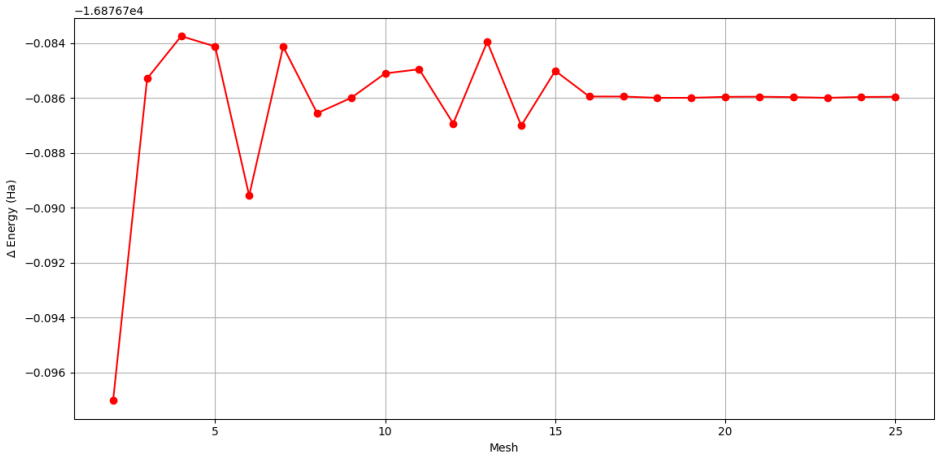

(b) GdCd with so

Figure 5 – k-points variations in function of energies differences of GdCd with spin polarization (sp) and spin polarization plus spin orbit (so) the x-axis represents points in x, y and z direction. Source: the Author.

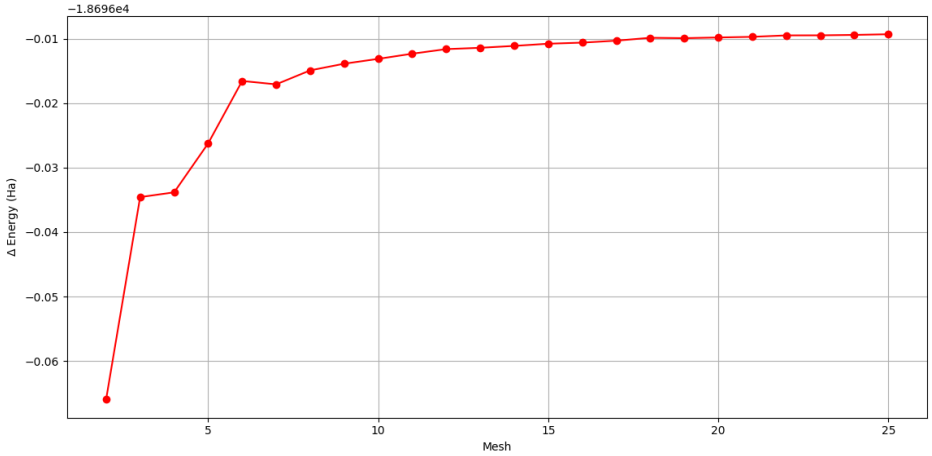

(a) ErCd with sp

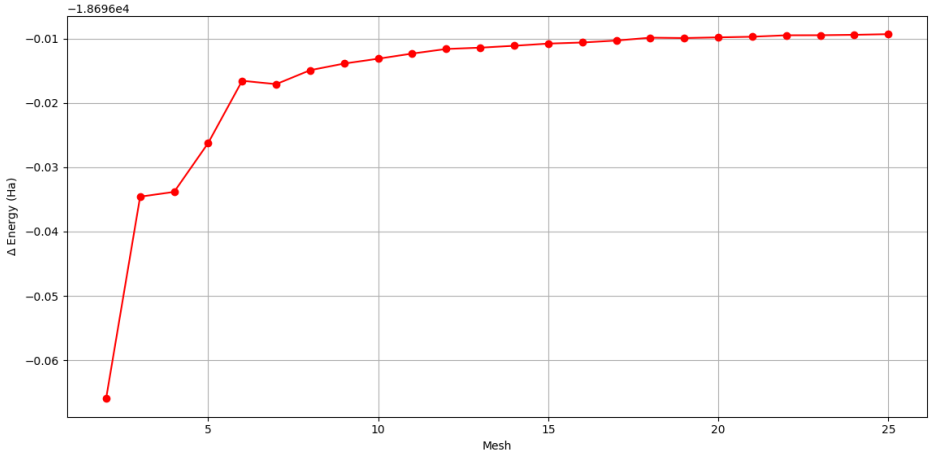

(b) ErCd with so

Figure 6 – k-points variations in function of energies differences of ErCd with spin polarization (sp) and spin polarization plus spin orbit (so) the x-axis represents points in x, y and z direction. Source: the Author.

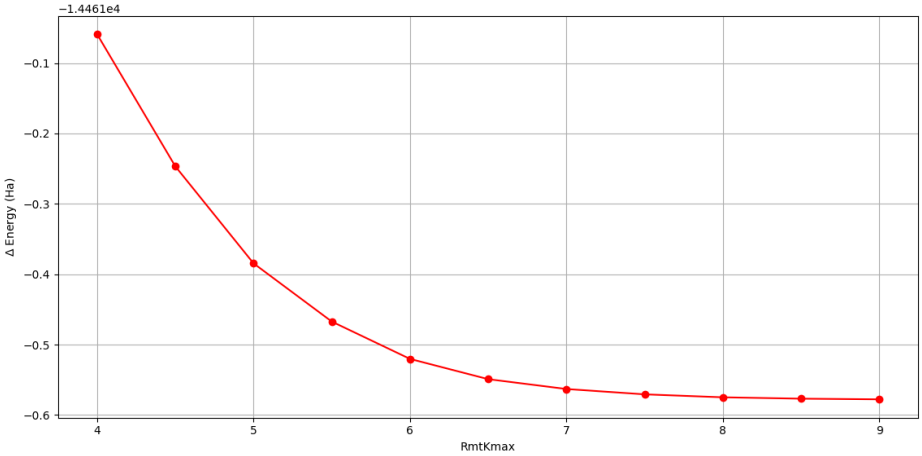

(a) CeCd with sp

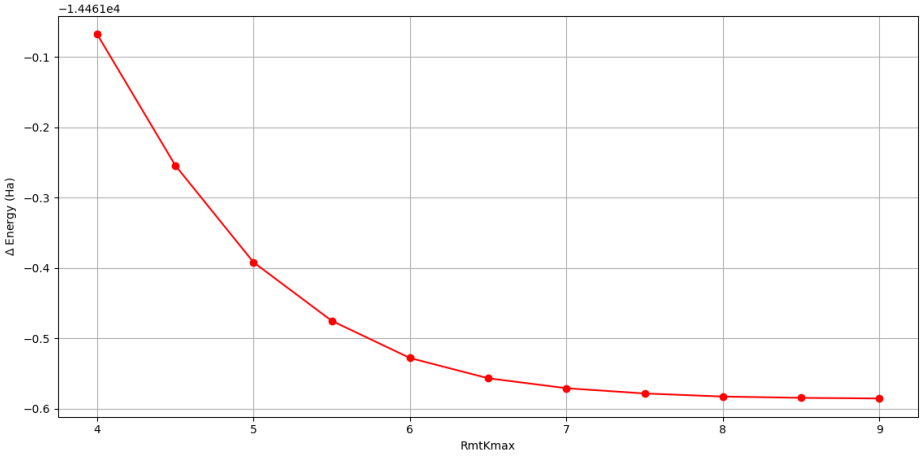

(b) CeCd with so

Figure 7 – $R_{mt}K_{max}$ variations in function of energies differences of CeCd with spin polarization (sp) and spin polarization plus spin orbit (so). Source: the Author.

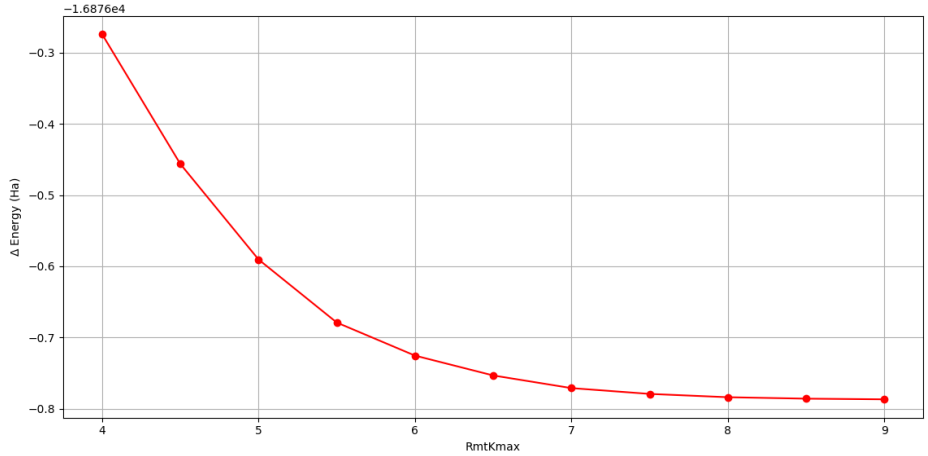

(a) GdCd with sp

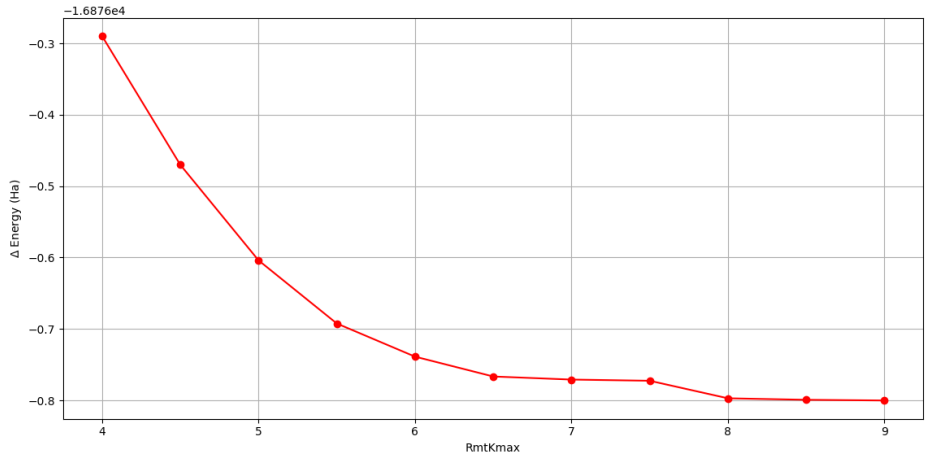

(b) GdCd with so

Figure 8 – $R_{mt}K_{max}$ variations in function of energies differences of GdCd with spin polarization (sp) and spin polarization plus spin orbit (so). Source: the Author.

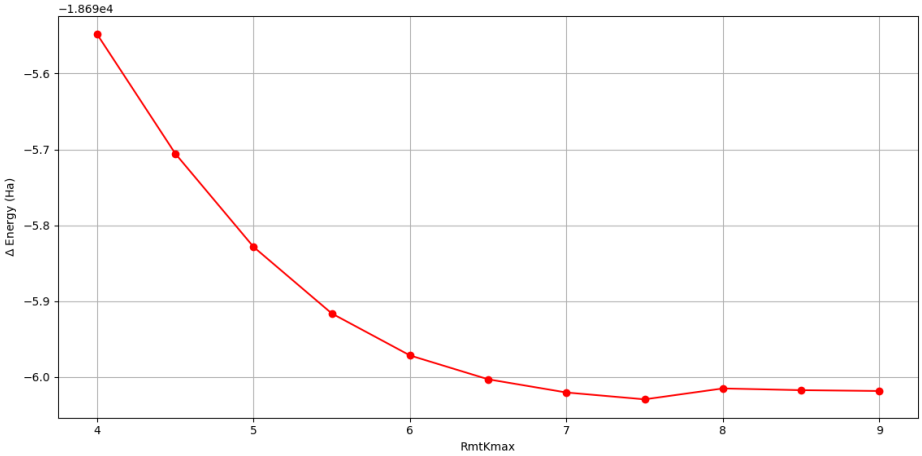

(a) ErCd with sp

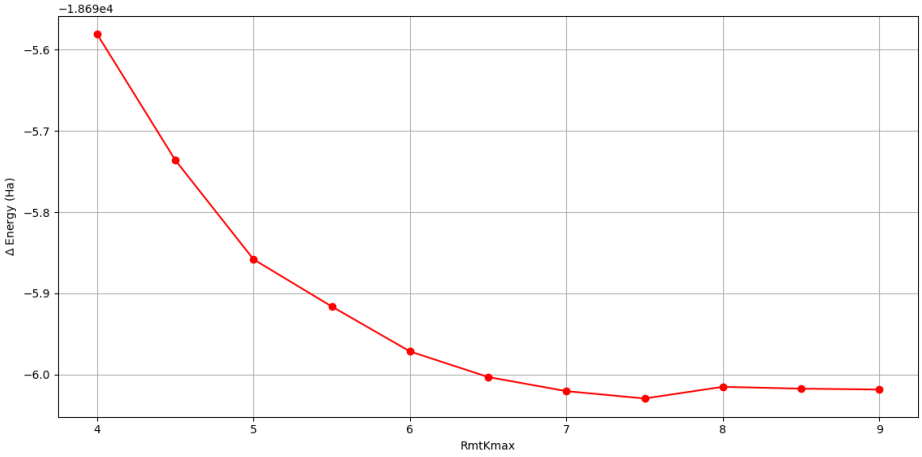

(b) ErCd with so

Figure 9 – $R_{mt}K_{max}$ variations in function of energies differences of ErCd with spin polarization (sp) and spin polarization plus spin orbit (so). Source: the Author.

Therefore, for the three compounds exemplified here (in calculations with or without spin-orbit interaction), we arrive at the ideal values of 8 for $R_{mt}K_{max}$ and $15 \times 15 \times 15$ for k-points. These values will be used for the rest of the series.

Calculations with or without spin-orbit coupling showed practically identical results, implying that the optimization process can be developed in both.

The DFT is all centered on the ground state of the system, since the Hohenberg-Kohn theorems apply only to that state, then it is very important that the experimental results for comparison are at low temperatures, thus representing the ground state properties.

3.2 Volume Optimization

In all the compounds of the serie, we developed calculations where we used the experimental lattice parameters as our initial point and varied the volume in steps of 1%, both in compression and expansion, until +15% (maximum expansion) and -15% (maximum compression), so we can find the crystalline cell of minimum energy.

After these calculations, graphs energy per volume were plotted Figures. 10, 11, and Figure 12. We also fitted a theoretical curve using the following Equation of State.

$$E(\eta) = E_0 + \frac{9B_0V_0}{16}(\eta^2 - 1)^2(6 + B_0'(\eta^2 - 1) - 4\eta^2) \tag{3.1}$$

this equation is called the *Birch-Muningham* equation and V_0 is the volume at zero pressure, B_0 is the Bulk modulus at zero pressure, B_0' is the pressure derivative and E_0 is the total energy at zero pressure are fitting parameters, $\eta = (\frac{V}{V_0})^{1/3}$.

Thus, we report in the Table 2 the theoretical values obtained for the crystalline cell with minimum energy. Remember that we show here only the graphs for CeCd, GdCd and ErCd; the rest of the graphs are in the Appendix D.

Ahead are the graphs of the compounds.

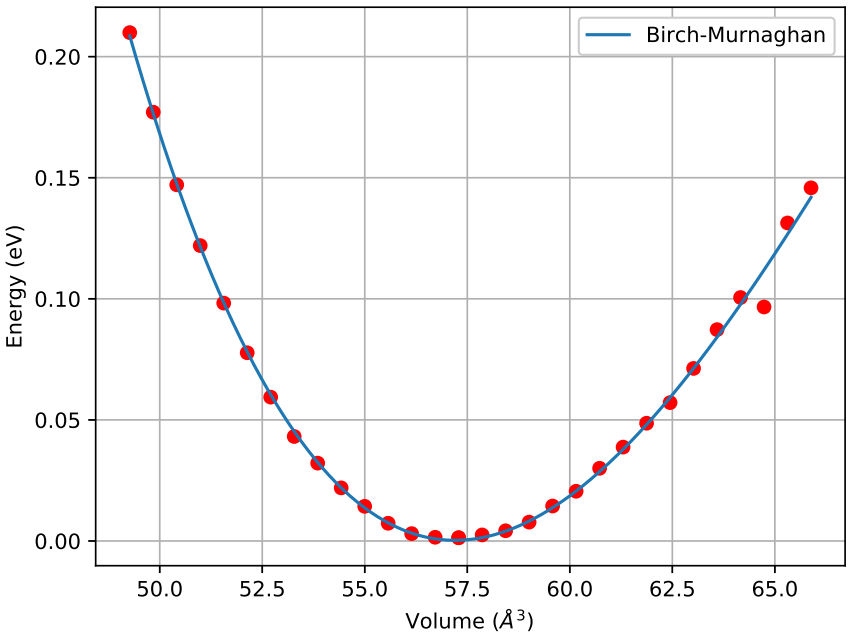

(a) CeCd with sp

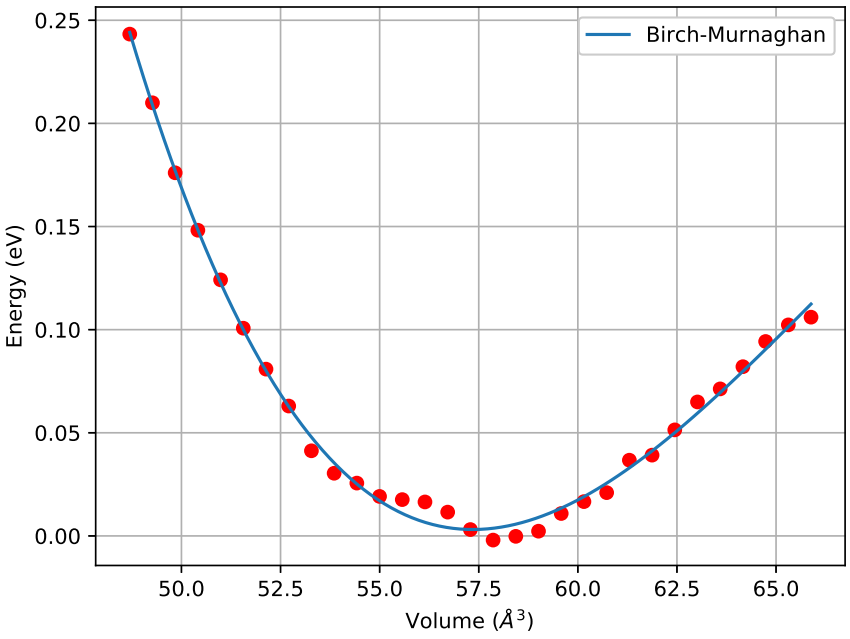

(b) CeCd with so

Figure 10 – Volume variations in function of energies differencies of CeCd with spin polarization (sp) and spin polarization plus spin orbit (so). Source: the Author.

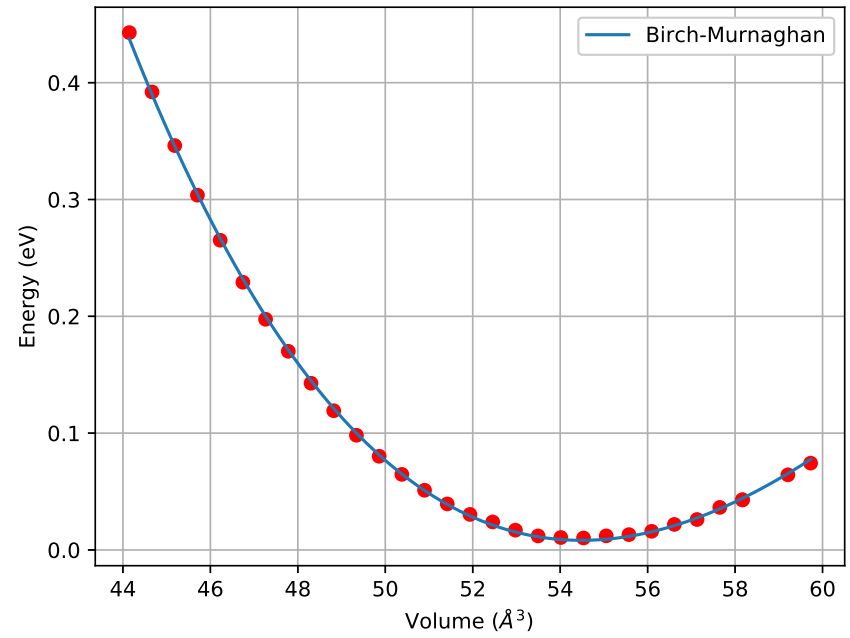

(a) GdCd with sp

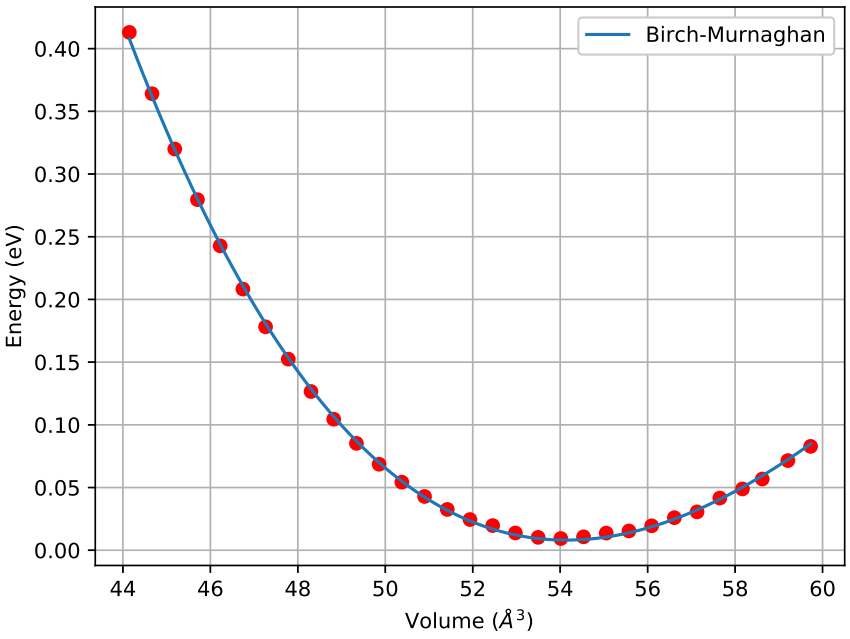

(b) GdCd with so

Figure 11 – Volume variations in function of energies differencies of GdCd with spin polarization (sp) and spin polarization plus spin orbit (so). Source: the Author.

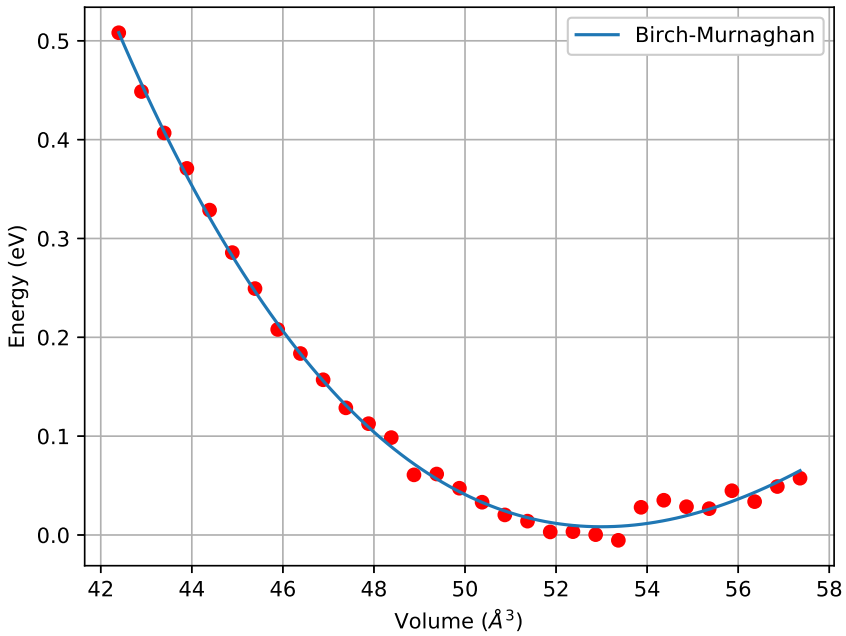

(a) ErCd with sp

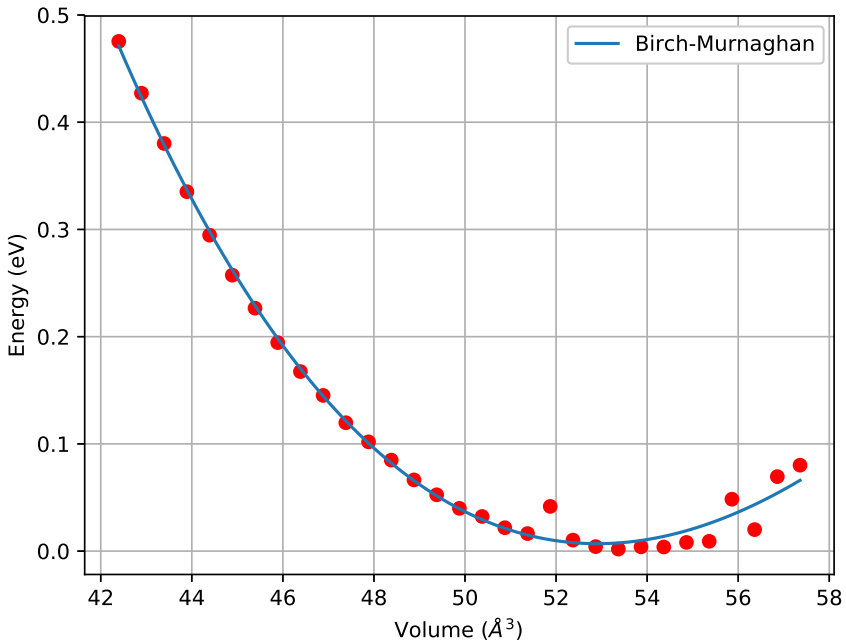

(b) ErCd with so

Figure 12 – Volume variations in function of energies differencies of ErCd with spin polarization (sp) and spin polarization plus spin orbit (so). Source: the Author.

Table 2 – Table with calculated values of lattice parameters and volume for each compound.

Compound	Theo. Lattice Parameter (Å)	Theo. Volume (Å^3)
CeCd	3.853	57.198 (sp)
	3.849	57.044 (so)
PrCd	3.895	59.097 (sp)
	3.860	57.513 (so)
NdCd	3.919	60.190 (sp)
	3.920	60.263 (so)
PmCd	3.900	59.344 (sp)
	3.879	58.382 (so)
SmCd	3.908	59.678 (sp)
	3.900	59.323 (so)
EuCd	3.945	61.383 (sp)
	3.928	60.598 (so)
GdCd	3.791	54.487 (sp)
	3.783	54.133 (so)
TbCd	3.760	53.182 (sp)
	3.752	52.802 (so)
DyCd	3.773	53.721 (sp)
	3.760	53.147 (so)
HoCd	3.780	54.032 (sp)
	3.778	53.912 (so)
ErCd	3.756	52.991 (sp)
	3.754	52.907 (so)
TmCd	3.799	54.840 (sp)
	3.756	53.002 (so)
YbCd	3.755	53.806 (sp)
	3.747	52.611 (so)

Our theoretical results in the great majority are bigger than the experimental value, this could be a characteristic of the code, we could see in the graphs that in the part of expansion, the points become less ordered considering the theoretical curve, this caused a less accurate fitting.

Our objective in these calculations is to find the less energetic lattice parameters for the crystalline cell, even when the experimental value is smaller than the theoretical, we use the theoretical.

3.3 Summary

Before we go on to the calculations indeed we give a brief summary of what was done until now:

We made the unit cell with CsCl structure to be our unit cell of all compounds, with experimental lattice parameters taken from [35, 41, 40, 42]. The muffin-tin radius is:

2.8 a.u. for RE and 2.6 a.u. for Cd. We start the optimization by the $R_{mt}K_{max}$ parameter arriving at the optimized value of 8.0 and use this value in the optimization of the k-points where we found the optimized value of $15 \times 15 \times 15$. We also did the volume variation to choose the less energetic lattice parameters for each compound, all the optimization process were made with spin polarization only (sp) and with spin polarization plus spin orbit coupling (so) to check if the two configurations results in some difference in the optimized parameters which we already saw that do not influence in the optimization process.

3.4 FP-LAPW ELK Code

ELK works with tasks, in its input files the first field is called "tasks" followed by numbers, Figure 13 show a picture of an input ELK's file where each number designates a specific task.

```
tasks
0
1
10
100

spincore
.true.
```

Figure 13 – Block showing the tasks part in ELK input file elk.in. Source: the Author

The task 0 is responsible for determining the energy of the ground state from atomic densities, it is in fact the convergence of the calculation. Task 1 is the restart of the calculation of the ground state starting from the density written in the file STATE.OUT, a file that is only created after the execution of task 0. Task 10 is responsible for generating the density of states (DOS), total, partial and interstices. The last task that we use, task 110 is actually the task responsible for calculating the hyperfine parameters in atomic sites, regarding the hyperfine magnetic field only the Fermi contact term is calculated in ELK.

We remember that ELK does not only have these four tasks (0, 1, 10, 110), but more than 80 tasks, all described in the code manual [14]. With our goals, only these four tasks were necessary, then we only describe these.

4 Results and Discussion

4.1 Methodology

Before starting the hyperfine field calculations we performed a test to determine if the time to group the tasks in sequence or perform one at a time will present significant differences, for these, we made a calculations passing through the four tasks in the CeCd compound with only spin polarization, the results of these calculations are illustrated in Table 3:

Table 3 – Table with time elapsed for two tasks configurations.

Calculus Type	Time (s)
Grouped tasks	15.36
Separated tasks	630.72

Remembering that the time of the separated tasks was counted considering only the calculation time of the running machine, it did not take into account the time spent to start the calculation again after the end of a previous task. Thus, we can see that for the tasks used in this work, using them all at once in the input file is much more efficient.

4.2 Hiperfyne Magnetic Fields on RECd Compounds

Since ELK works with tasks, as was discussed at the beginning of this chapter, we have results for calculating the hyperfine magnetic field and DOS of all volumes that we vary during volume optimization.

For comparison and beginning of discussion, Table 4 shows the experimental values measured by Cavalcante et. al, [13] using the technique PAC[1], and theoretical values also calculated in the work [13] using the code WIEN2k together with the values calculated in this work in the minimum volumes. Remembering that we are reporting the Hyperfine Magnetic Field in the cadmium atom.

[1] Perturbed Angular Correlation Spectroscopy.

Table 4 – Experimental and Calculated Value of Magnetic Hyperfine Field at Cadmium atom in RECd compounds.

Compound	B_{hf}(T)sp(ELK)	B_{hf}(T)so(ELK)	B_{hf}(T)(WIEN2k)[13]	B_{hf}(T)(Exp.)[13]
CeCd	-14.25	-13.68	-5.75	5.10
PrCd	-16.23	-14.51	-13.92	—-
NdCd	-21.31	-21.27	-15.89	17.4
PmCd	-24.46	-24.28	——	——
SmCd	-23.72	-22.93	-21.98	21.1
EuCd	-28.10	-28.51	——	——
GdCd	-39.27	-38.15	-35.11	30.8
TbCd	-27.48	-26.40	-25.67	25.6
DyCd	-20.03	-20.03	-17.91	20.0
HoCd	-14.28	-12.64	-11.74	10.3
ErCd	-7.18	-7.06	-6.22	6.9
TmCd	-3.35	-2.76	——	—-
YbCd	-0.38	-0.83	——	—-

In this Table 4, *sp* stands for spin polarized only, *so* spin polarized plus spin orbit coupling, the values which are missing is because the experiment reported in the paper of Fabio et al. [13] was not performed on these compounds and in the literature we cannot find any value for the B_{hf} of the respectives compounds not theoretical neither experimental.

We could see that all the values calculated using the ELK code with spin polarization only are above the experimental value (CeCd is 179% above being the highest value and DyCd is 0.15% above being the lowest value). The good agreement between calculated and experimental values of B_{hf} is unusual for DFTs methods and its not expected [44, 16, 11]. This happens because a neglect of the orbital and dipolar contributions by the code and the majority of the magnetization arises from the s polarized states. To deal with this issue, all the calculations made on ELK must take account of the core spin polarization at least, but additionally to that any s state of semi-core must be moved to the core and the problem be treated with full Dirac equation. A point that suggests a better agreement when the full Dirac equation is used is the values with spin orbit coupling which diminishes the discrepancy between the theoretical value and the experimental. Until the version of the code used in this work (5.2.14) no one of these issues is taken into account.

It is possible to change the species file considering all the s states as core states, ELK allows this, but we did no t do this because our intention is to test the code "out of the box" without changes in your source files.

Another possible explanation about these values is that our cells is not the least energetic, like we used the theoretical values fitted in the graphs of volume optimization and these values is bigger than the experimental, this could indicate that the cell is not in your minimum and so it is not represents the ground state of the system causing some

discrepancy in these values but this will not take into account the huge discrepancy for some compounds.

4.3 Density of States of RECd compounds

The density of states (DOS) is an important theoretical quantity for understanding the bonding in a compound. In order to get the nature change of the band gap, the total density of states and partial density of states are calculated for all the series, as shown in the Figures below.

All the DOS here are calculated with *sp* and after with *so*.

4.3.1 CeCd

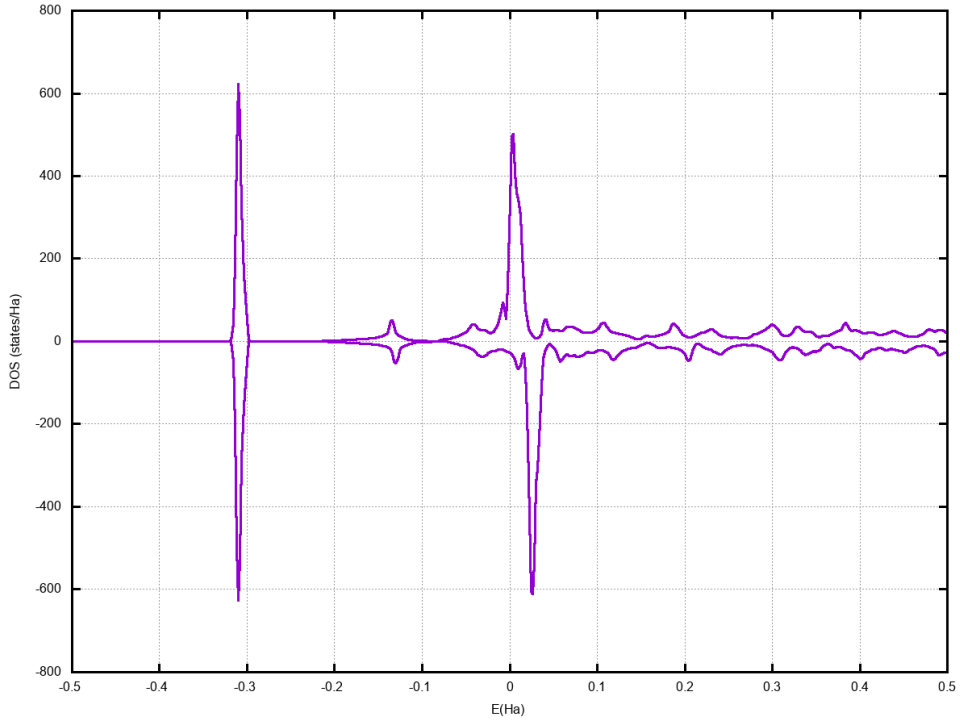

(a) CeCd Total DOS with sp.

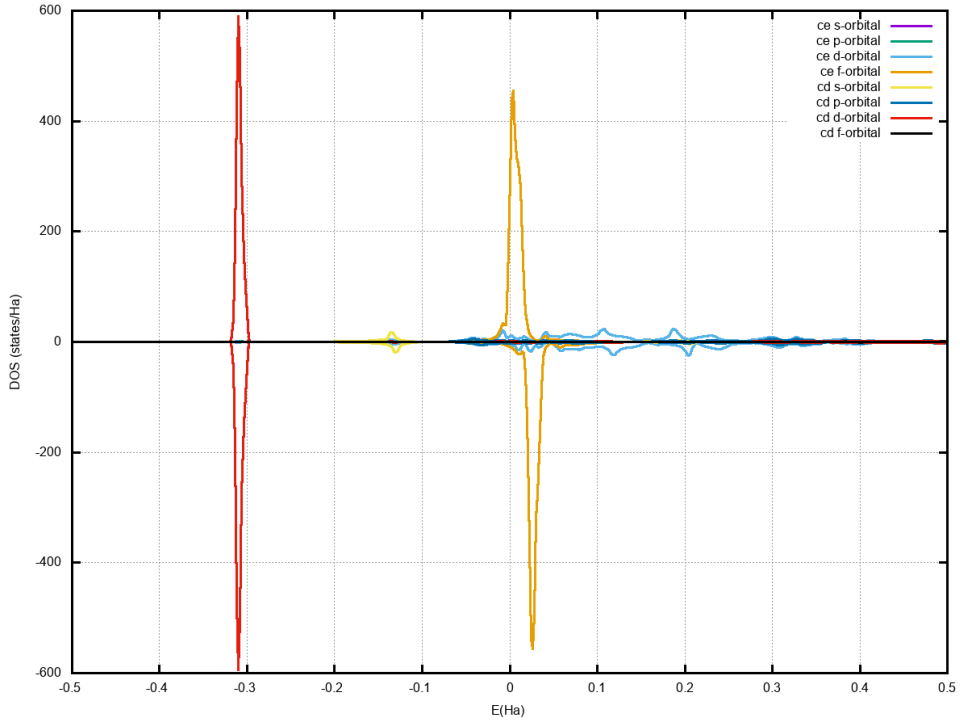

(b) CeCd Partial DOS with sp

Figure 14 – Total and Partial DOS of CeCd with spin spolarized (sp). Source: the Author.

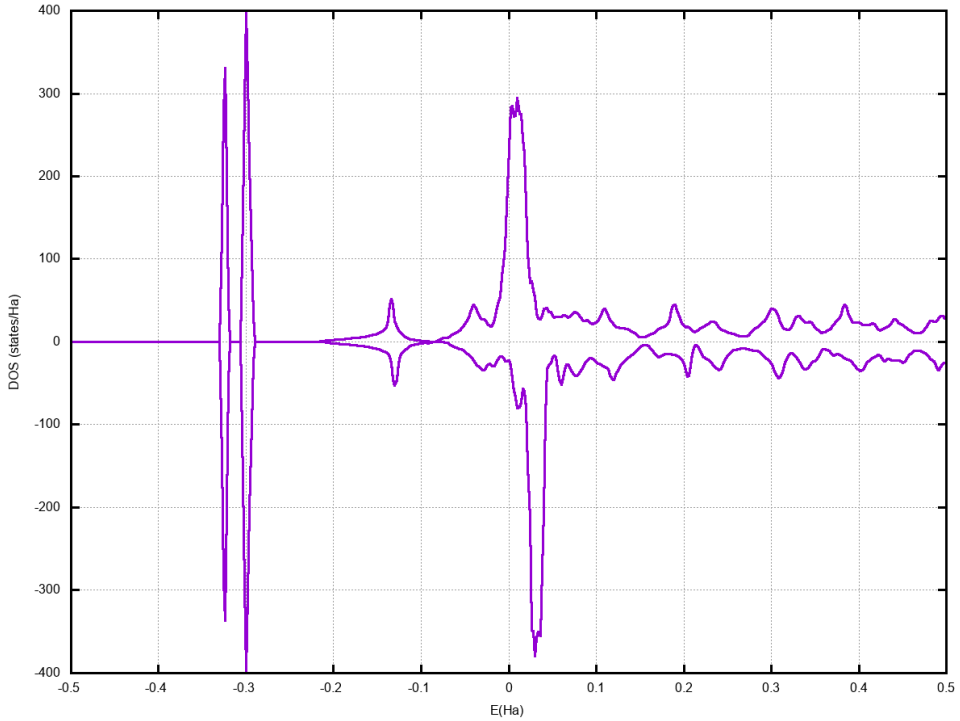

(a) CeCd Total DOS with so.

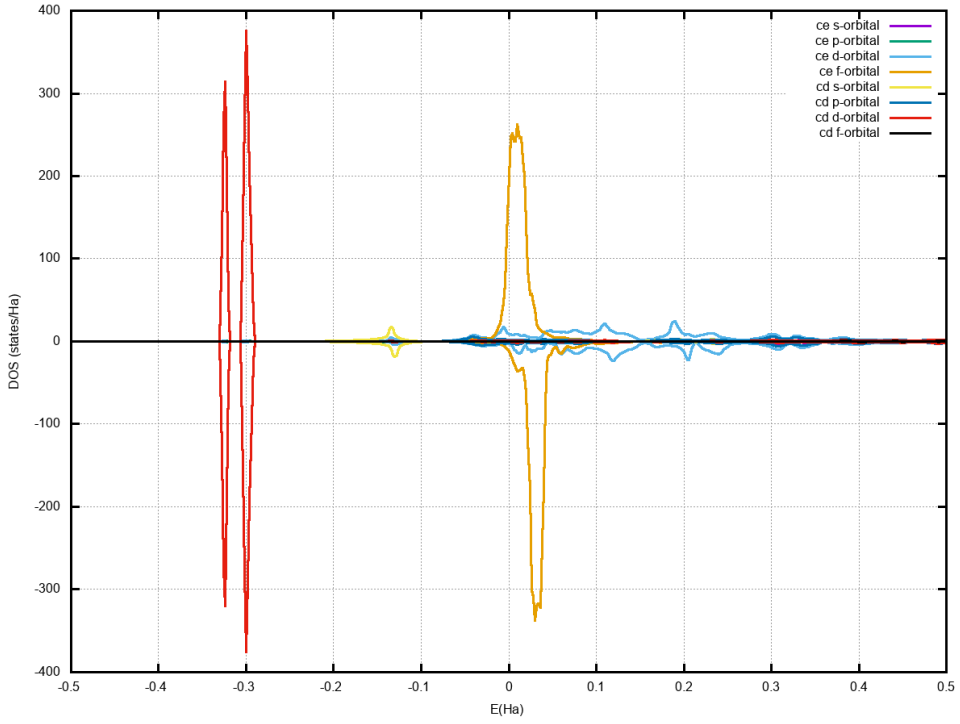

(b) CeCd Partial DOS with so

Figure 15 – Total and Partial DOS of CeCd with spin spolarized + spin orbit (so). Source: the Author.

4.3.2 PrCd

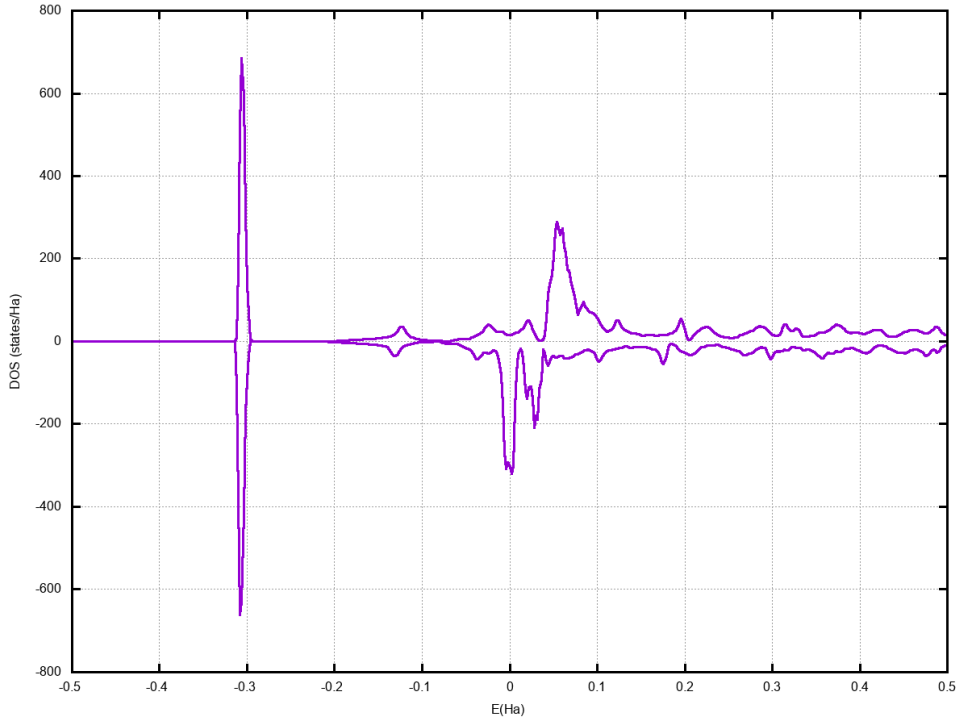

(a) PrCd Total DOS with sp

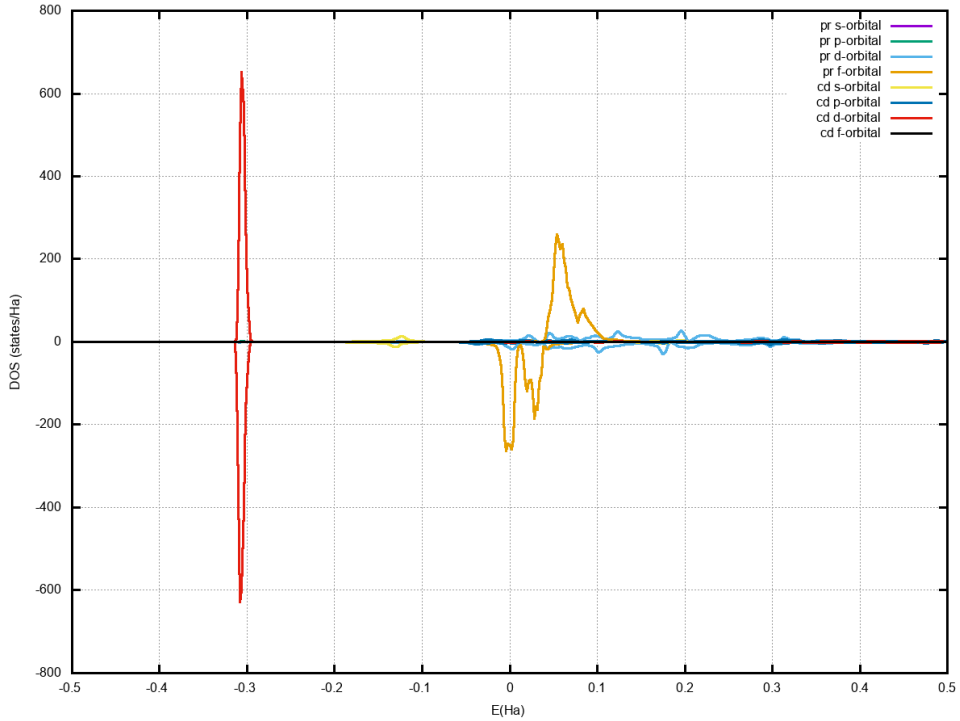

(b) PrCd Partial DOS with sp

Figure 16 – Total and Partial DOS of PrCd with spin spolarized (sp). Source: the Author.

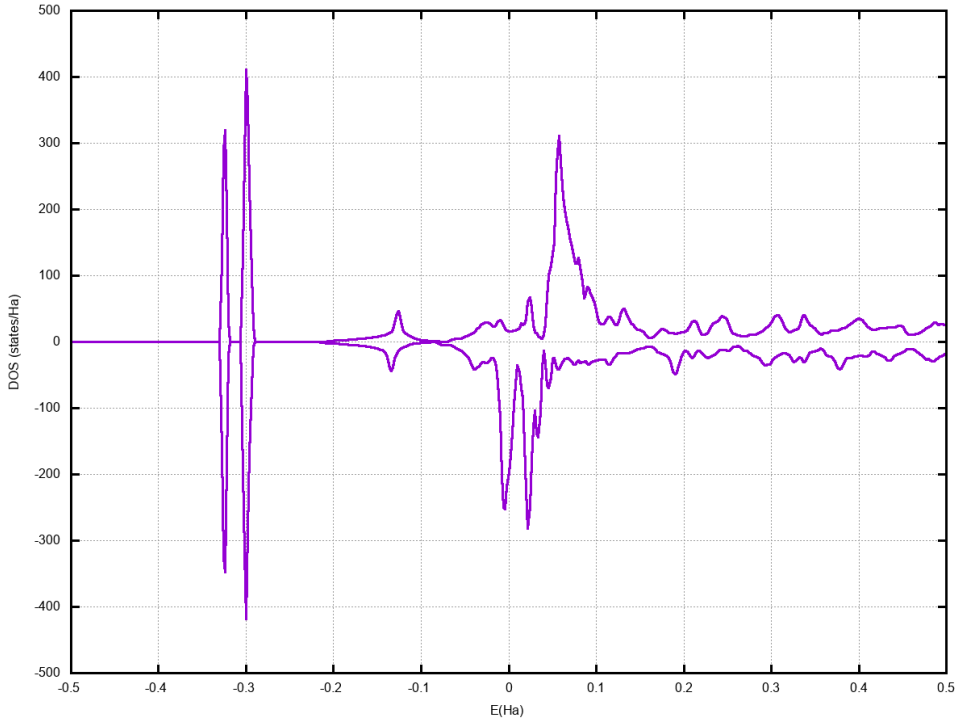

(a) PrCd Total DOS with so

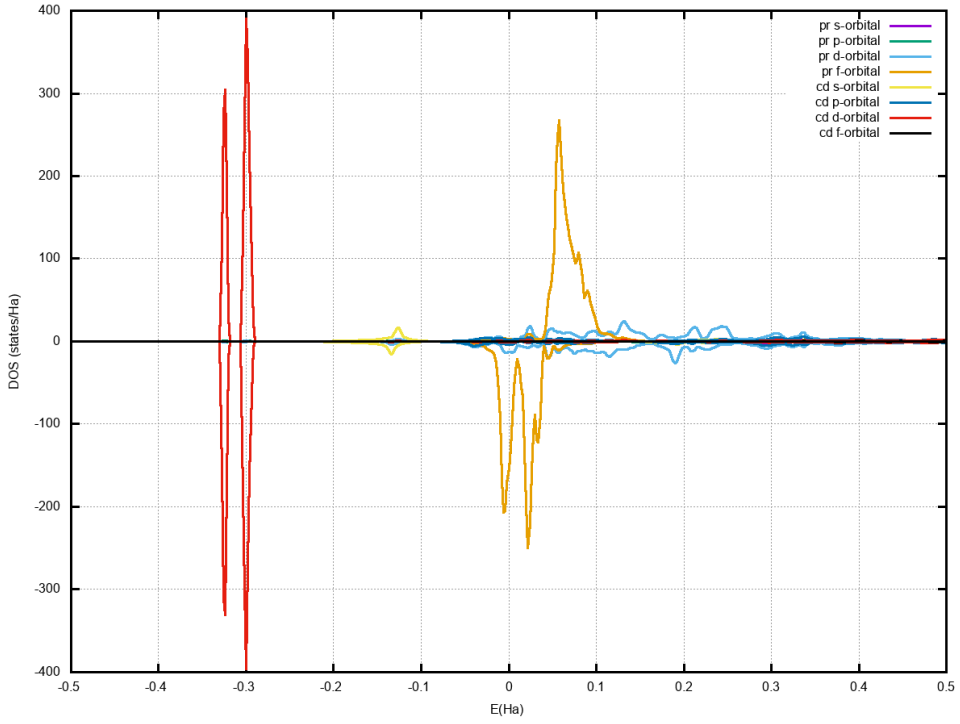

(b) PrCd Partial DOS with so

Figure 17 – Total and Partial DOS of PrCd with spin spolarized + spin orbit (so). Source: the Author.

4.3.3 GdCd

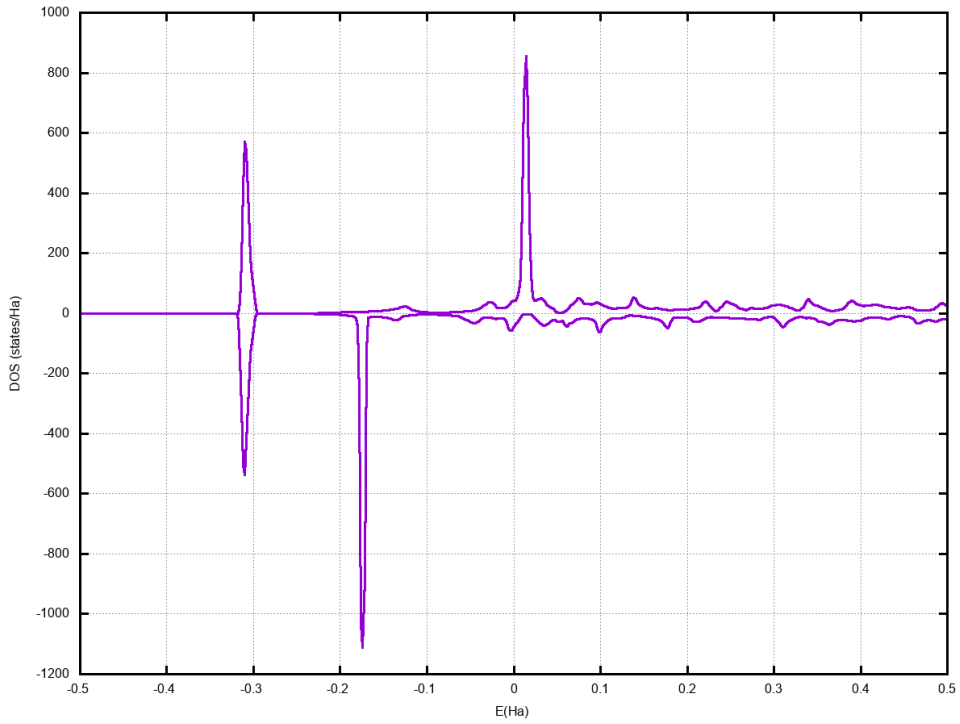

(a) GdCd Total DOS with sp

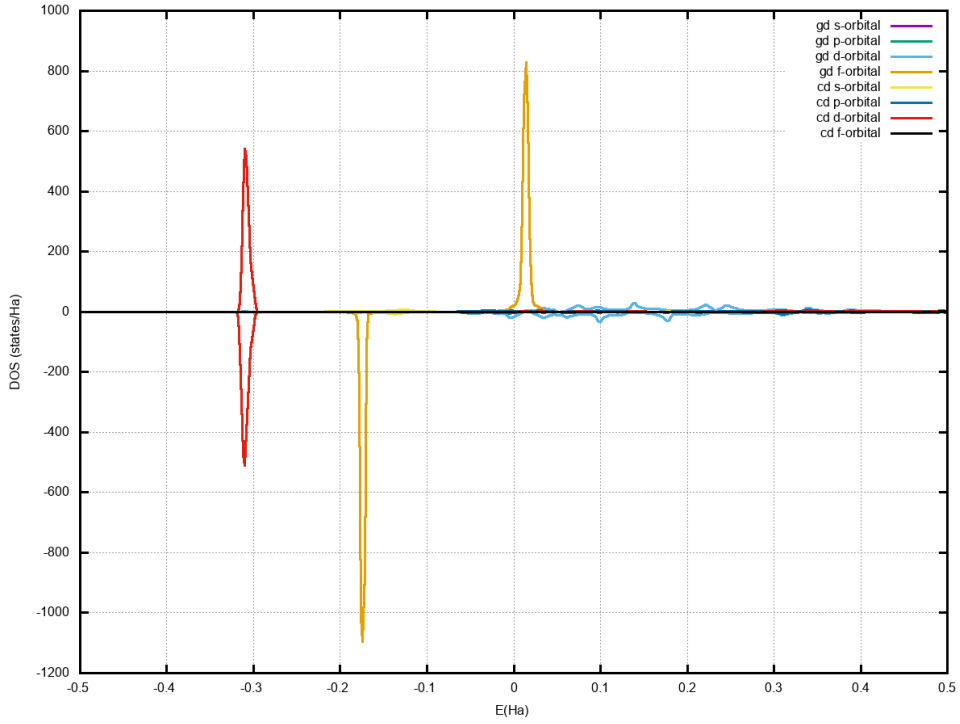

(b) GdCd Partial DOS with sp

Figure 18 – Total and Partial DOS of GdCd with spin spolarized (sp). Source: the Author.

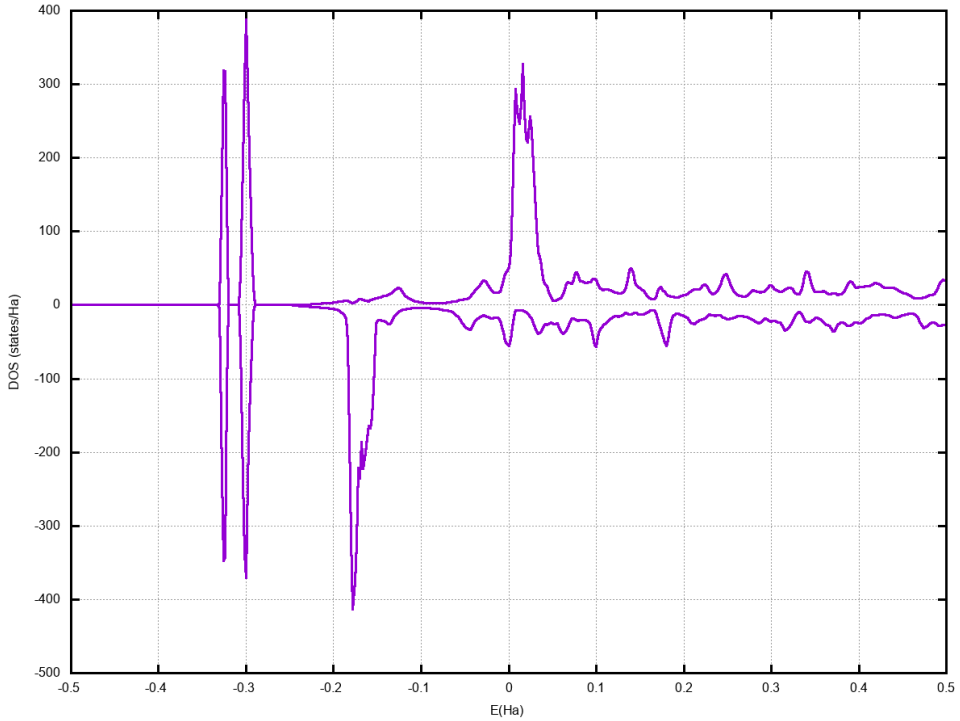

(a) GdCd Total DOS with so

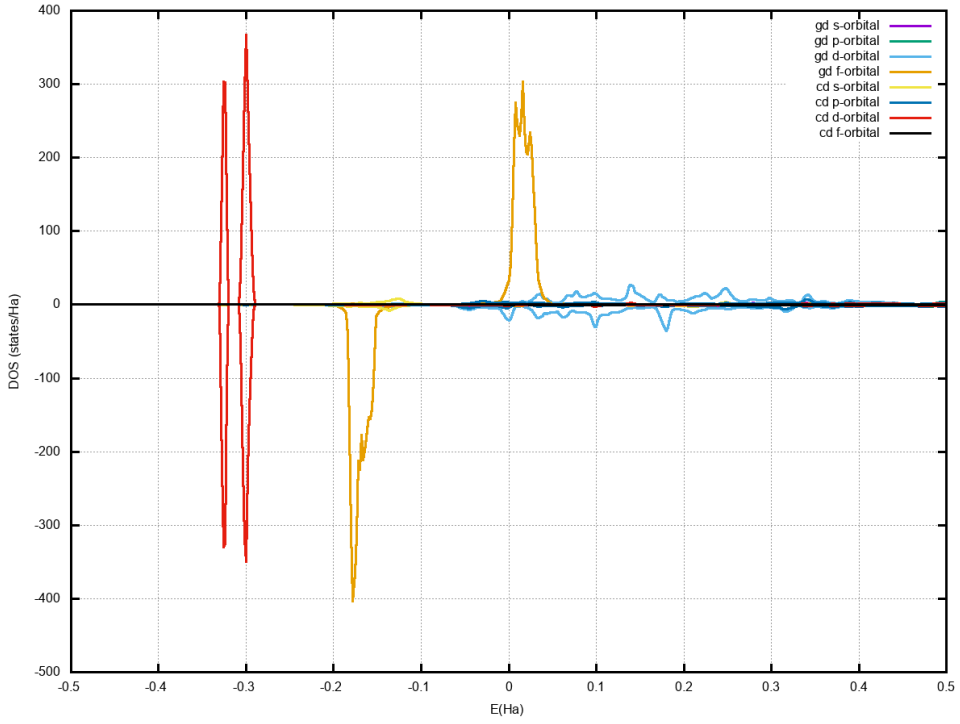

(b) GdCd Partial DOS with so

Figure 19 – Total and Partial DOS of GdCd with spin spolarized + spin orbit (so). Source: the Author.

4.3.4 NdCd

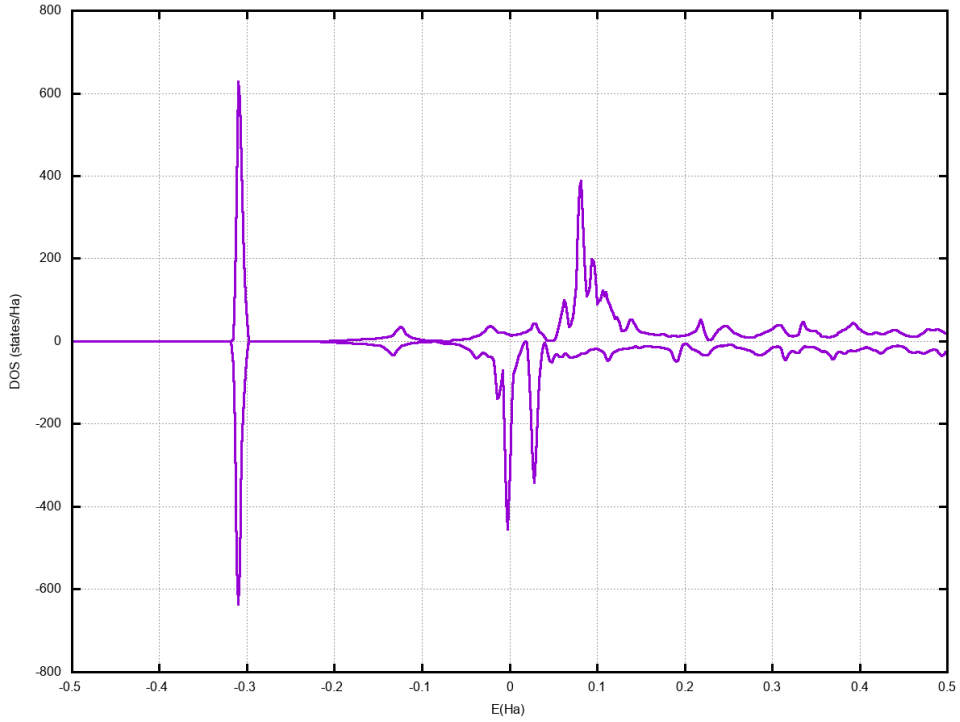

(a) NdCd Total DOS with sp

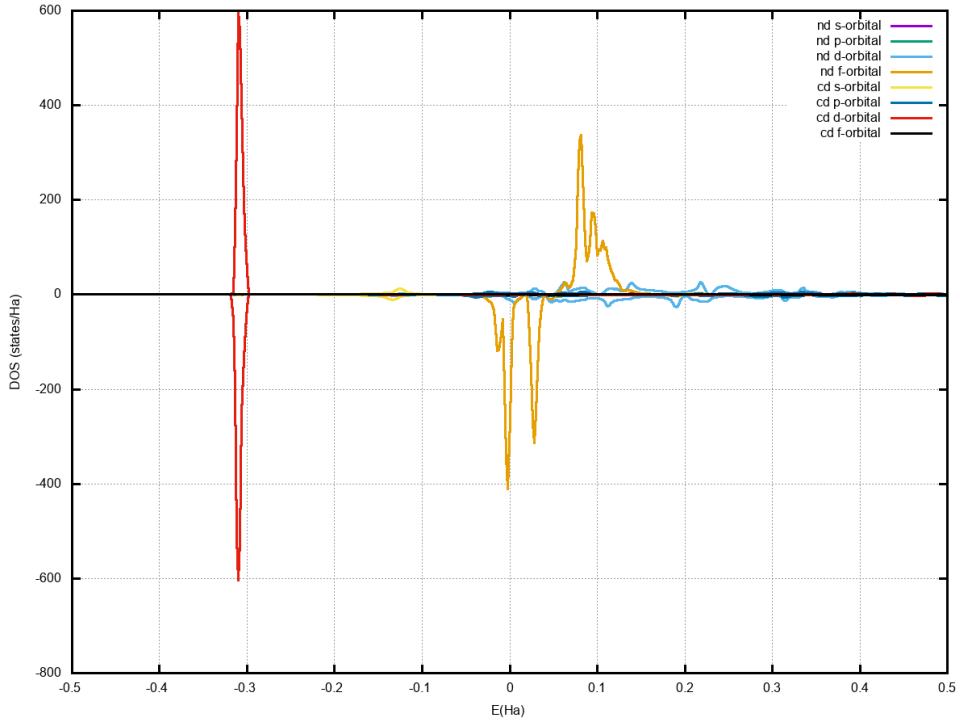

(b) NdCd Partial DOS with sp

Figure 20 – Total and Partial DOS of NdCd with spin spolarized (sp). Source: the Author.

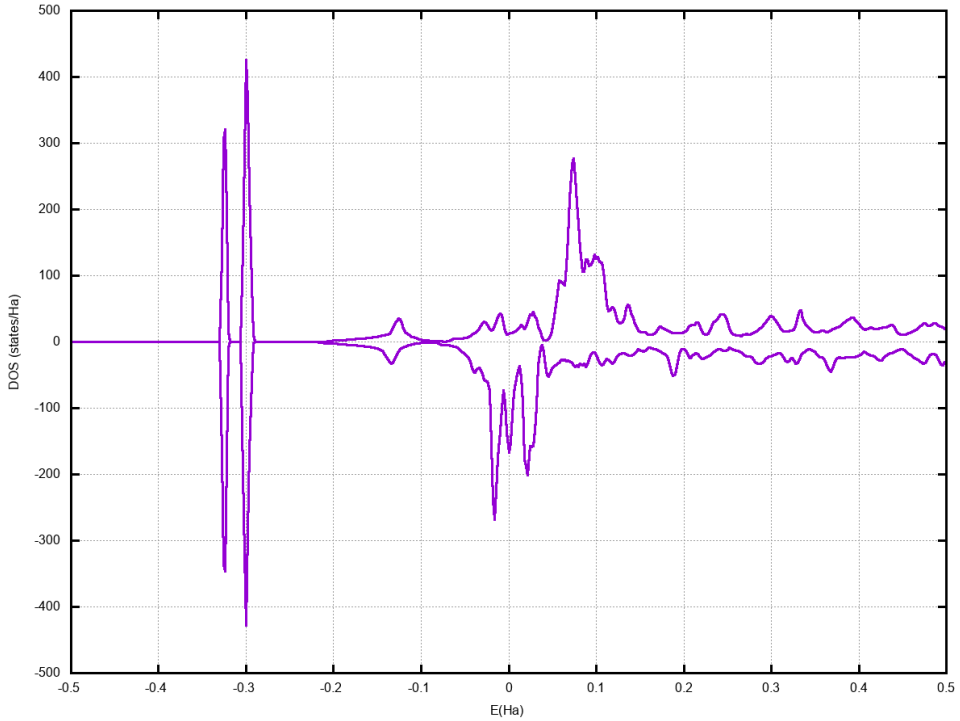

(a) NdCd Total DOS with so

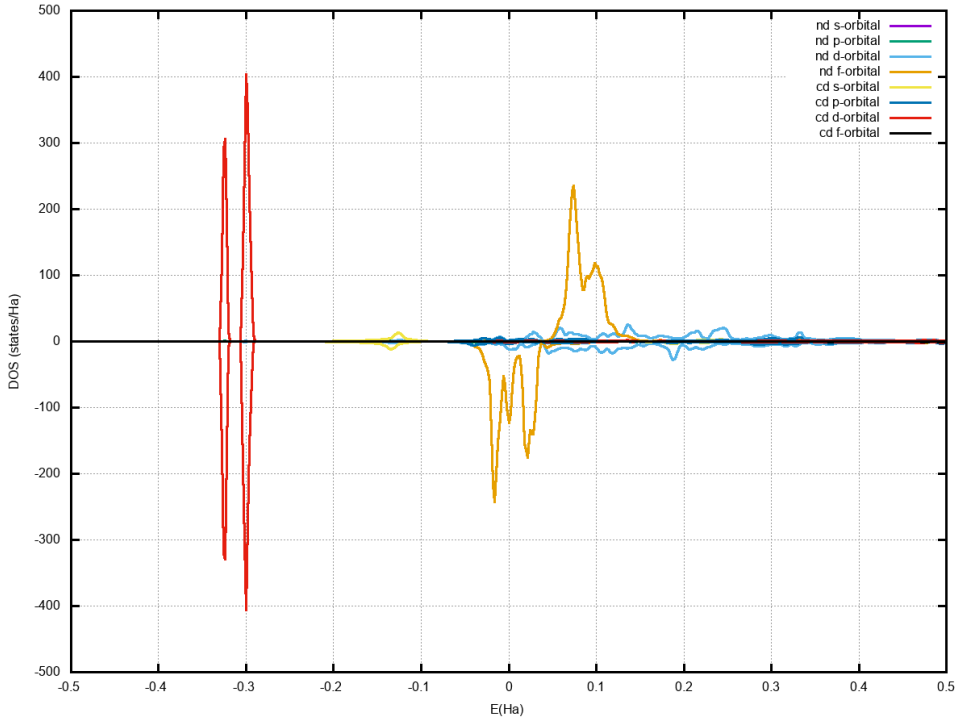

(b) NdCd Partial DOS with so

Figure 21 – Total and Partial DOS of NdCd with spin spolarized + spin orbit (so). Source: the Author.

4.3.5 SmCd

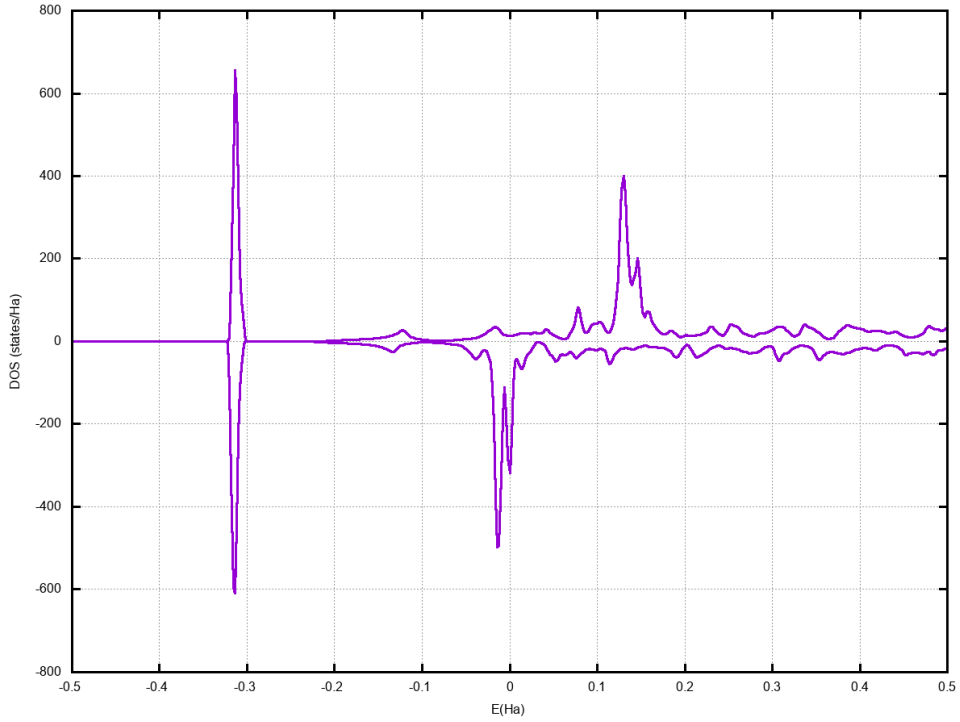

(a) SmCd Total DOS with sp

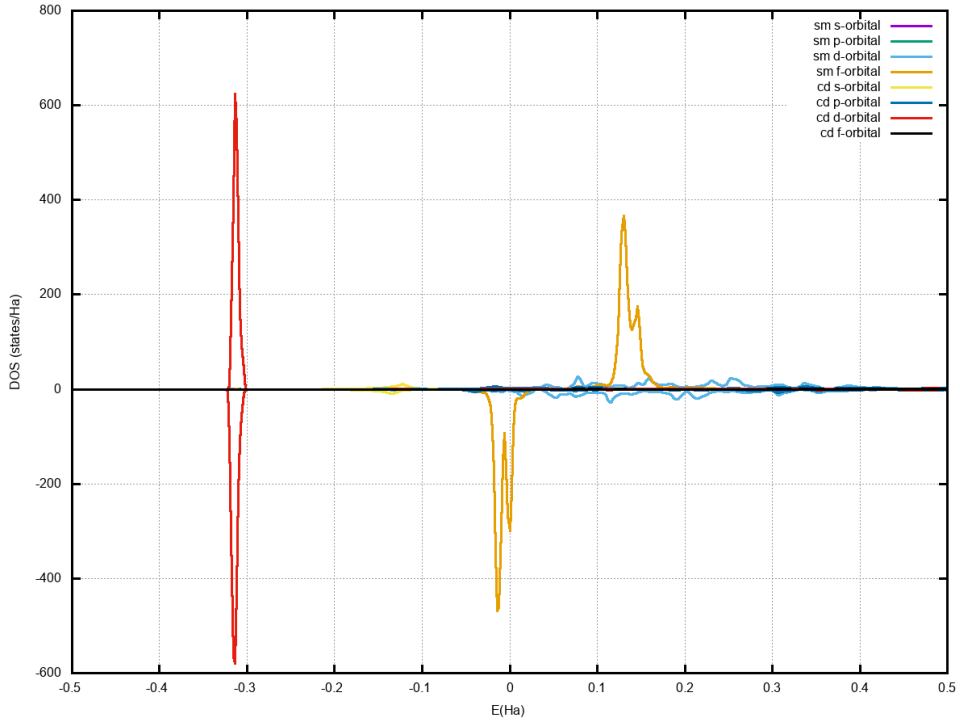

(b) SmCd Partial DOS with sp

Figure 22 – Total and Partial DOS of SmCd with spin spolarized (sp). Source: the Author.

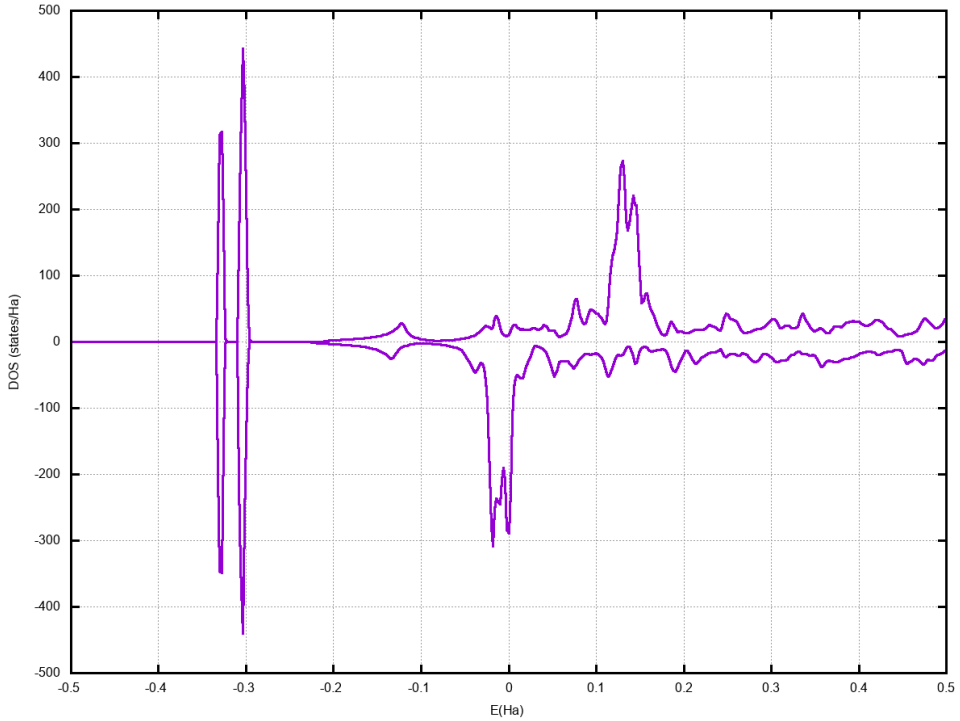

(a) SmCd Total DOS with so

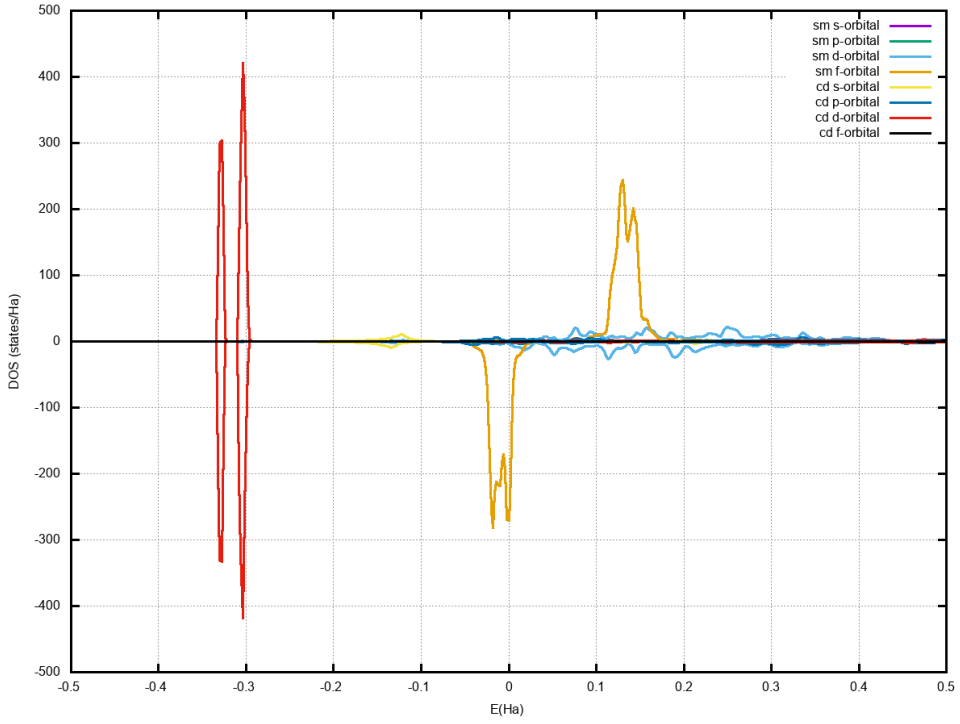

(b) SmCd Partial DOS with so

Figure 23 – Total and Partial DOS of SmCd with spin spolarized + spin orbit (so). Source: the Author.

4.3.6 TbCd

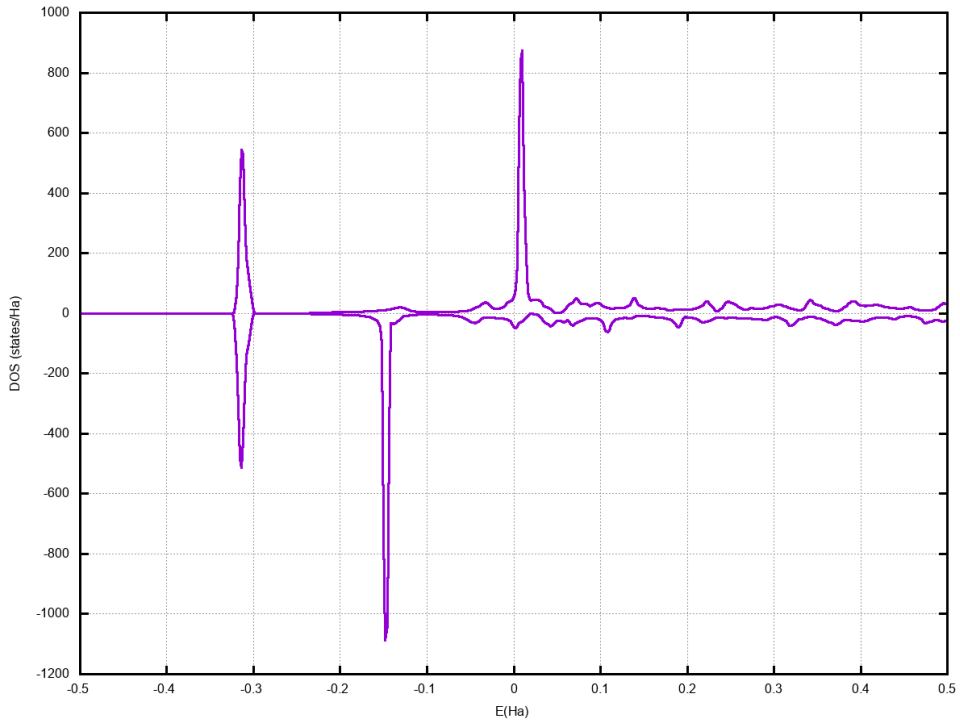

(a) TbCd Total DOS with sp

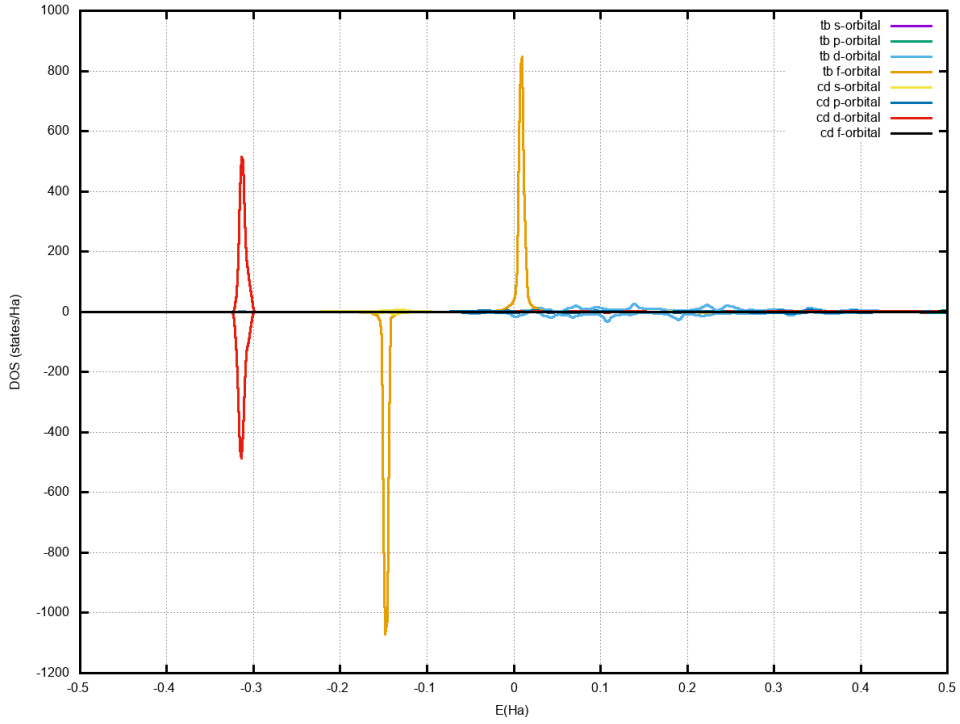

(b) TbCd Partial DOS with sp

Figure 24 – Total and Partial DOS of TbCd with spin spolarized (sp). Source: the Author.

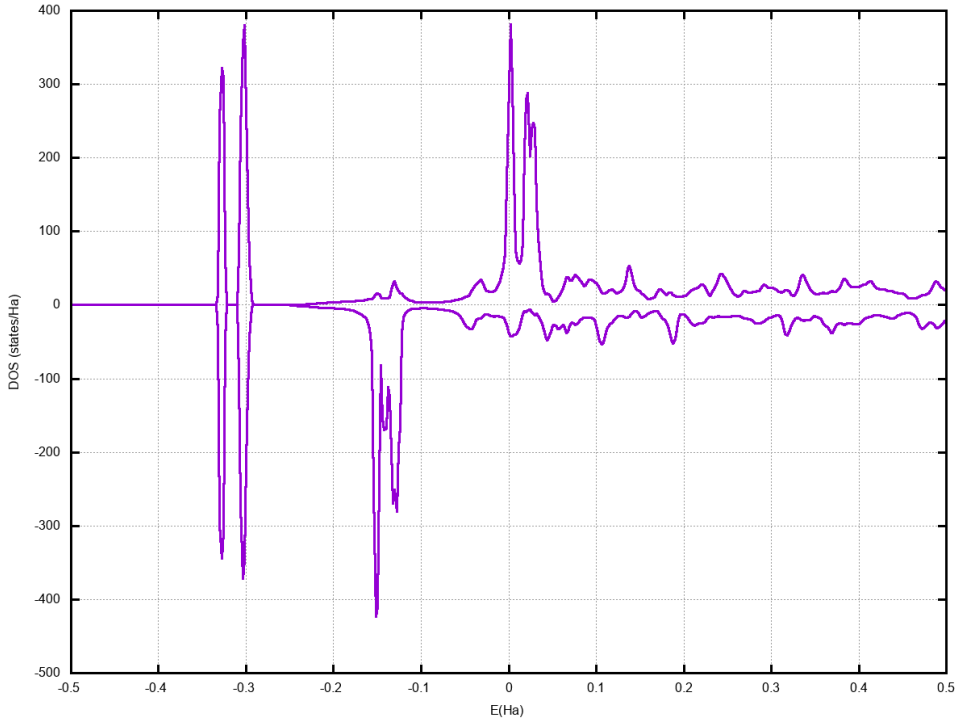

(a) TbCd Total DOS with so

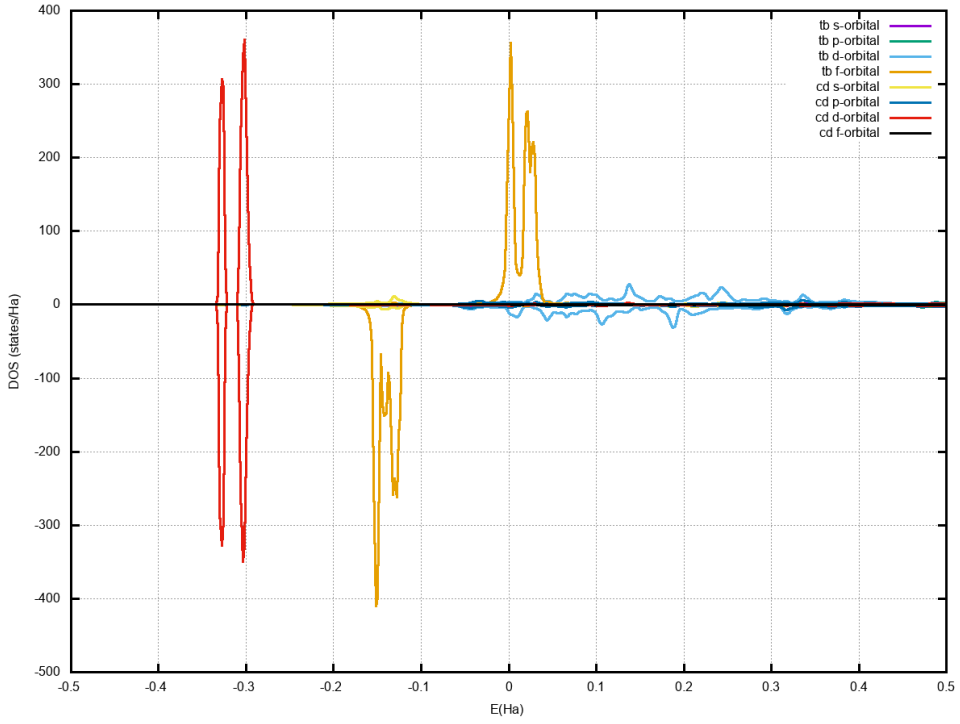

(b) TbCd Partial DOS with so

Figure 25 – Total and Partial DOS of CeCd with spin spolarized + spin orbit (so). Source: the Author.

4.3.7 DyCd

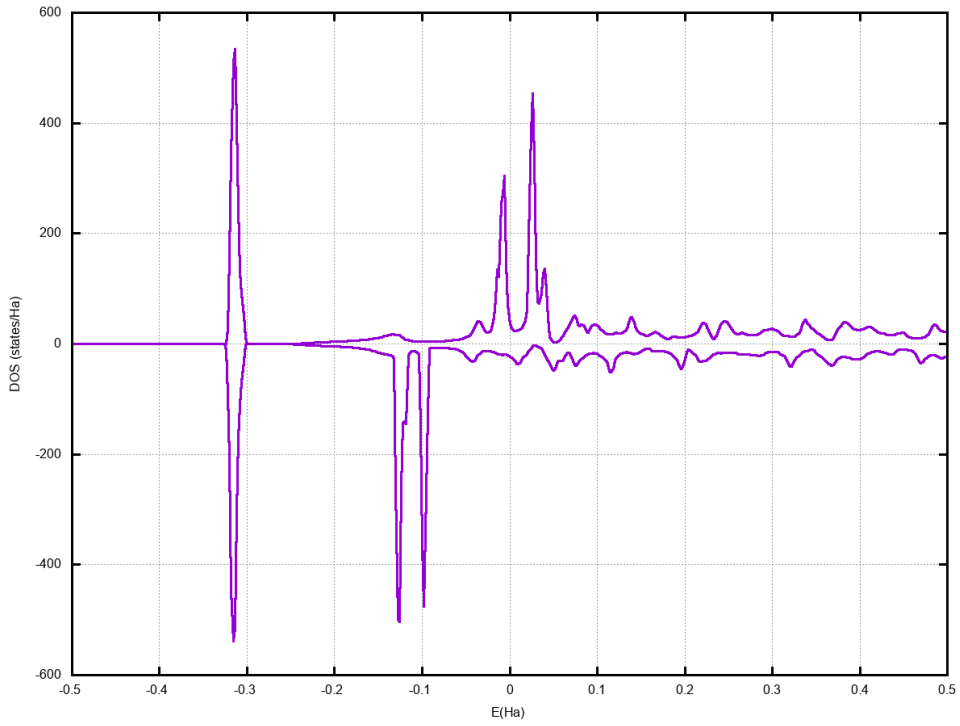

(a) DyCd Total DOS with sp

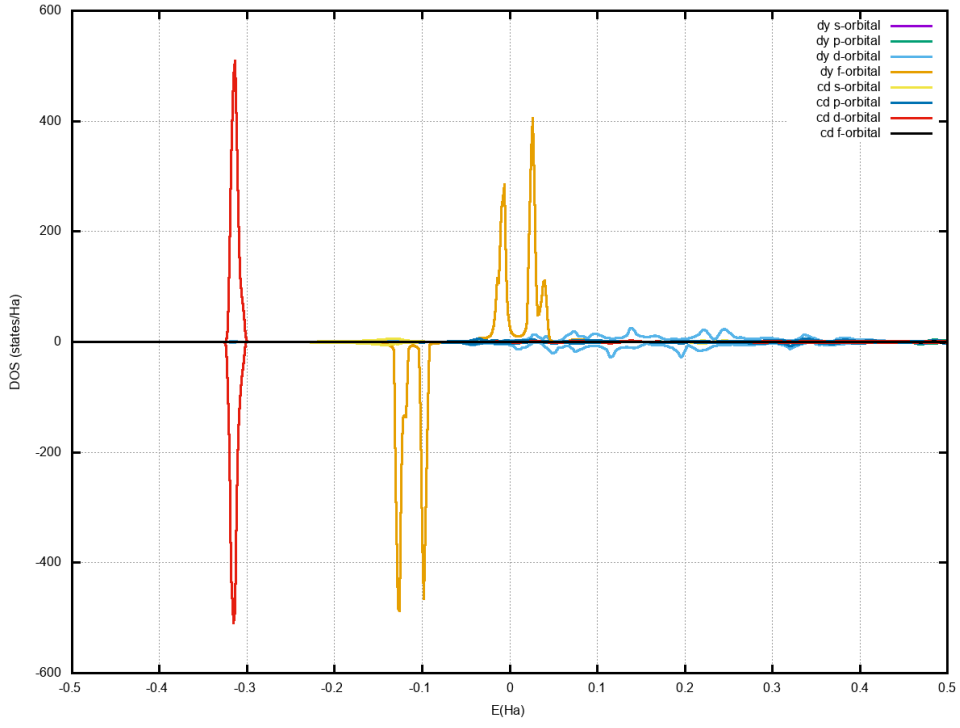

(b) DyCd Partial DOS with sp

Figure 26 – Total and Partial DOS of DyCd with spin spolarized (sp). Source: the Author.

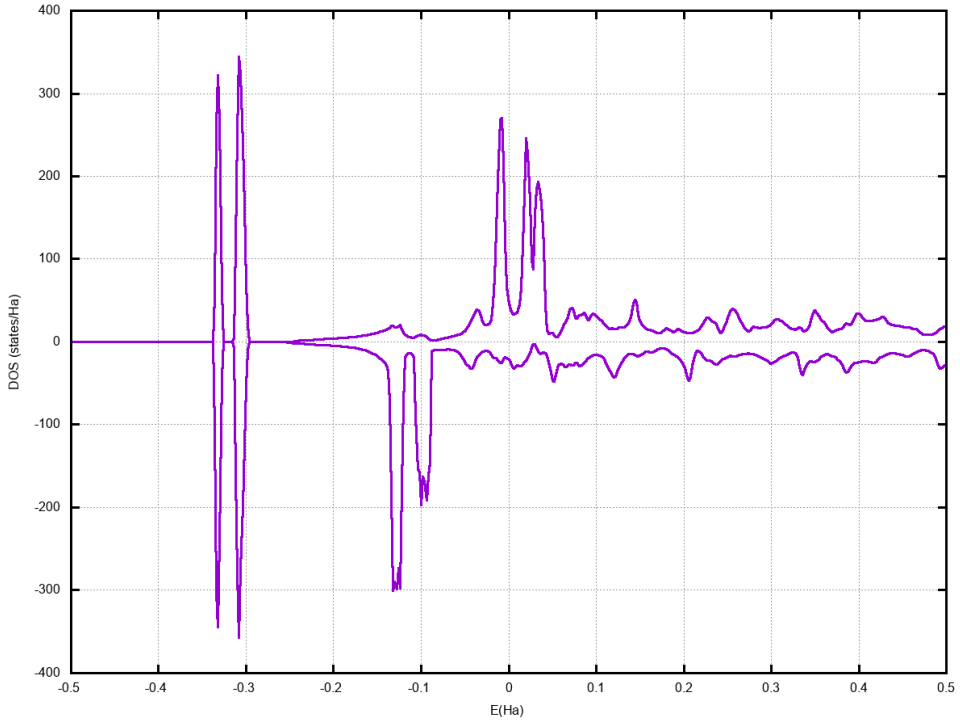

(a) DyCd Total DOS with so

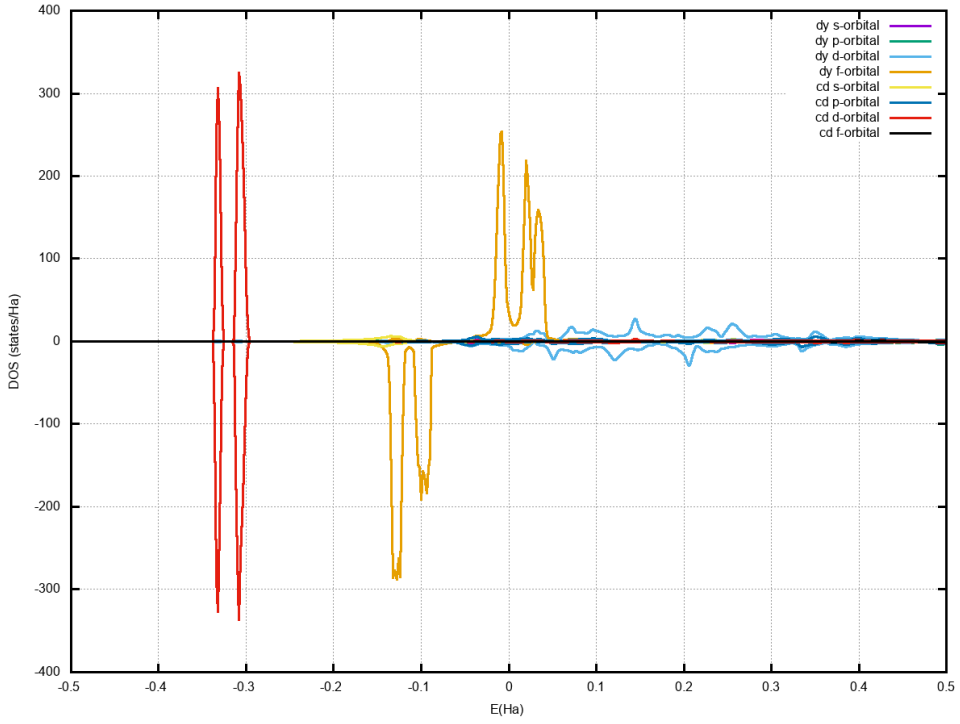

(b) DyCd Partial DOS with so

Figure 27 – Total and Partial DOS of DyCd with spin spolarized + spin orbit (so). Source: the Author.

4.3.8 HoCd

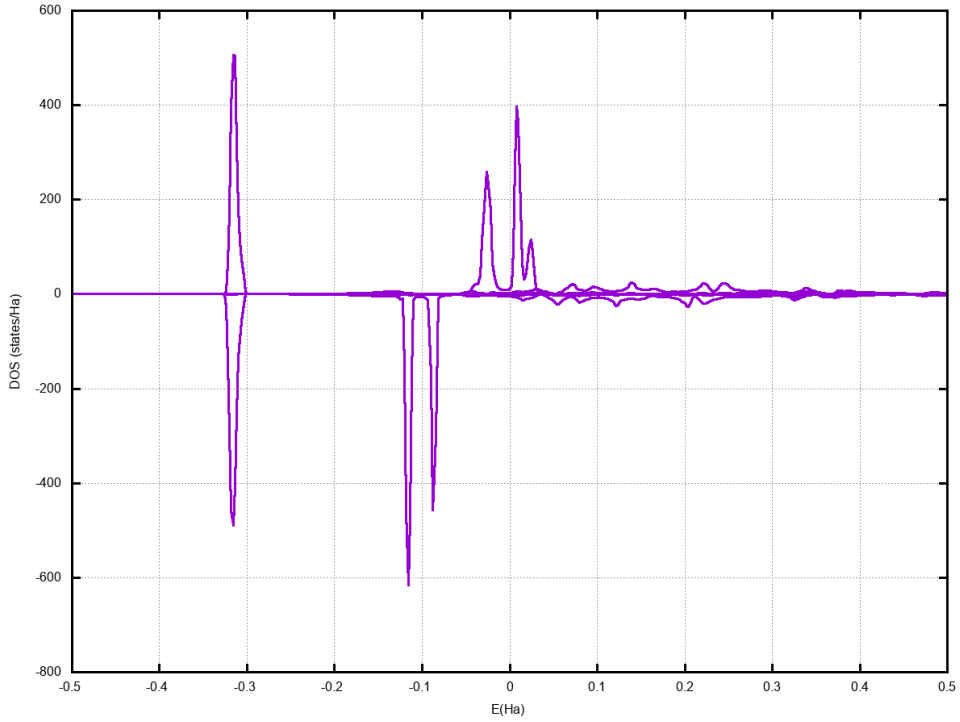

(a) HoCd Total DOS with sp

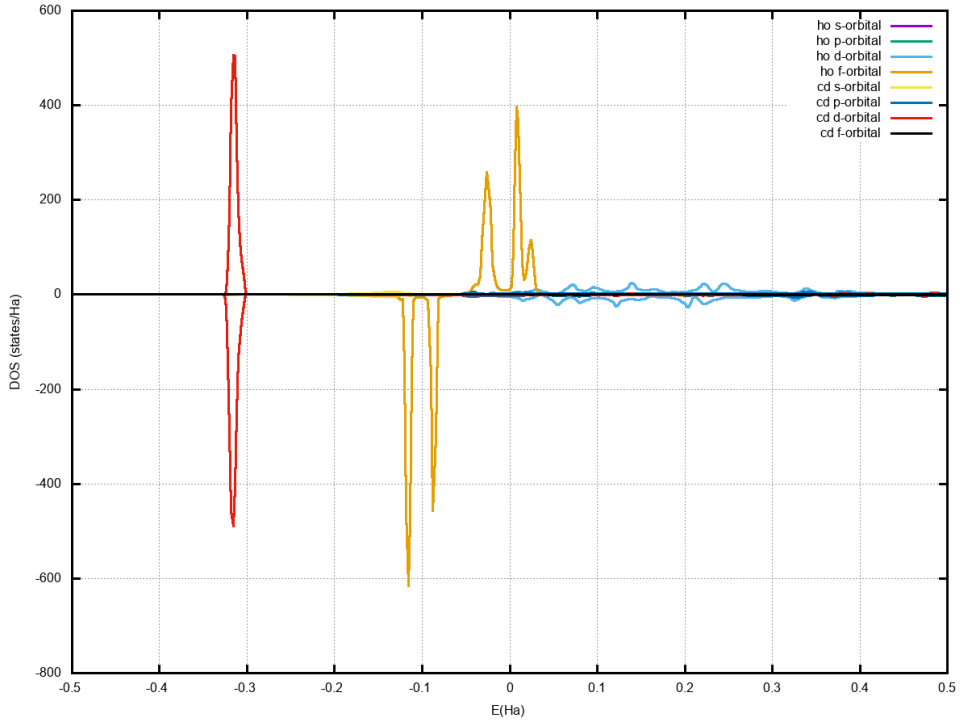

(b) HoCd Partial DOS with sp

Figure 28 – Total and Partial DOS of HoCd with spin spolarized (sp). Source: the Author.

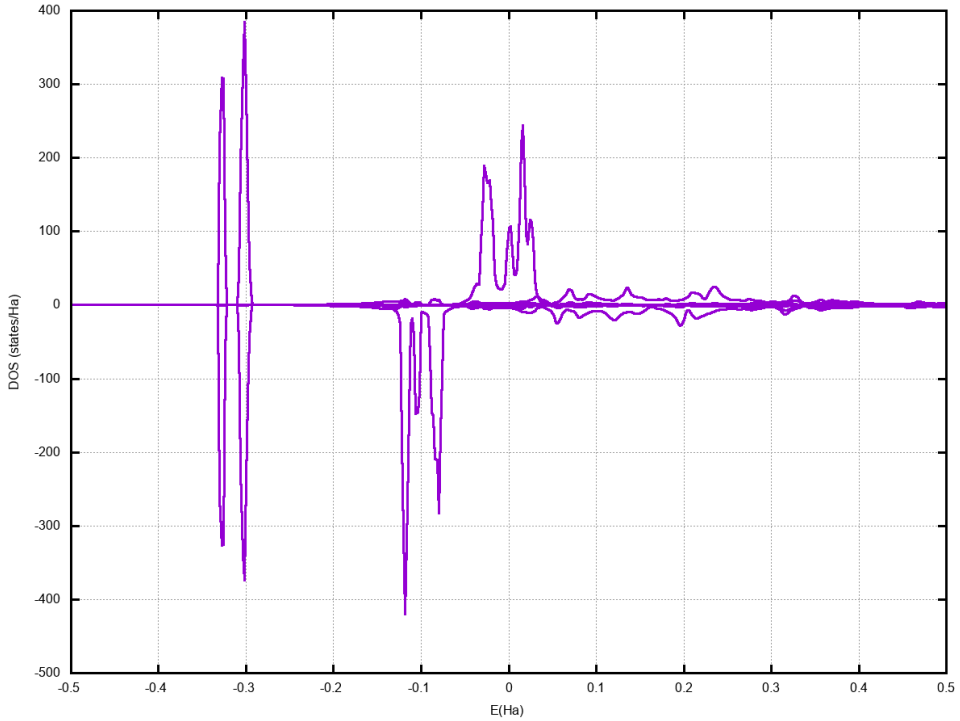

(a) HoCd Total DOS with so

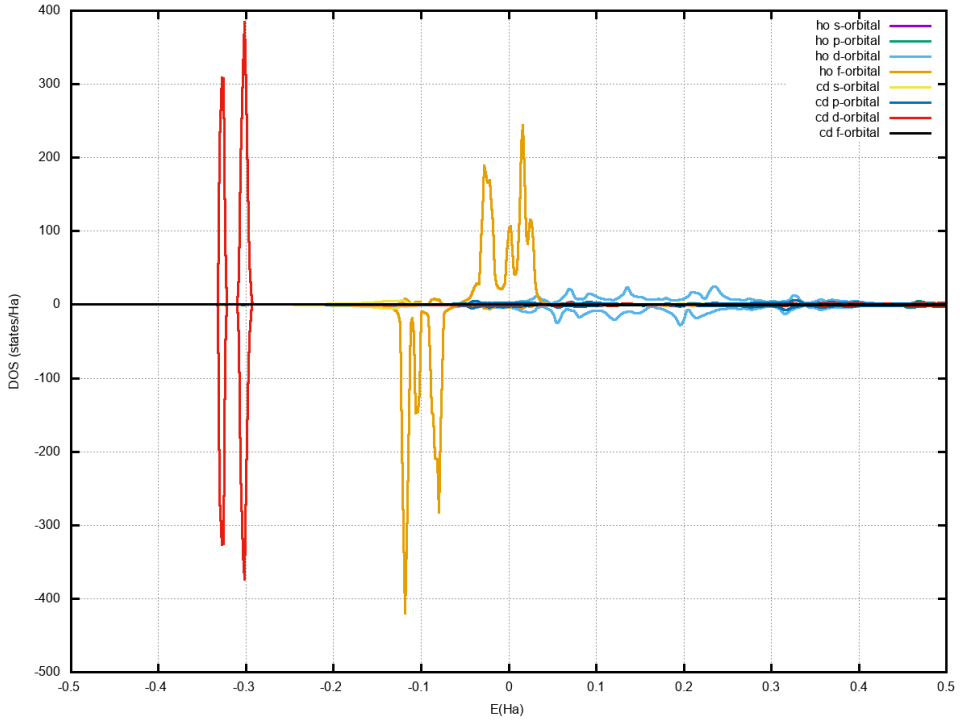

(b) HoCd Partial DOS with so

Figure 29 – Total and Partial DOS of HoCd with spin spolarized + spin orbit (so). Source: the Author.

4.3.9 ErCd

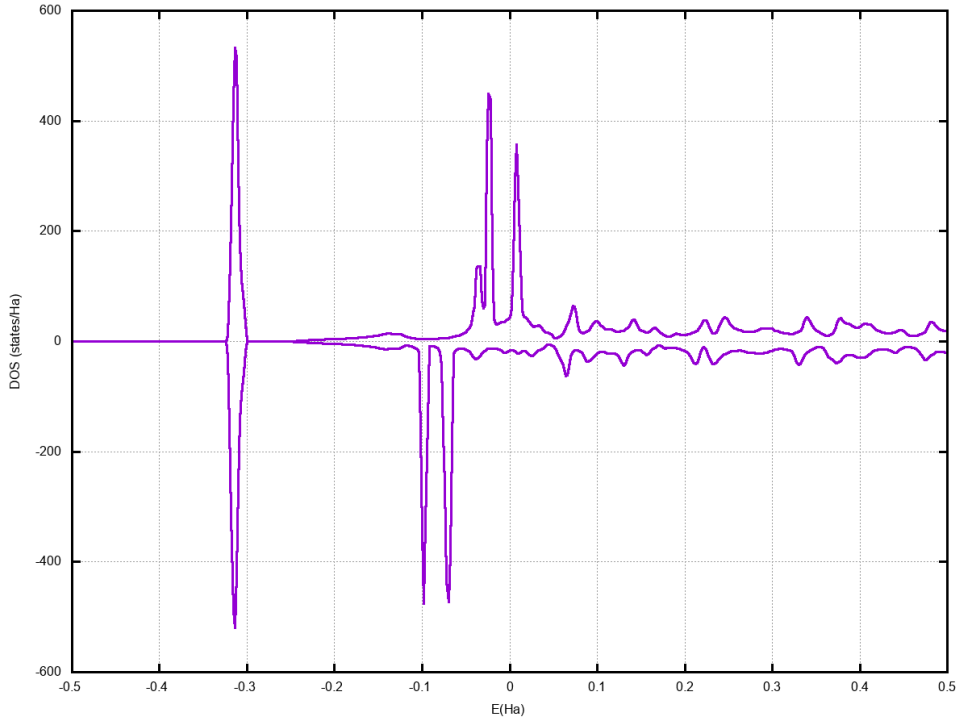

(a) ErCd Total DOS with sp

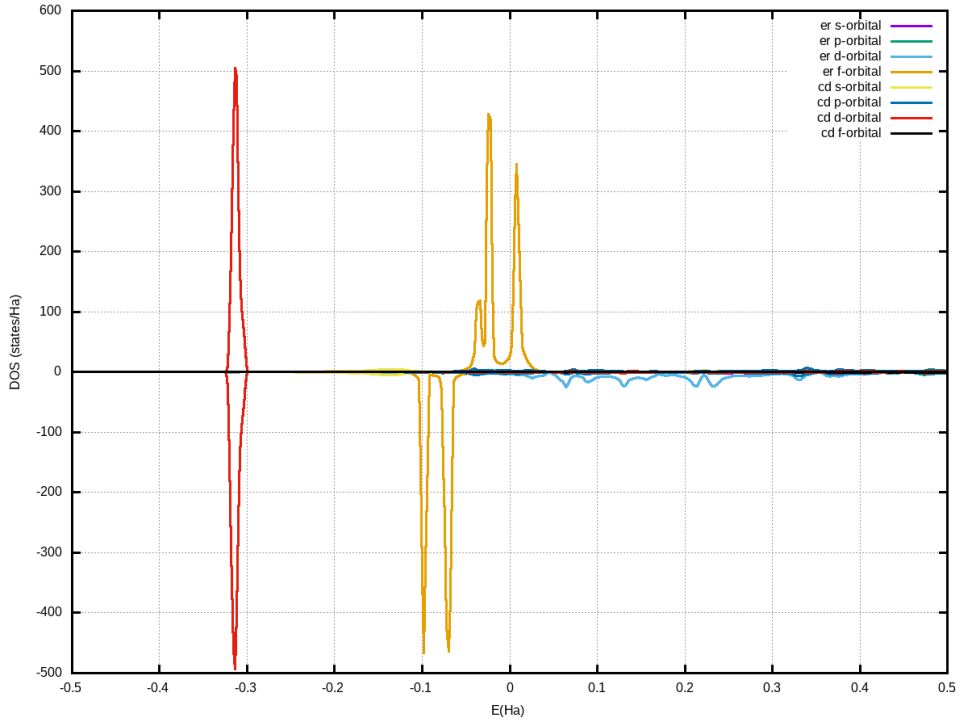

(b) ErCd Partial DOS with sp

Figure 30 – Total and Partial DOS of ErCd with spin spolarized (sp). Source: the Author.

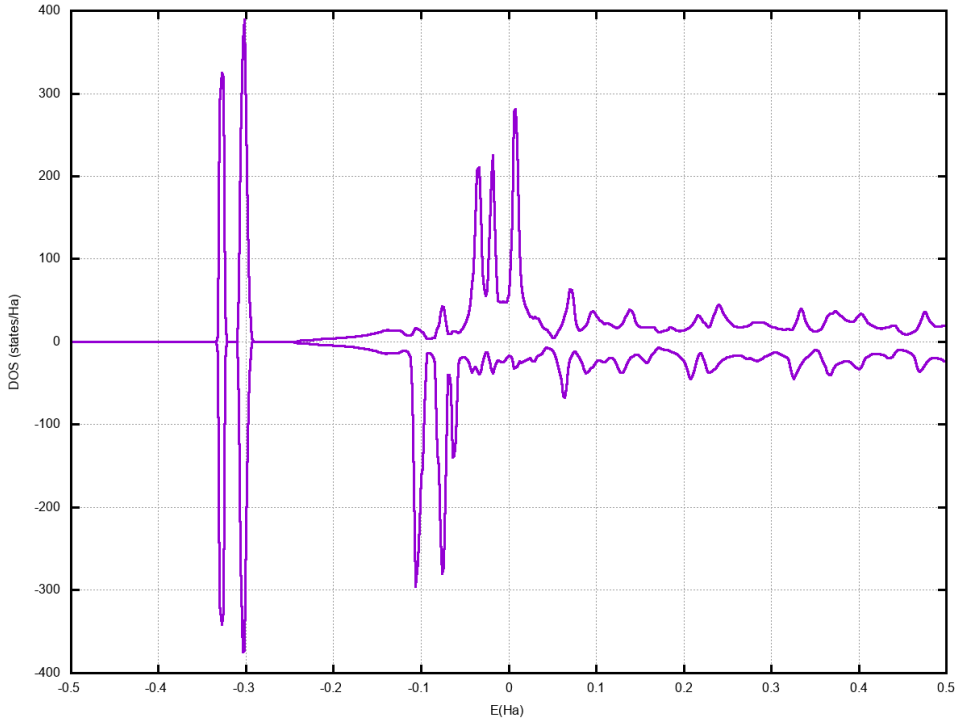

(a) ErCd Total DOS with so

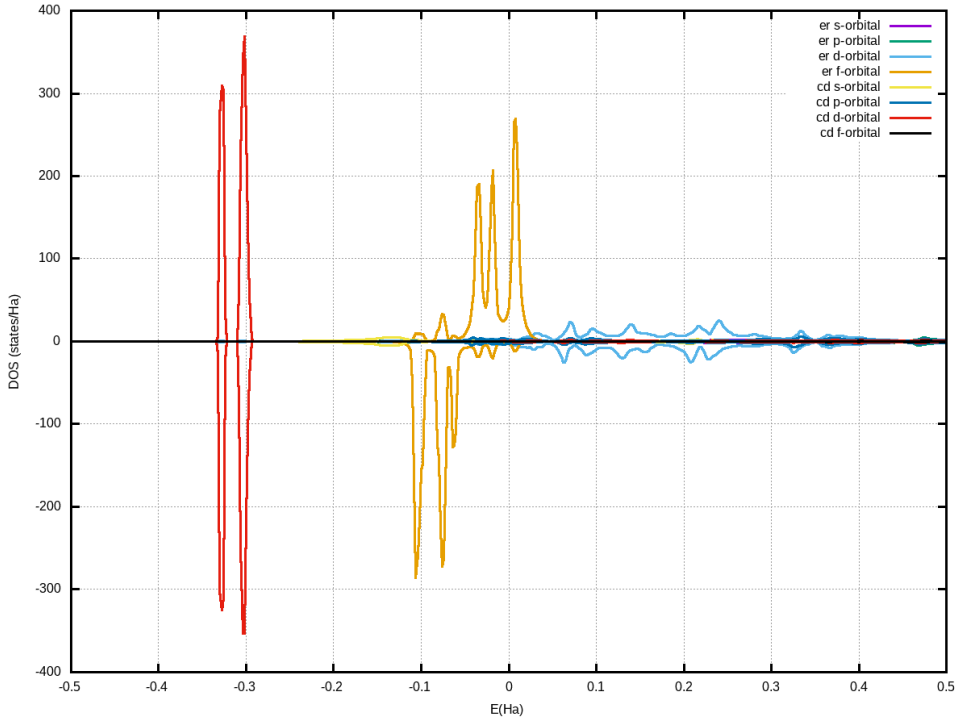

(b) ErCd Partial DOS with so

Figure 31 – Total and Partial DOS of ErCd with spin spolarized + spin orbit (so). Source: the Author.

4.3.10 EuCd

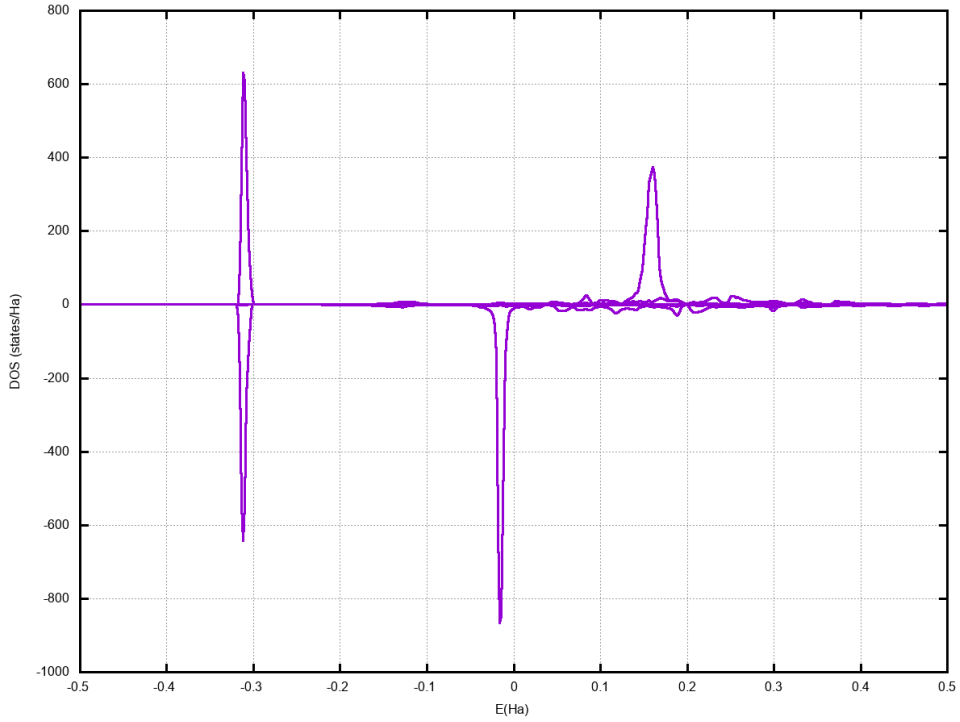

(a) EuCd Total DOS with sp

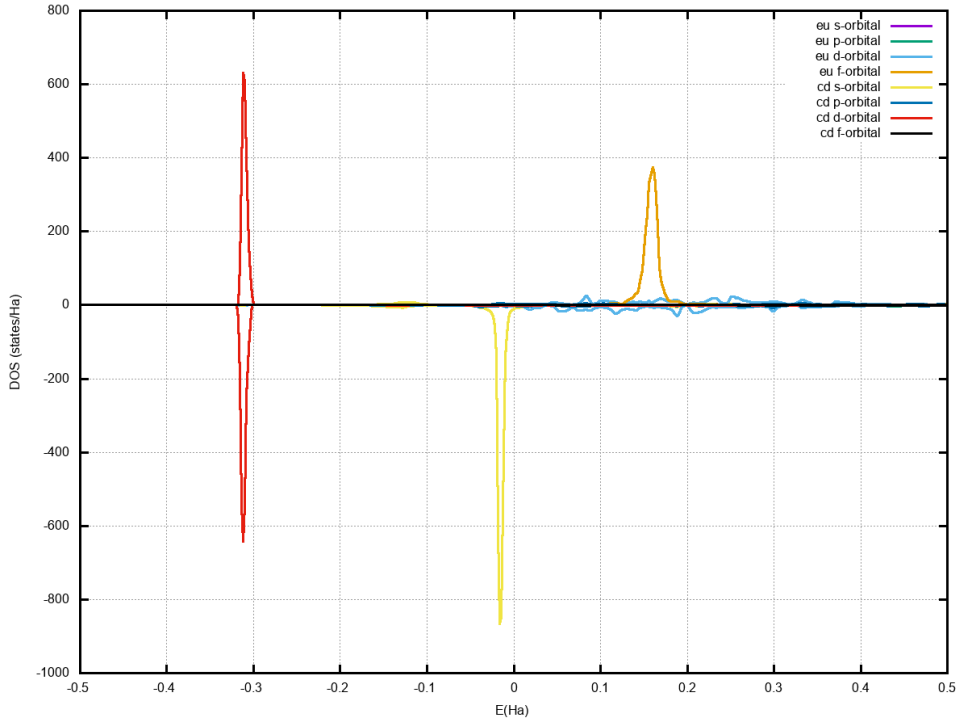

(b) EuCd Partial DOS with sp

Figure 32 – Total and Partial DOS of EuCd with spin spolarized (sp). Source: the Author.

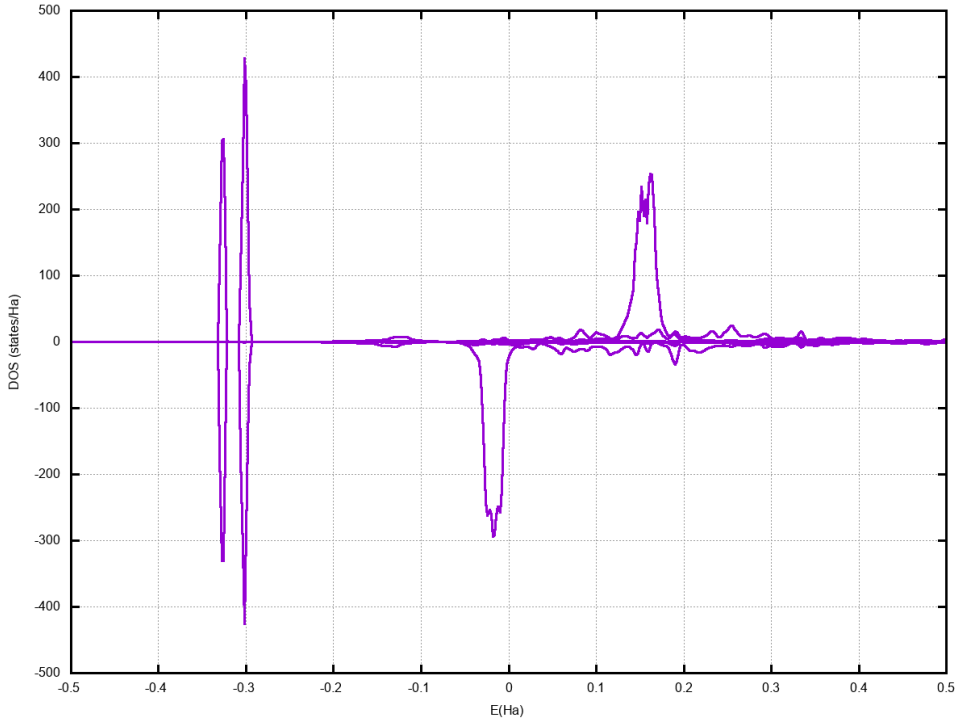

(a) EuCd Total DOS with so

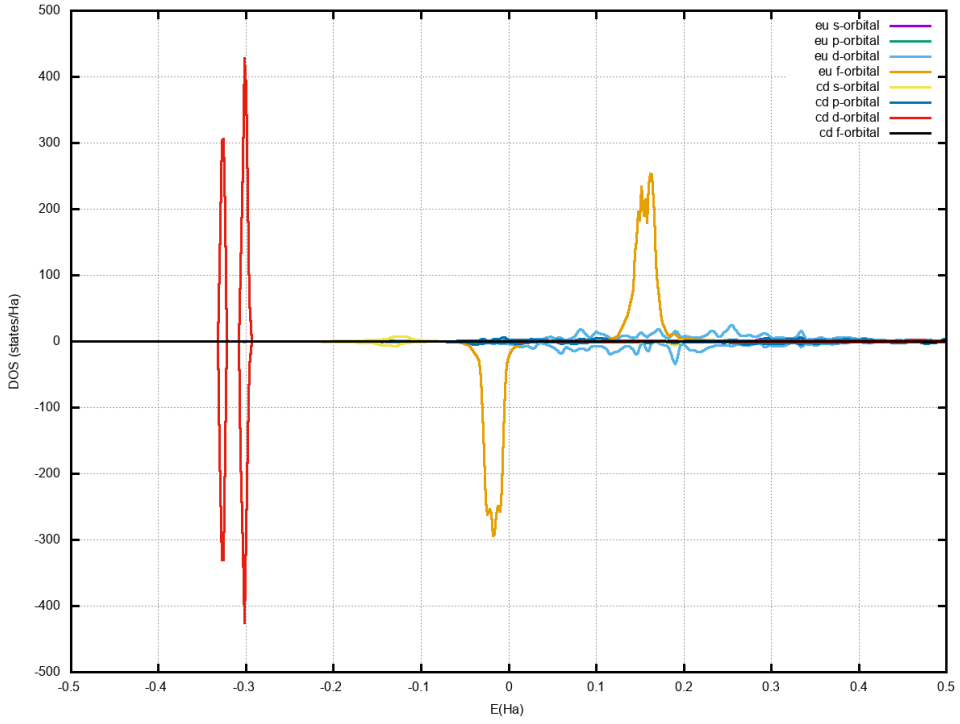

(b) EuCd Partial DOS with so

Figure 33 – Total and Partial DOS of EuCd with spin spolarized + spin orbit (so). Source: the Author.

4.3.11 TmCd

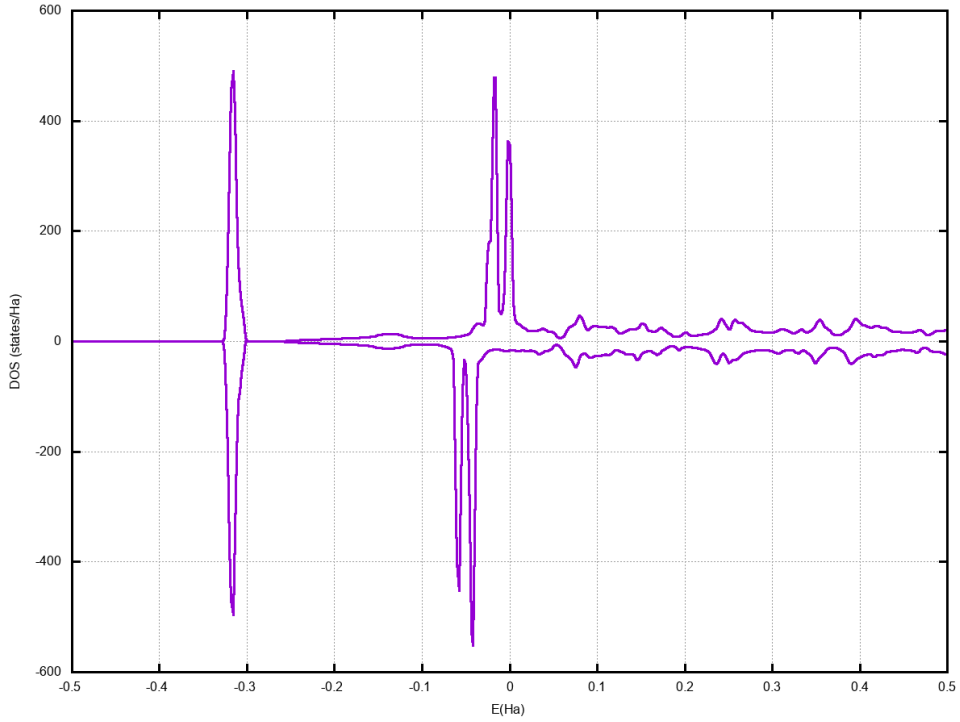

(a) TmCd Total DOS with sp

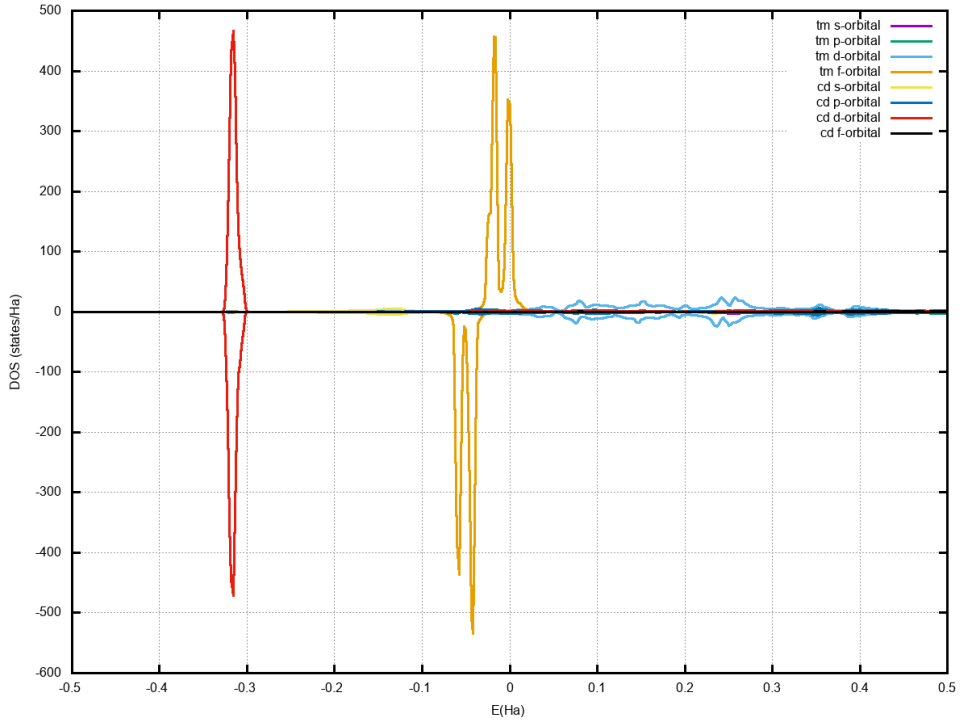

(b) TmCd Partial DOS with sp

Figure 34 – Total and Partial DOS of TmCd with spin spolarized (sp). Source: the Author.

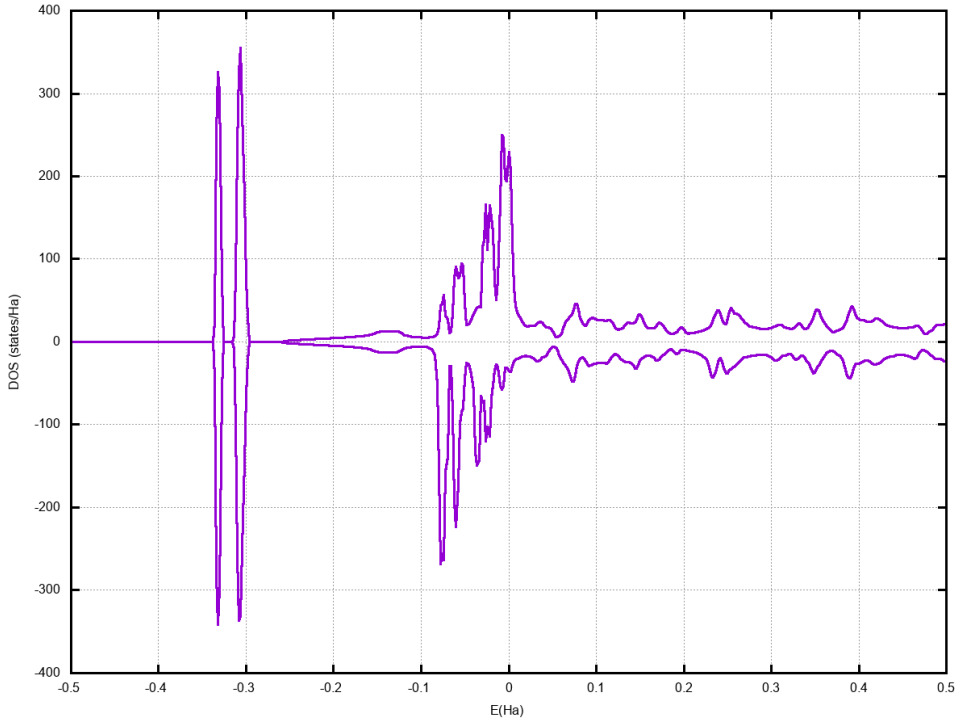

(a) TmCd Total DOS with so

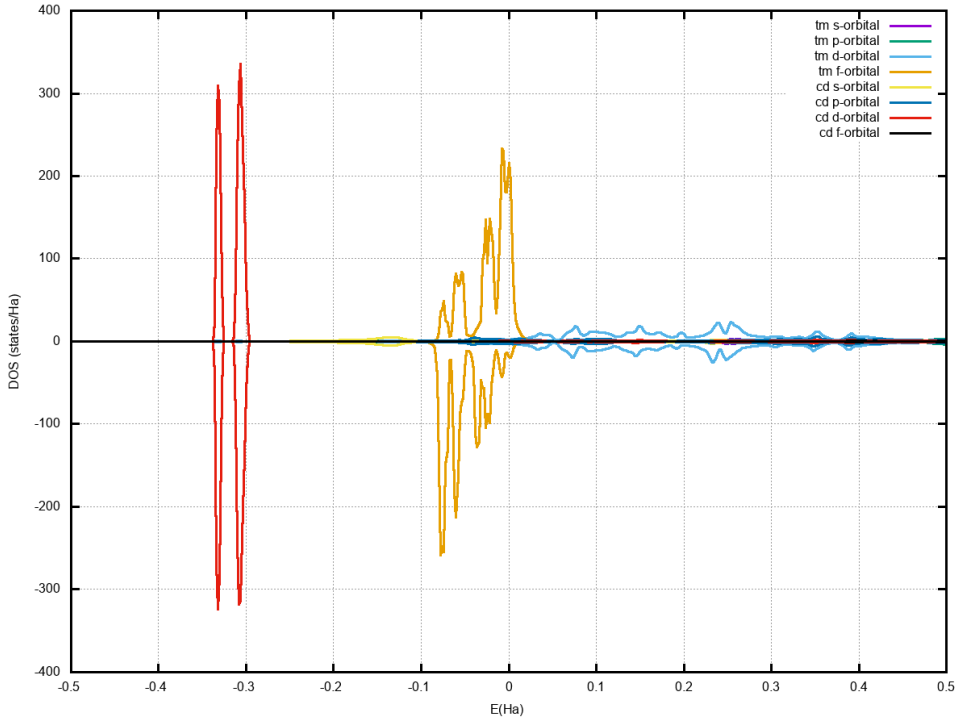

(b) TmCd Partial DOS with so

Figure 35 – Total and Partial DOS of TmCd with spin spolarized + spin orbit (so). Source: the Author.

4.3.12 YbCd

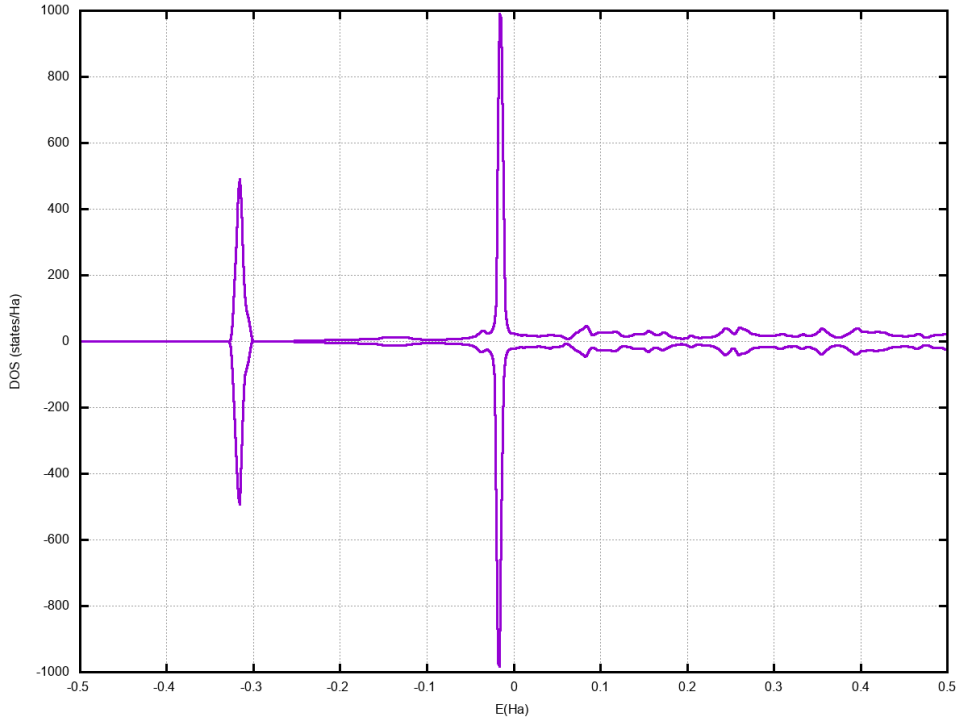

(a) YbCd Total DOS with sp

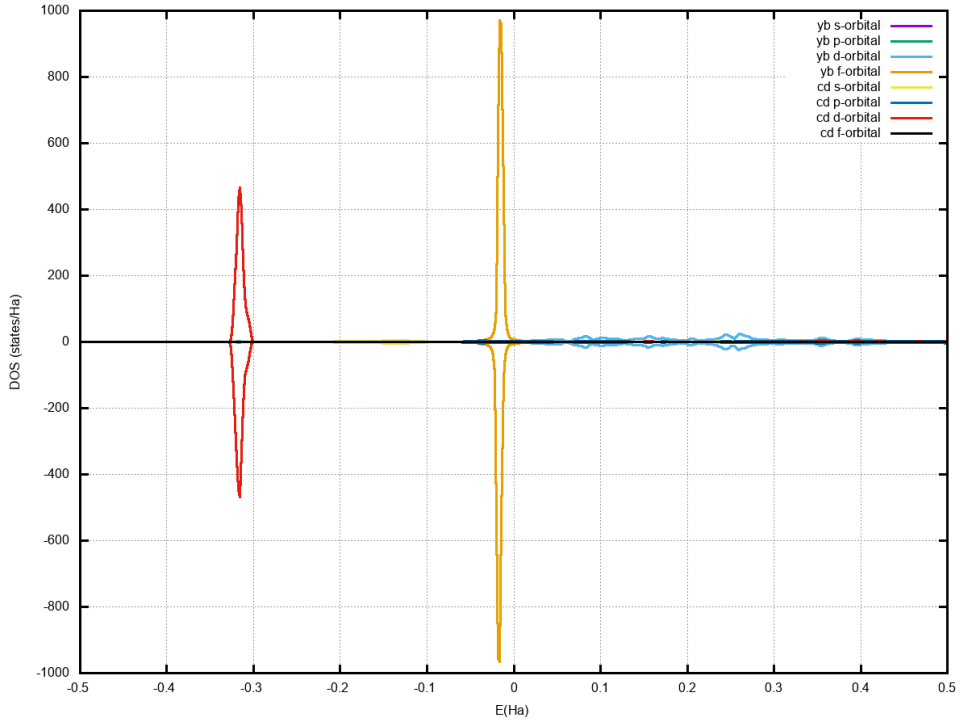

(b) YbCd Partial DOS with sp

Figure 36 – Total and Partial DOS of YbCd with spin spolarized (sp). Source: the Author.

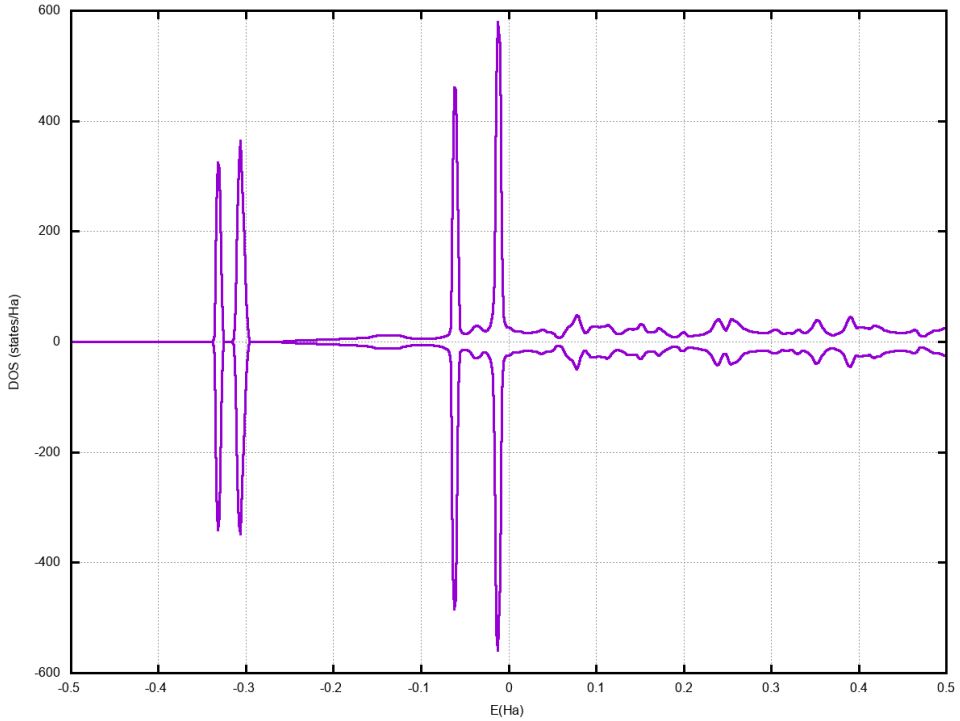

(a) YbCd Total DOS with so

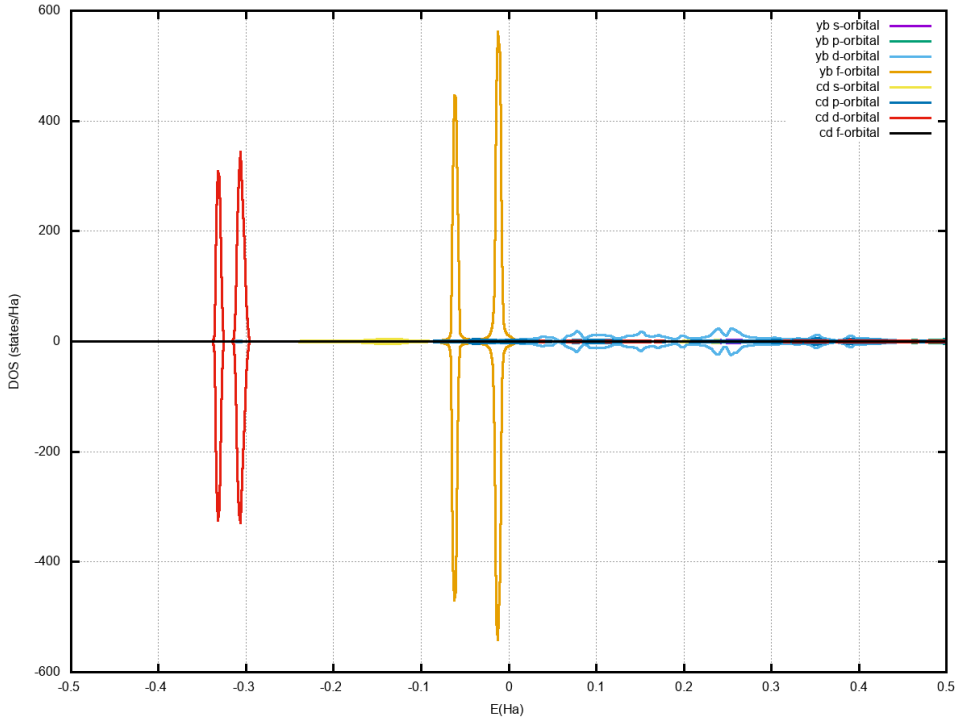

(b) YbCd Partial DOS with so

Figure 37 – Total and Partial DOS of YbCd with spin spolarized + spin orbit (so). Source: the Author.

4.4 Conclusions about the DOS

We begin this conclusion analyzing the Cd atom in all the DOS plots. In all the compounds the Cd atom has your d orbital localized around $E = -0.3Ha$ for positive spins and negative spins. With only spin polarization there is just one peak in the positive direction and one peak in the negative direction indicating that the electron's states are in majority in this energy. When we add the spin orbit coupling these two peaks unfold in four, two in a few levels below $E = -0.3$ in the positive and negative direction and another in $E = -0.3$ also in positive and negative direction.

Considering the RE atoms, some compounds showed some hybridization between the d orbital and f orbital around the Fermi level. With only spin polarization this hybridization is not so accentuated, when the spin orbit coupling is added to the calculus, both orbitals get more delocalized given more hybridizated states. The compounds which show this kind of hybridization are: CeCd with sp and so around $E = 0Ha$ for positive and negative spins, PrCd with sp and so aroun $E = 0Ha$ for negative spins and $E = 0.1Ha$ for positive spins, GdCd showed very little hybridization only with so and only for positive spins around $E = 0Ha$. NdCd also showed little hybridization for positive spins around $E = 0.1Ha$, with sp and a little more accentuated for so, SmCd followed the pattern of NdCd, the difference is that the hybridization is around $E = 0.15$ for positive spins.

TbCd, DyCd, HoCd, ErCd, EuCd, TmCd and YbCd practically shows no hybridization between the d and f orbital of the RE atom. This predominance of f states near the Fermi level for RE atoms ins which is responsible for the magnetic moments of these atoms.

5 Determination of th ane Hyperfine Magnetic Field in CeCd with DFT+U

With a more pedagogical objective we decided treat the CeCd compound using the DFT+U formalism, this compound has some peculiarities (like his only $4f$ electron) and showed a huge discrepancy between the calculated and experimental value of MHF, because this we choose it for this study.

We employ the same methodology used before but with the Orbital Polarization Method (OPM) added to treat the $4f$ shell of the Ce atom - generating a dependence of the U and J parameters in the cell's energy. It is worth mentioning that the total energies obtained with DFT + U cannot be compared to the energies achieved without the use of orbital polarization.

The correlation and exchange parameters were, respectively, $U = 0.6Ry$ and $J = 0Ry$ (with $U_{eff} = 0.6Ry$). This value of U is found in the literature, with J been 10% of U; however (as already mentioned), they depend on each calculation (here we we choose $J = 0$) and the orbital polarization is in fact a function of U_{eff} (Eq. 1.32).

Thus, we could be making some mistake associated with the use of these values in our calculations; however, it is minimized (or practically extinguished) with the fact that we compare the energies of the phases only when they are generated in exactly the same way.

The volume in the calculations within the DFT + U was also varied up to -15% (compression) to +15% (expansion) in relation to the volume obtained through the experimental lattice parameters in intervals of 1%.

We do not expect a significant change in the magnetic hyperfine field at cadmium sites because the DFT+U affect only the electronic configuration of the rare-earth ions, changing also the localized magnetic moment. [45]

5.1 Hiperfyne Magnetic Field of CeCd compound

We use the same methodology reported in the last chapter, of using all the tasks of ELK grouped. The difference of these calculus with the calculus reported in the last chapter is the use of the parameter U. For this parameter we choose arbitrarily a value of $U = 0.25Ha$ [46], we also made two set of calculus, one with only spin polarized (sp), and other with sp plus spin-orbit coupling (so) with U, in both spins configurations but with U. We show these results in the Table 5.

Table 5 – Experimental and Calculated Value of Magnetic Hyperfine Field at Cadmium atom in CeCd compound.

Compound	B_{hf}(T)sp(ELK)	B_{hf}(T)so(ELK)	B_{hf}(T)(WIEN2k)[13]	B_{hf}(T)(Exp.)[13]
CeCd	-14.25	-13.68	-5.75	5.10
CeCd + U	-7.58	-6.94	–	–

Without U the value of the B_{hf} field not agree with the experimental value, there is some discussion regarding the cubic structure used in this work for CeCd. Fujiware et. al. [47] argues that CeCd has a phase transition, considering it a hexagonal and not a cubic, but in this work they do not did any x-ray measurements only magnetization to claim this phase transition but this could be the reason that our values disagree so much from experimental. When we use the U parameter our values are much better, U contributes to make the $4f$ unique electron in Ce to be more located rising the field value, some more investigations for another U values and hexagonal structure could help improve this agreement between theory and experiment.

5.2 Density of States of CeCd

Like we did in our last chapter, we also plot the DOS for CeCd, with U and sp and with U and so. These graphs are shown in Figure **??**.

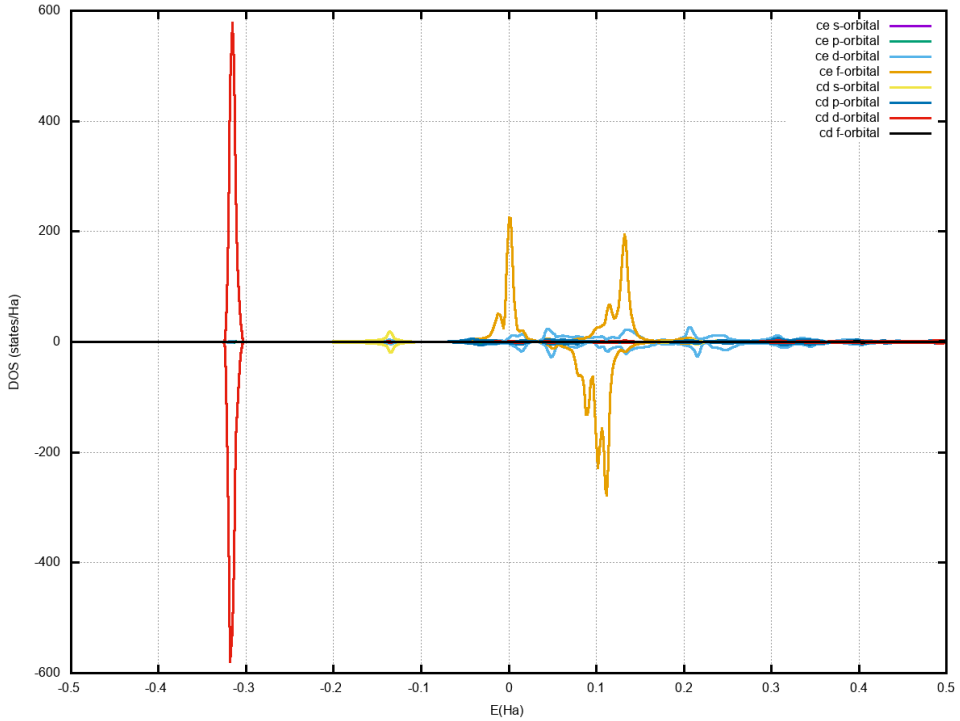

(a) CeCd DOS with sp + U

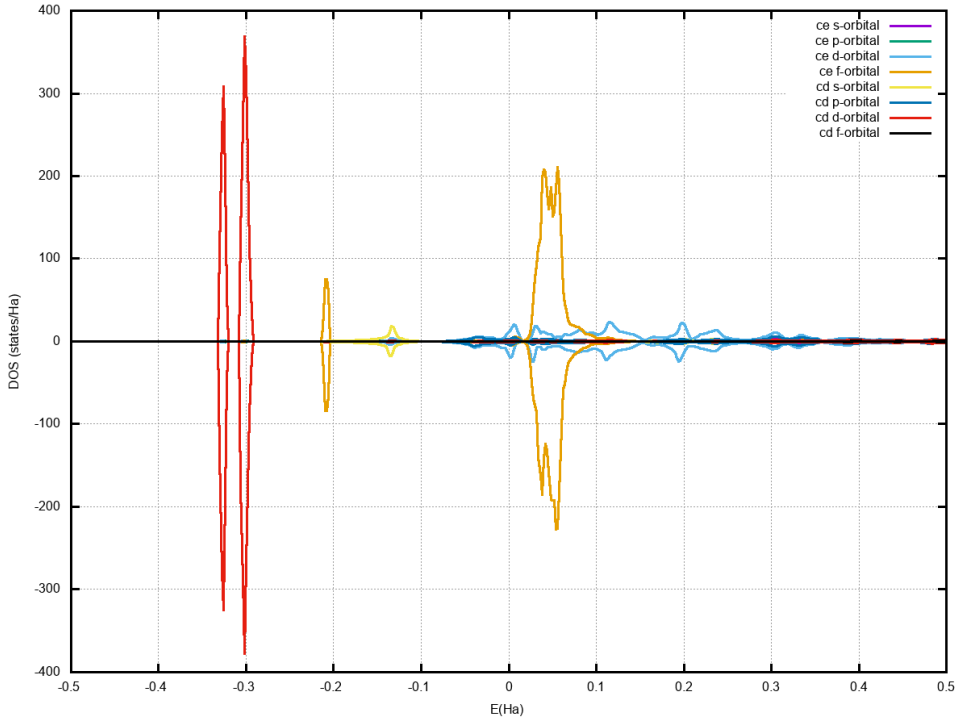

(b) CeCd DOS with so + U

Figure 38 – Partial DOS of CeCd with spin polarized and spin orbit coupling plus U parameter. Source: the Author.

It is possible to see with these DOS plots that the U parameter affects much more the f orbital of Cerium, agreeing with what we said earlier, that the only $4f$ electron will be more localized with this, making our calculations more close to the experimental situation.

Here it is worth to mention that the DFT+U do not represent very well the Kohn-Sham wave functions at the core, because it is consider the self-interaction in these states which is not a physical effect, this is responsible for some failures in represent magnetic systems.

Conclusion

In conclusion, we have studied the hyperfine interaction in the RECd compounds. We have verified the performance of FP-LAPW ELK code and calculated the values of the Magnetic Hyperfine Field (see Table 1.4) in two configurations of spin to test our methodology, as well as the code itself. We have also produced results for the hyperfine magnetic field in YbCd which emphasizes the originality of this work. Experimentally these values are hard to obtain, as the sample preparation influences the results [13]. The ELK code in its current version does not separate the contributions for the hyperfine field, which may explain the discrepancy between our calculated values and the values from Cavalcante *et al.* We have also proposed a methodology inspired by WIEN2k, from the parameter optimization to the calculation of physical quantities.

Since ELK is a free and open source code with more than 80 tasks, it could be a good choice to start in the field of first principles calculations. The down side of the code is the lack of detailed information about it, its manual is not very detailed, so this work intends to change the situation and, thus, attract more attention to the code. Regarding its user friendly philosophy (which indeed it sticks to), a lot of its functionalities are hidden from the user which forces the user to look straight into the source code. It could be a difficult task for the user, but, on the up side there is a possibility to change the code if it is needed making it more suitable for the user's needs.

Considering our results, we observed that the use of spin orbit coupling improves our results indicating that this effect is important in the compounds studied, a treatment with full Dirac's equation may be the right formalism to study the magnetism in rare earth compounds. Our density of states showed hybridization of the orbitals d and f in the rare earth atoms in some compound that remains in agreement with the findings of Fujii *et al.* and indicates that Campbell's model has a certain role in the description of these effects. We also showed that the formalism of DFT+U even with the ad hoc potential term improves our results for CeCd, so the use of this methodology may be necessary to study the magnetism in the rest of the series.

We would also like to conclude emphasizing the originality of this work regarding the use of the FP-LAPW ELK code (to our knowledge, there are no other work developed in Brazil using this code), as well as the difficulty of studying the magnetism in RECd compounds, a field causing a lot of debate for at least forty years. We hope that this work sheds some light to some aspects in the field and becomes inspirational for the new research, both experimental and theoretical, in all the series of RECd compounds.

Bibliography

[1] John Seaman. *Rare Earths and Clean Energy: Analyzing China's Upper Hand*. Gouvernance européenne et géopolitique de l'énergie, 2010.

[2] Fabio Cavalcante et al. "A method to determine contributions to the hyperfine field at Ce probes in magnetic hosts: Application to Ce impurities at RE sites in REAg (RE = Gd, Tb, Dy, Ho) compounds". In: *Journal of Alloys and Compounds* 660 (Dec. 2015). DOI: 10.1016/j.jallcom.2015.11.081.

[3] G. Schatz and A. Weidinger. *Nuclear Condensed Matter Physics: Nuclear Methods and Applications*. Willey US, 1996.

[4] A. P. Guimarães. *Magnetism and Magnetic Resonance in Solids*. Willey US, 1998.

[5] Elton N. Kaufmann and Reiner J. Vianden. "The electric field gradient in noncubic metals". In: *Rev. Mod. Phys.* 51 (1 Jan. 1979), pp. 161–214. DOI: 10.1103/RevModPhys.51.161. URL: https://link.aps.org/doi/10.1103/RevModPhys.51.161.

[6] R. O. Jones. "Density functional theory: Its origins, rise to prominence, and future". In: *Rev. Mod. Phys.* 87 (3 Aug. 2015), pp. 897–923. DOI: 10.1103/RevModPhys.87.897. URL: https://link.aps.org/doi/10.1103/RevModPhys.87.897.

[7] P Blaha, Karlheinz Schwarz, and P Herzig. "First-Principles Calculation of the Electric Field Gradient of Li 3 N". In: *Physical review letters* 54 (Apr. 1985), pp. 1192–1195. DOI: 10.1103/PhysRevLett.54.1192.

[8] D. J. Singh and L. Nordstrom. *Planewaves, Pseudopotentials and the LAPW Method*. Springer-Verlag US, 2006. DOI: 10.1007/978-0-387-29684-5.

[9] D. Richard et al. "*Abinitio* LSDA and LSDA + U study of pure and Cd-doped cubic lanthanide sesquioxides". In: *Phys. Rev. B* 88 (16 Oct. 2013), p. 165206. DOI: 10.1103/PhysRevB.88.165206. URL: https://link.aps.org/doi/10.1103/PhysRevB.88.165206.

[10] L. A. Errico et al. "Anisotropic Relaxations Introduced by Cd Impurities in Rutile $\mathbf{TiO_2}$: First-PrinciplesCalculations and Experimental Support". In: *Phys. Rev. Lett.* 89 (5 July 2002), p. 055503. DOI: 10.1103/PhysRevLett.89.055503. URL: https://link.aps.org/doi/10.1103/PhysRevLett.89.055503.

[11] M. V. Lali ć et al. "First-principles calculations of hyperfine fields in the $CeIn_3$ intermetallic compound". In: *Phys. Rev. B* 65 (5 Dec. 2001), p. 054405. DOI: 10.1103/PhysRevB.65.054405. URL: https://link.aps.org/doi/10.1103/PhysRevB.65.054405.

[12] C. Sena et al. “Charge distribution and hyperfine interactions in the vicinity of impurity sites in In2O3 doped with Fe, Co, and Ni”. In: *Journal of Magnetism and Magnetic Materials* 387 (2015), pp. 165–178. ISSN: 0304-8853. DOI: https://doi.org/10.1016/j.jmmm.2015.03.092. URL: http://www.sciencedirect.com/science/article/pii/S0304885315003479.

[13] F. H. M. Cavalcante et al. “Magnetic hyperfine interactions on Cd sites of the rare-earth cadmium compounds RCd (R = Ce, Pr, Nd, Sm, Gd, Tb, Dy, Ho, and Er)”. In: *Phys. Rev. B* 94 (6 Aug. 2016), p. 064417. DOI: 10.1103/PhysRevB.94.064417. URL: https://link.aps.org/doi/10.1103/PhysRevB.94.064417.

[14] J. K. Dewhurst et al. *ELK FP-LAPW code*. 2017. URL: http://elk.sourceforge.net/ (visited on 07/30/2017).

[15] P. Blaha et al. “Calculations of electric field gradients in solids: How theory can complement experiment”. In: *Hyperfine Interactions* 126.1 (July 2000), pp. 389–395. ISSN: 1572-9540. DOI: 10.1023/A:1012614510955. URL: https://doi.org/10.1023/A:1012614510955.

[16] Pavel Novak et al. “Self-interaction correction and contact hyperfine field”. In: *Phys. Rev. B* 67 (Apr. 2003). DOI: 10.1103/PhysRevB.67.140403.

[17] P. Novák and V. Chlan. “Contact hyperfine field at Fe nuclei from density functional calculations”. In: *Phys. Rev. B* 81 (17 May 2010), p. 174412. DOI: 10.1103/PhysRevB.81.174412. URL: https://link.aps.org/doi/10.1103/PhysRevB.81.174412.

[18] S. Blügel et al. “Hyperfine fields of 3d and 4d impurities in nickel”. In: *Phys. Rev. B* 35 (7 Mar. 1987), pp. 3271–3283. DOI: 10.1103/PhysRevB.35.3271. URL: https://link.aps.org/doi/10.1103/PhysRevB.35.3271.

[19] P. A. M. Dirac and R. H. Fowler. “Quantum mechanics of many-electron systems”. In: *Proc. R. Soc. Lond. A* 123 (792 Apr. 1929). DOI: https://doi.org/10.1098/rspa.1929.0094. URL: https://royalsocietypublishing.org/doi/abs/10.1098/rspa.1929.0094.

[20] P. Hohenberg and W. Kohn. “Inhomogeneous Electron Gas”. In: *Phys. Rev.* 136 (3B Nov. 1964), B864–B871. DOI: 10.1103/PhysRev.136.B864. URL: https://link.aps.org/doi/10.1103/PhysRev.136.B864.

[21] W. Kohn and L. J. Sham. “Self-Consistent Equations Including Exchange and Correlation Effects”. In: *Phys. Rev.* 140 (4A Nov. 1965), A1133–A1138. DOI: 10.1103/PhysRev.140.A1133. URL: https://link.aps.org/doi/10.1103/PhysRev.140.A1133.

[22] Asier Eiguren and Claudia Ambrosch-Draxl. "Spin polarization and relativistic electronic structure of the 11 H/W(110) surface". In: *New Journal of Physics* 11.1 (Jan. 2009), p. 013056. DOI: 10.1088/1367-2630/11/1/013056. URL: https://doi.org/10.1088%2F1367-2630%2F11%2F1%2F013056.

[23] Jeffrey C. Grossman, Lubos Mitas, and Krishnan Raghavachari. "Structure and Stability of Molecular Carbon: Importance of Electron Correlation". In: *Phys. Rev. Lett.* 75 (21 Nov. 1995), pp. 3870–3873. DOI: 10.1103/PhysRevLett.75.3870. URL: https://link.aps.org/doi/10.1103/PhysRevLett.75.3870.

[24] W. Kohn, A. D. Becke, and R. G. Parr. "Density Functional Theory of Electronic Structure". In: *The Journal of Physical Chemistry* 100.31 (1996), pp. 12974–12980. DOI: 10.1021/jp9606691. eprint: https://doi.org/10.1021/jp9606691. URL: https://doi.org/10.1021/jp9606691.

[25] Axel D. Becke. "Density-functional thermochemistry. V. Systematic optimization of exchange-correlation functionals". In: *The Journal of Chemical Physics* 107.20 (1997), pp. 8554–8560. DOI: 10.1063/1.475007. eprint: https://doi.org/10.1063/1.475007. URL: https://doi.org/10.1063/1.475007.

[26] Bjørk Hammer et al. "Multidimensional Potential Energy Surface for H_2 Dissociation over Cu(111)". In: *Phys. Rev. Lett.* 73 (10 Sept. 1994), pp. 1400–1403. DOI: 10.1103/PhysRevLett.73.1400. URL: https://link.aps.org/doi/10.1103/PhysRevLett.73.1400.

[27] J. C. Slater. "Wave Functions in a Periodic Potential". In: *Phys. Rev.* 51 (10 May 1937), pp. 846–851. DOI: 10.1103/PhysRev.51.846. URL: https://link.aps.org/doi/10.1103/PhysRev.51.846.

[28] S. Cottenier. *Density Functional Theory and the family of (L)APW-methods. A Step-by-Step Introduction*. Institut voor Kern-en Stralingsfysica, 2002. URL: http://www.wien2k.at/reg_user/textbooks.

[29] O. Krogh Andersen. "Linear methods in band theory". In: *Phys. Rev. B* 12 (8 Oct. 1975), pp. 3060–3083. DOI: 10.1103/PhysRevB.12.3060. URL: https://link.aps.org/doi/10.1103/PhysRevB.12.3060.

[30] Vladimir I. Anisimov, Jan Zaanen, and Ole K. Andersen. "Band theory and Mott insulators: Hubbard U instead of Stoner I". In: *Phys. Rev. B* 44 (3 July 1991), pp. 943–954. DOI: 10.1103/PhysRevB.44.943. URL: https://link.aps.org/doi/10.1103/PhysRevB.44.943.

[31] V. I. Anisimov et al. "Density-functional theory and NiO photoemission spectra". In: *Phys. Rev. B* 48 (23 Dec. 1993), pp. 16929–16934. DOI: 10.1103/PhysRevB.48.16929. URL: https://link.aps.org/doi/10.1103/PhysRevB.48.16929.

[32] M. T. Czy żyk and G. A. Sawatzky. "Local-density functional and on-site correlations: The electronic structure of La_2CuO_4 and $LaCuO_3$". In: *Phys. Rev. B* 49 (20 May 1994), pp. 14211–14228. DOI: 10.1103/PhysRevB.49.14211. URL: https://link.aps.org/doi/10.1103/PhysRevB.49.14211.

[33] G. Rollmann et al. "First-principles calculation of the structure and magnetic phases of hematite". In: *Phys. Rev. B* 69 (16 Apr. 2004), p. 165107. DOI: 10.1103/PhysRevB.69.165107. URL: https://link.aps.org/doi/10.1103/PhysRevB.69.165107.

[34] H. Fujii et al. "Magnetic properties of CeCd and NdCd single crystals". In: *Journal of Magnetism and Magnetic Materials* 52.1 (1985), pp. 428–430. ISSN: 0304-8853. DOI: https://doi.org/10.1016/0304-8853(85)90323-3. URL: http://www.sciencedirect.com/science/article/pii/0304885385903233.

[35] K. H. J. Buschow. "Magnetic properties of CsCl-type rare-earth cadmium compounds". In: *The Journal of Chemical Physics* 61.11 (1974), pp. 4666–4670. DOI: 10.1063/1.1681788. eprint: https://doi.org/10.1063/1.1681788. URL: https://doi.org/10.1063/1.1681788.

[36] M. A. Ruderman and C. Kittel. "Indirect Exchange Coupling of Nuclear Magnetic Moments by Conduction Electrons". In: *Phys. Rev.* 96 (1 Oct. 1954), pp. 99–102. DOI: 10.1103/PhysRev.96.99. URL: https://link.aps.org/doi/10.1103/PhysRev.96.99.

[37] I A Campbell. "Indirect exchange for rare earths in metals". In: *Journal of Physics F: Metal Physics* 2.3 (May 1972), pp. L47–L50. DOI: 10.1088/0305-4608/2/3/004. URL: https://doi.org/10.1088%2F0305-4608%2F2%2F3%2F004.

[38] Jianping Long. "First-principles investigations of the physical properties of RCd (R=Ce, La, Pr, Nd)". In: *Physica B: Condensed Matter* 407.24 (2012), pp. 4831–4836. ISSN: 0921-4526. DOI: https://doi.org/10.1016/j.physb.2012.09.022. URL: http://www.sciencedirect.com/science/article/pii/S0921452612008782.

[39] Per Söderlind et al. "Ground-state properties of rare-earth metals: an evaluation of density-functional theory". In: *Journal of Physics: Condensed Matter* 26.41 (Sept. 2014), p. 416001. DOI: 10.1088/0953-8984/26/41/416001. URL: https://doi.org/10.1088%2F0953-8984%2F26%2F41%2F416001.

[40] D H Ryan et al. "170Yb Mössbauer study of the YbCd5.7binary quasi-crystal and related phases". In: *Journal of Physics: Condensed Matter* 13.45 (Oct. 2001), pp. 10159–10163. DOI: 10.1088/0953-8984/13/45/304. URL: https://doi.org/10.1088%2F0953-8984%2F13%2F45%2F304.

[41] K Buschow. "Intermetallic compounds of rare earths and non-magnetic metals". In: *Reports on Progress in Physics* 42.8 (Aug. 1979), pp. 1373–1477. DOI: 10.1088/0034-4885/42/8/003. URL: https://doi.org/10.1088%2F0034-4885%2F42%2F8%2F003.

[42] Jens Jensen and Allan R. Mackintosh. *Rare Earth Magnetism - Structures and Excitations*. Clarendon Press, 1991.

[43] John P. Perdew, Kieron Burke, and Matthias Ernzerhof. "Generalized Gradient Approximation Made Simple". In: *Phys. Rev. Lett.* 77 (18 Oct. 1996), pp. 3865–3868. DOI: 10.1103/PhysRevLett.77.3865. URL: https://link.aps.org/doi/10.1103/PhysRevLett.77.3865.

[44] S.K. Mohanta et al. "First-principles calculation of the electric field gradient and magnetic hyperfine field in rare-earth metals (Gd to Lu) and dilute alloys with Cd". In: *Solid State Communications* 150.37 (2010), pp. 1789–1793. ISSN: 0038-1098. DOI: https://doi.org/10.1016/j.ssc.2010.07.012. URL: http://www.sciencedirect.com/science/article/pii/S003810981000414X.

[45] Juarez L. F. Da Silva et al. "Hybrid functionals applied to rare-earth oxides: The example of ceria". In: *Phys. Rev. B* 75 (4 Jan. 2007), p. 045121. DOI: 10.1103/PhysRevB.75.045121. URL: https://link.aps.org/doi/10.1103/PhysRevB.75.045121.

[46] J. Filho et al. "The Ce electronic ground state in CeMn 2Ge 2 determined by 140Ce PAC spectroscopy and electronic structure calculations". In: *Physica B-condensed Matter - PHYSICA B* 389 (Feb. 2007), pp. 73–76. DOI: 10.1016/j.physb.2006.07.027.

[47] Hideoki Kadomatsu et al. "Magnetic and structural phase transition of CeCd at hydrostatic pressure". In: *Physics Letters A* 94.3 (1983), pp. 178–180. ISSN: 0375-9601. DOI: https://doi.org/10.1016/0375-9601(83)90377-8. URL: http://www.sciencedirect.com/science/article/pii/0375960183903778.

[48] M. Born and R. Oppenheimer. "Zur Quantentheorie der Molekeln". In: *Annalen der Physik* 389.20 (1927), pp. 457–484. DOI: 10.1002/andp.19273892002. eprint: https://onlinelibrary.wiley.com/doi/pdf/10.1002/andp.19273892002. URL: https://onlinelibrary.wiley.com/doi/abs/10.1002/andp.19273892002.

APPENDIX A – Born-Oppenheimer Approximation

A first approximation that we will use to simplify the Hamiltonian (1.2), is the Born - Oppenheimer approximation [48]. The nuclei have the mass of the order of 1000 times bigger than the electrons, they move in a much slower way and then we can consider them "frozen". That is, the electrons now will be considered moving under a potential generated by the frozen nuclei. This make the term in our Hamiltonian responsible for the nuclei kinetic energy to be zero and the potential of nucleus-nucleus interaction be static, reducing it to a constant, hence our Hamiltonian is now written as follows:

$$\hat{H}_{ele} = -\frac{\hbar^2}{2}\sum_i \frac{\nabla^2_{\vec{r_i}}}{m_e} - \frac{1}{4\pi\epsilon_0}\sum_{i,j}\frac{e^2 Z_i}{|\vec{R_i} - \vec{r_j}|} + \frac{1}{8\pi\epsilon_0}\sum_{i\neq j}\frac{e^2}{|\vec{r_i} - \vec{r_j}|} \tag{A.1}$$

where $\hat{H}_{ele}$ means Electronic Hamiltonian.

APPENDIX B – Proofs of the Hohenberg-Kohn's Theorems

In this appendix we prove the two Hohenberg-Kohn's theorems which form the base of DFT. These proofs follow the proofs shown in [Springborg].

Before we start the proof, let's make some preliminary considerations. We consider a system of N electrons that move in some external potential. For the system of interest the external potential is that of the nuclei. We do not know this potential in advance. We assume that we have measured some electron density in an experiment, but we do not know what system it belongs to. However, we will assume that it is the density of the ground state.

We know N since

$$N = \int \rho(\vec{r}) d\vec{r} \tag{B.1}$$

We can then specify the kinetic-energy part of the total N-electron Hamilton operator. Since we have N electrons, it must be

$$\sum_{i=1}^{N} -\frac{1}{2}\nabla_{\vec{r}_i}^2 \tag{B.2}$$

In addition, that part of Hammilton operator that originates from the electron-electron interactions is

$$\sum_{i>j=1}^{N} \frac{1}{|\vec{r}_i - \vec{r}_j|} \equiv V(\vec{r}_1, \vec{r}_2, ..., \vec{r}_N) \tag{B.3}$$

The total Hamilton operator is thus

$$\hat{H} = \sum_{i=1}^{N} -\frac{1}{2}\nabla_{\vec{r}_i}^2 + \sum_{i=1}^{N} V_{ext}(\vec{r}_i) + V(\vec{r}_1, \vec{r}_2, ..., \vec{r}_N) \tag{B.4}$$

We do not know V_{ext}, but we know the electron density $\rho(\vec{r})$. Therefore the first theorem says:

Theorem 1: *The external potential $V_{ext}(\vec{r})$ that act in a system of interacting particles is determined uniquely by the electronic density of the fundamental state, $\rho_0(\vec{r})$, except by a constant.*

Proof: Let's assume that we have two different Hamilton operators,

$$\hat{H}_1 = \sum_{i=1}^{N} -\frac{1}{2}\nabla_{\vec{r}_i}^2 + \sum_{i=1}^{N} V_{ext,1}(\vec{r}_i) + V(\vec{r}_1, \vec{r}_2, ..., \vec{r}_N) \tag{B.5}$$

and

$$\hat{H}_2 = \sum_{i=1}^{N} -\frac{1}{2}\nabla_{\vec{r}_i}^2 + \sum_{i=1}^{N} V_{ext,2}(\vec{r}_i) + V(\vec{r}_1, \vec{r}_2, ..., \vec{r}_N) \tag{B.6}$$

The external potentials $V_{ext,1}$ and $V_{ext,2}$ are assumed to differ by more than an additive constant. Then, we have two *different* wavefunctions for the ground states,

$$\hat{H}_1\Psi_1 = E_1\Psi_1 \tag{B.7}$$

$$\hat{H}_2\Psi_2 = E_2\Psi_2 \tag{B.8}$$

where

$$\Psi_1 \neq \Psi_2 \tag{B.9}$$

Notice that we will not have to specify these; we just need to know that they exist. However, both Ψ_1 and Ψ_2 give the *same* electron density (this is the basic assumption),

$$\rho(\vec{r}) = \sum_{i=1}^{N} \int ... \int \Psi_1^*(\vec{r}_1, \vec{r}_2, ..., \vec{r}_N)\delta(\vec{r}_i - \vec{r})\Psi_1(\vec{r}_1, \vec{r}_2, ..., \vec{r}_N)d\vec{r}_1 d\vec{r}_2 ... d\vec{r}_N \tag{B.10}$$

$$\rho(\vec{r}) = \sum_{i=1}^{N} \int ... \int \Psi_2^*(\vec{r}_1, \vec{r}_2, ..., \vec{r}_N)\delta(\vec{r}_i - \vec{r})\Psi_2(\vec{r}_1, \vec{r}_2, ..., \vec{r}_N)d\vec{r}_1 d\vec{r}_2 ... d\vec{r}_N \tag{B.11}$$

The variational principles tells us that

$$\langle\Psi|\hat{H}_1|\Psi\rangle > \langle\Psi_1|\hat{H}_1|\Psi_1\rangle = E_1 \tag{B.12}$$

where Ψ is any N-electron wavefunction *different* from Ψ_1. We now *choose*

$$\Psi = \Psi_2 \tag{B.13}$$

and then obtain

$$\begin{aligned} E_1 < \langle\Psi_2|\hat{H}_1|\Psi_2\rangle &= \langle\Psi_2|\hat{H}_1 - \hat{H}_2 + \hat{H}_2|\Psi_2\rangle \\ &= \langle\Psi_2|\hat{H}_1 - \hat{H}_2|\Psi_2\rangle + \langle\Psi_2|\hat{H}_2|\Psi_2\rangle \\ &= \langle\Psi_2|\sum_{i=1}^{N} V_{ext,1}(\vec{r}_i) - \sum_{i=1}^{N} V_{ext,2}(\vec{r}_i)|\Psi_2\rangle + E_2 \\ &= \int \rho(\vec{r})[V_{ext,1}(\vec{r} - V_{ext,2}(\vec{r})]d\vec{r} + E_2 \end{aligned} \tag{B.14}$$

We have here used that the difference between $\hat{H}_1$ and $\hat{H}_2$ is only the difference in the external potentials, and that Ψ_1 and Ψ_2 produce the same electron density.

We repeat the above procedure for the case where Ψ_1 and Ψ_2 have been interchanged,

$$\langle\Psi|\hat{H}_2|\Psi\rangle > \langle\Psi_2|\hat{H}_2|\Psi_2\rangle = E_2 \tag{B.15}$$

where Ψ is any N-electron wave function *different* from Ψ_2. We choose

$$\Psi = \Psi_1 \tag{B.16}$$

$$\begin{aligned} E_2 < \langle\Psi_1|\hat{H}_2|\Psi_1\rangle &= \langle\Psi_1|\hat{H}_2 - \hat{H}_1 + \hat{H}_1|\Psi_1\rangle \\ &= \langle\Psi_1|\hat{H}_2 - \hat{H}_1|\Psi_1\rangle + \langle\Psi_1|\hat{H}_1|\Psi_1\rangle \\ &= \langle\Psi_1|\sum_{i=1}^{N} V_{ext,2}(\vec{r}_i) - \sum_{i=1}^{N} V_{ext,1}(\vec{r}_i)|\Psi_1\rangle + E_1 \\ &= \int \rho(\vec{r})[V_{ext,2}(\vec{r} - V_{ext,1}(\vec{r})]d\vec{r} + E_1 \end{aligned} \tag{B.17}$$

Eq. (B.14) gives

$$E_1 - E_2 < \int \rho(\vec{r})[V_{ext,1}(\vec{r}) - V_{ext,2}(\vec{r})]d\vec{r} \tag{B.18}$$

or (multiplying by -1),

$$E_2 - E_1 > \int \rho(\vec{r}[V_{ext,2}(\vec{r}) - V_{ext,1}(\vec{r})]d\vec{r} \tag{B.19}$$

On the other hand, Eq. (B.17) gives

$$E_2 - E_1 < \int \rho(\vec{r})[V_{ext,2}(\vec{r}) - V_{ext,1}(\vec{r})]d\vec{r} \tag{B.20}$$

Eq. (B.19) and Eq. (B.20) cannot both be true. Therefore, we have a contradiction, and something in our assumptions must be wrong. That is, we can not have two *different* external potentials that produce the same electron density. This means that the electron density $\rho(\vec{r})$ defines *all* terms in Hamilton operator, and therefore we can *in principle* determine the complete N-electron wavefunction for the ground state by only knowing the electron density. □ Now for the second theorem:

Theorem 2: *A universal functional could be defined for the energy $E[\rho(\vec{r})]$ in terms of the electronic density $\rho(\vec{r})$ and, for a given external potential $V_{ext}(\vec{r})$, this functional has a global minimum in the exact density of the fundamental state $\rho_0(\vec{r})$.*

Proof: First we assume that we know the functional of ρthat gives us the total electronic energy E_e for the ground state. We also know that this density can - in principle - be calculated from some N-electron wavefunction, i.e., from the ground state wave function for the system of our interest, Ψ_0. Thus,

$$E_e = \langle \Psi_0 | \hat{H} | \Psi_0 \rangle \tag{B.21}$$

Since Ψ_0 is the ground state, E_e must be the smallest possible value of

$$\langle \Psi | \hat{H} | \Psi \rangle \tag{B.22}$$

i.e.,

$$E_e = \min_{\Psi} \langle \Psi | \hat{H} | \Psi \rangle \tag{B.23}$$

where we have specified that we vary Ψ.

Furthermore, we know that Ψ leads to the correct electron density ρ. We will therefore write explicitly

$$E_e = \min_{\Psi \to \rho} \langle \Psi | \hat{H} | \Psi \rangle \tag{B.24}$$

Thereby we have *formally* written E_e as a functional of ρ,

$$E_e = E_e[\rho] = \min_{\Psi \to \rho} \langle \Psi | \hat{H} | \Psi \rangle \tag{B.25}$$

What happens if we take that functional but insert a wrong density ρ'? Since $\rho \neq \rho'$, the two densities cannot be constructed from the same wave function. Therefore,

that wave function $\Psi^{'}$ that leads to the minimum of

$$E_e[\rho^{'}] = \min_{\Psi^{'} \to \rho^{'}} \langle \Psi^{'} | \hat{H} | \Psi^{'} \rangle \tag{B.26}$$

is not that of the ground state of the system. Therefore, any expectation value $\langle \Psi^{'} | \hat{H} | \Psi \rangle$ of Eq. (B.26), i.e., we have a variational principle for the density functionals,

$$E_e[\rho^{'}] \geq E_e[\rho] \tag{B.27}$$

and this is the second theorem. □

APPENDIX C – Step by Step FP-LAPW ELK code Tutorial

These tutorials are based on Tutorials from Professor Vitaly Romaka[1].

C.1 Ground State Energy of CeCd

In this tutorial we will learn how to prepare the input files (elk.in) of CeCd for ground state energy calculations. The ground state calculations run at T = 0 K and require the following crystallographic parameters: space group, atomic coordinates, and lattice constants.

C.1.1 Requirements

- Precompiled ELK 5.2.14

C.1.2 Input Parameters

- CeCd: space group: P1, $a = b = c = 3.855$ Å[35]

C.1.3 Crystal Structure Preparation

Before starting, create inside the working directory a directory with a convenient name where all the calculations will be stored. **Attention! The stage of crystal structure preparation is one of the most important and even small mistake would lead to the wrong electronic structure of the material.**

For the crystal structure preparation the program spacegroup is used. It is located inside the elk-5.2.14/src/spacegroup/ directory and is a part of the elk package. The input parameters for this program are located inside the spacegroup.in file which should be changed according to the given crystallographic parameters of CeCd. For the these the spacegroup.in file will look like this:

[1] https://sites.google.com/site/tinykpoint/elk-tutorial

```
'P1'                                          :hrmg
7.284894000     7.284894000     7.284894000 :a, b, c
90.0    90.0    90.0                          :bc, ac, ab
1       1       1                             :ncell
.true.                                        :primcell
2                                             :nspecies
'Ce'                                          :spsymb
1                                             :nwpos
0       0       0                             :wpos
'Cd'                                          :spsymb
1                                             :nwpos
0.5     0.5     0.5                           :wpos
```

Figure 39 – Block showing the input parameters of spacegroup functionality. Source: the Author

The first line (hrmg) contains the Hermann-Mauguin symbol of a space group (P1 identity group) and its origin choice (:2). The line (a, b, c) provides the lattice vector lengths in atomic units (a.u.). The next line (bc, ac, ab) gives the angles in degrees between the lattice vectors b and c (α), a and c (β), and a and b (γ). The line (ncell) sets the number of unit cells required in each direction of the basis vectors a, b, c, respectively and is used for superstructure creation. The line (primcell) defines if the primitive unit cell should be found (.true.) or not (.false.). If the Bravais lattice of the crystal is not primitive than setting (primcell) value to (.true.) could significantly speed up the ground state calculation. However in some cases like crystal structure optimization, superstructure creation or volumetric data visualization it may be necessary to make it (.false.). In this case the symmetry of the structure will be reduced to P1. The line (nspecies) gives the number of atomic species and the line (spsymb) atomic species symbol. The line (nwpo) sets the number of Wyckoff positions (atomic sites) and the line (wpos) provides fractional coordinates for the given Wyckoff position.

After saving the spacegroup.in file run the program spacegroup. Several files would be created in particular GEOMETRY.OUT, which contains all necessary crystallographic information in format suitable for the ELK program. The GEOMETRY.OUT file could be opened directly by some crystallographic visualization program to check the generated crystal structure before running the ground state calculations. Copy created spacegroup.in and GEOMETRY.OUT files for CeCd to your working directory.

C.1.4 Ground State Energy Calculation

At this stage the input file (elk.in) for the ground state energy calculation will be created. For the CeCd inside the working directory create an empty file elk.in and fill it with the following information:

```
tasks
0

xctype
20

autolinengy
true

mixtype
3

maxscl
100

nempty
10

sppath
'~/elk-5.2.14/species/'

ngridk
2       2       2
```

Figure 40 – Block showing the elk.in input file. Source: the Author

The tasks (0) corresponds to the ground state calculations starting from the atomic densities. The xctype (20) defines the type of exchange-correlation functional (GGA). The autolinengy (true) parameter sets the automatic determination of the fixed linearisation energies. Type of potential mixing (Broyden) is defined by the mixtype (3) parameter. The maxscl parameter gives the maximum number of self-consistent loops allowed. The number of empty states per atom and spin is set by the nempty (10) parameter. The sppath parameter gives the path where the species files can be found. The k-point mesh size is given by the ngridk (2 2 2) parameter. To add crystallographic information about the CeCd copy the following section from the GEOMETRY.OUT into the elk.in file:

```
scale
 1.0

scale1
 1.0

scale2
 1.0

scale3
 1.0

avec
   7.284894000       0.000000000       0.000000000
   0.000000000       7.284894000       0.000000000
   0.000000000       0.000000000       7.284894000

atoms
   2                                    : nspecies
'Ce.in'                                 : spfname
   1                                    : natoms; atpos, bfcmt below
    0.00000000    0.00000000    0.00000000    0.00000000  0.00000000  0.00000000
'Cd.in'                                 : spfname
   1                                    : natoms; atpos, bfcmt below
    0.50000000    0.50000000    0.50000000    0.00000000  0.00000000  0.00000000
```

Figure 41 – GEOMETRY.OUT file. Source: the Author

The avec parameter sets the lattice vectors of the crystal in atomic units. Save the elk.in file and run ELK program with elk.in as an argument. About a dozen of files will be created among them INFO.OUT (information on self-consistent loop), TOTENERGY.OUT (total energy in Hartree (Ha) for every self-consistent loop), DTOTENERGY.OUT (energy difference between two consecutive self- consistent loops), and STATE.OUT (density and potential data). After the calculations are finished the quality of the calculations should be improved by increasing the k-point mesh size. To do this change the tasks value from 0 to 1 (to resume the ground-state calculations using density from STATE.OUT)and increase the ngridk from 2 2 2 to 10 10 10 (to get more precise total energy value).

After completion of the ground state calculations for CeCd on a $10 \times 10 \times 10$ k-point mesh you gotta have a lot of .OUT files which have information about Ground State Energy and other properties. You could return to the elk.in file, put more tasks and obtain more physical parameters.

APPENDIX D – Graphs of Optimization Parameters

In this appendix we show the graphs used for the optimization of the parameters $R_{mt}K_{max}$, k-poins mesh and volume of the rest of the compounds.

All the graphs are groupped for each compounds.

D.0.1 PrCd

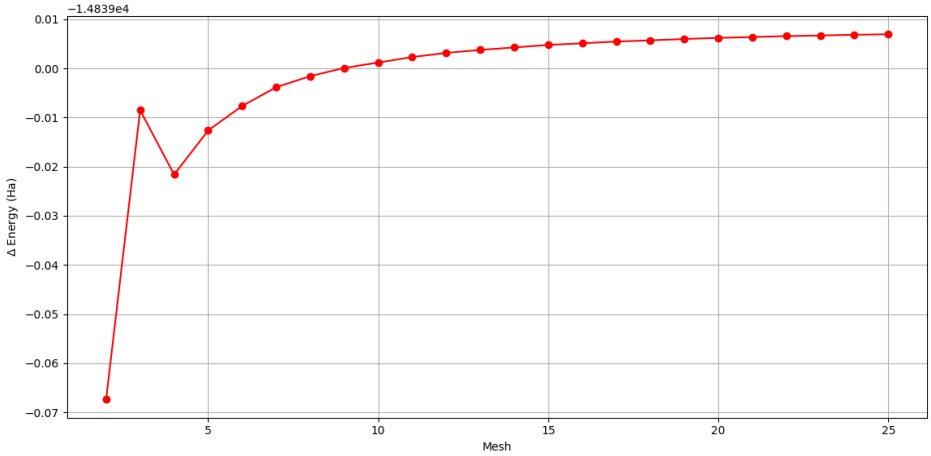

(a) PrCd with sp

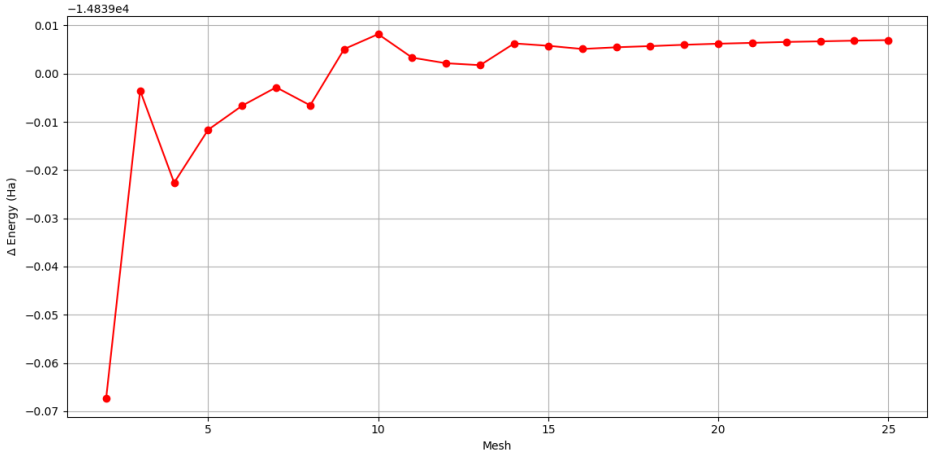

(b) PrCd with so

Figure 42 – k-points variations in function of energies differences of PrCd with spin polarization (sp) and spin polarization plus spin orbit (so) the x-axis represents points in x, y and z direction. Source: the Author.

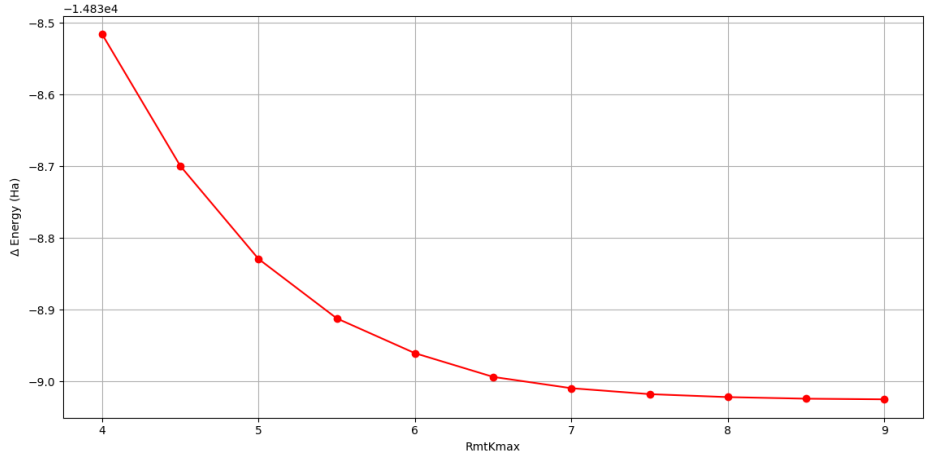

(a) PrCd with sp

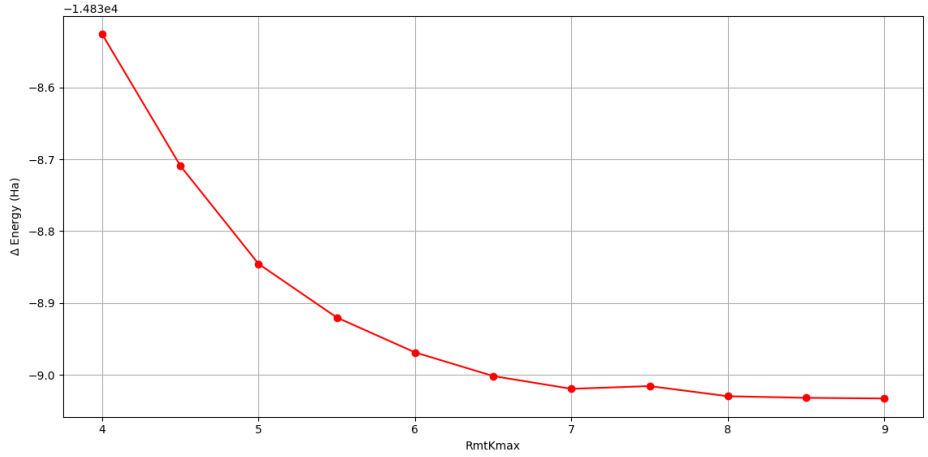

(b) PrCd with so

Figure 43 – $R_{mt}K_{max}$ variations in function of energies differences of CeCd with spin polarization (sp) and spin polarization plus spin orbit (so). Source: the Author.

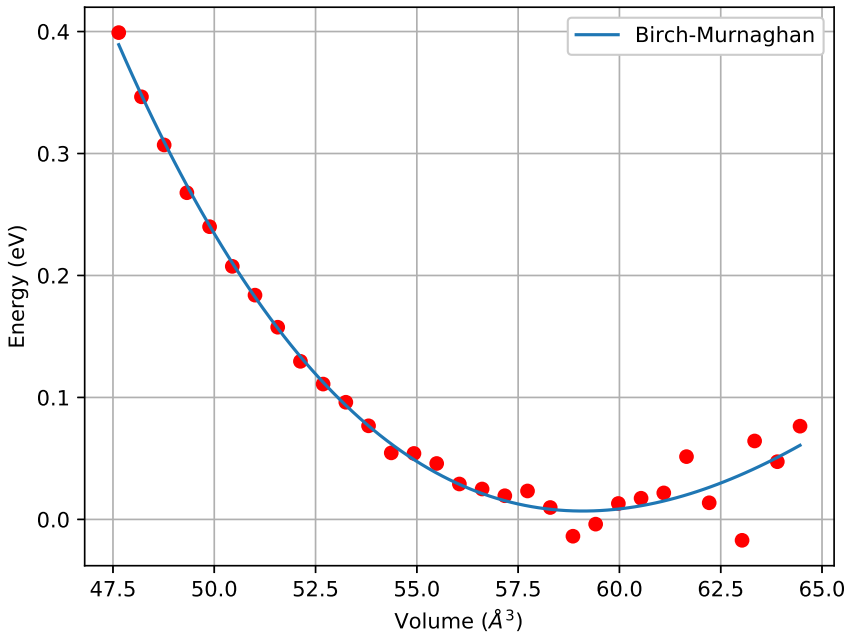

(a) PrCd with sp

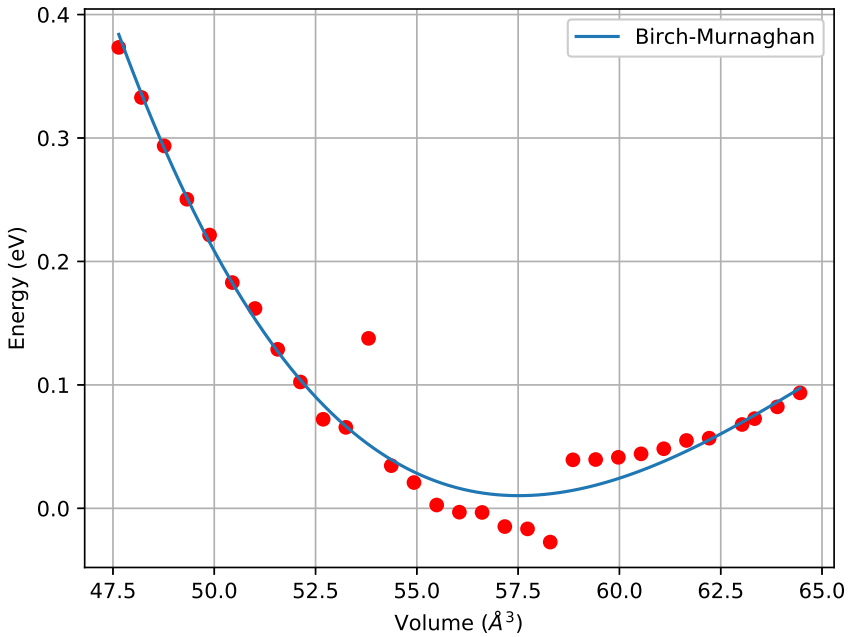

(b) PrCd with so

Figure 44 – Volume variations in function of energies differencies of PrCd with spin polarization (sp) and spin polarization plus spin orbit (so). Source: the Author.

D.0.2 NdCd

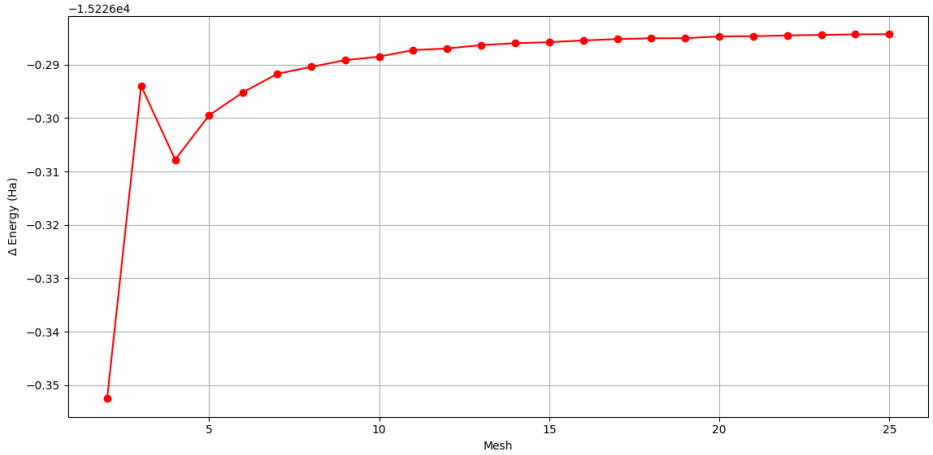

(a) NdCd with sp

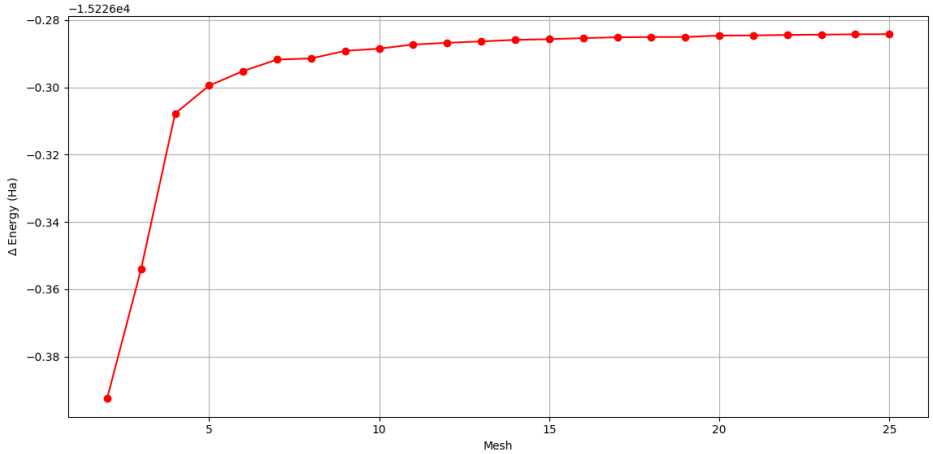

(b) NdCd with so

Figure 45 – k-points variations in function of energies differences of NdCd with spin polarization (sp) and spin polarization plus spin orbit (so) the x-axis represents points in x, y and z direction. Source: the Author.

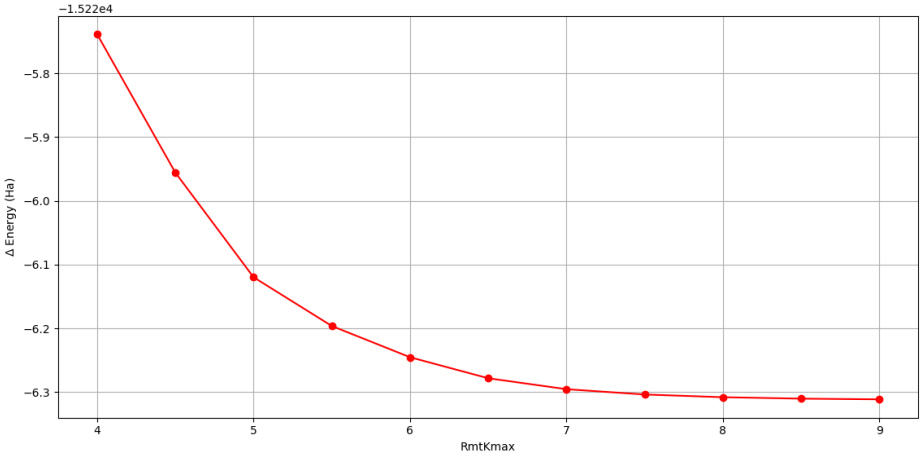

(a) NdCd with sp

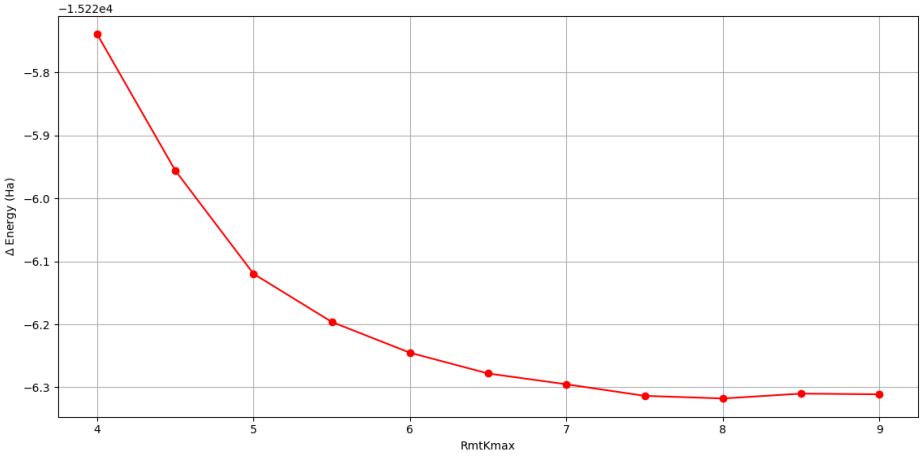

(b) NdCd with so

Figure 46 – $R_{mt}K_{max}$ variations in function of energies differences of NdCd with spin polarization (sp) and spin polarization plus spin orbit (so). Source: the Author.

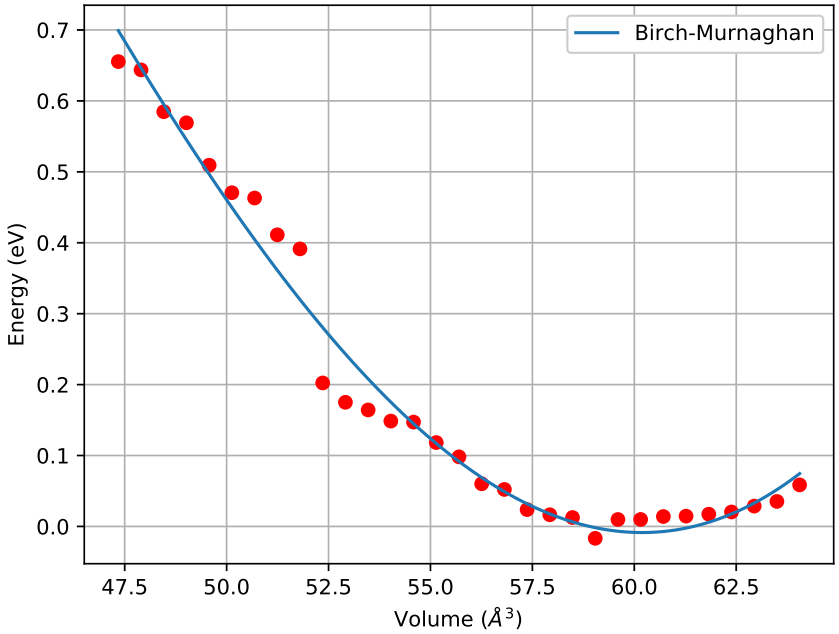

(a) NdCd with sp

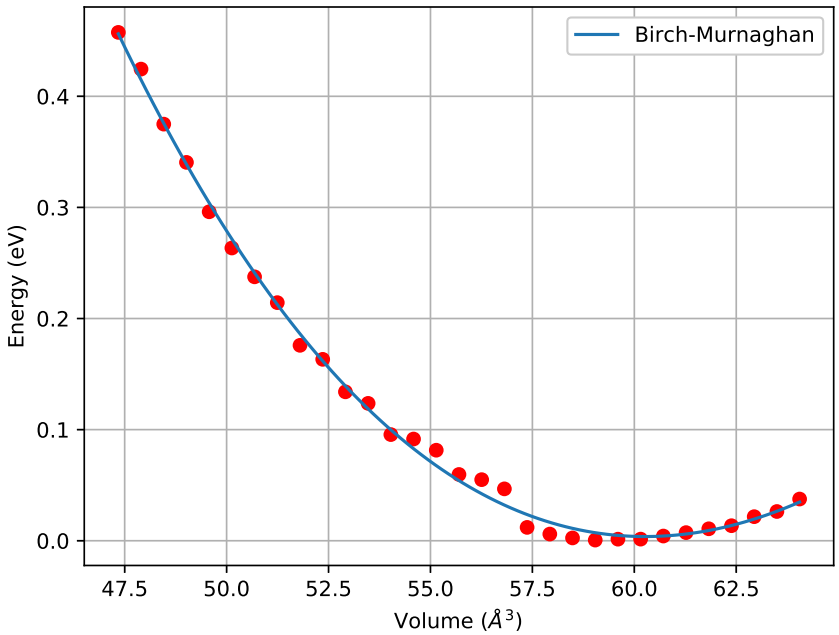

(b) NdCd with so

Figure 47 – Volume variations in function of energies differencies of NdCd with spin polarization (sp) and spin polarization plus spin orbit (so). Source: the Author.

D.0.3 SmCd

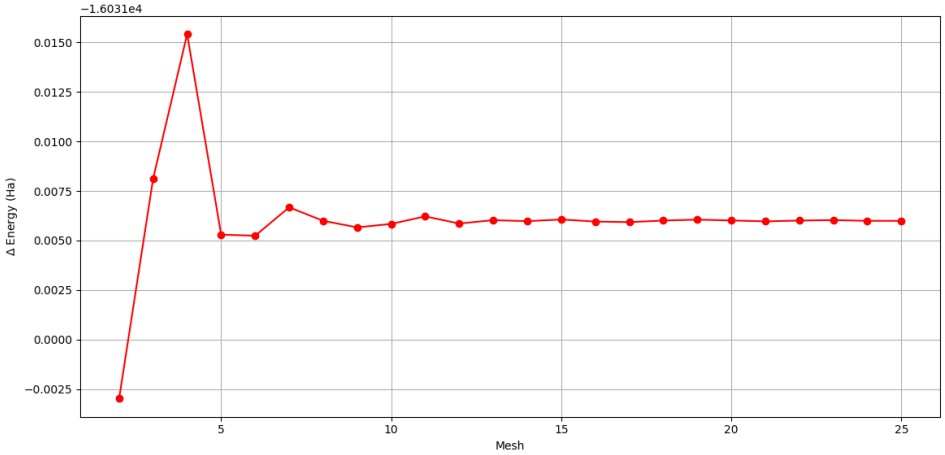

(a) SmCd with sp

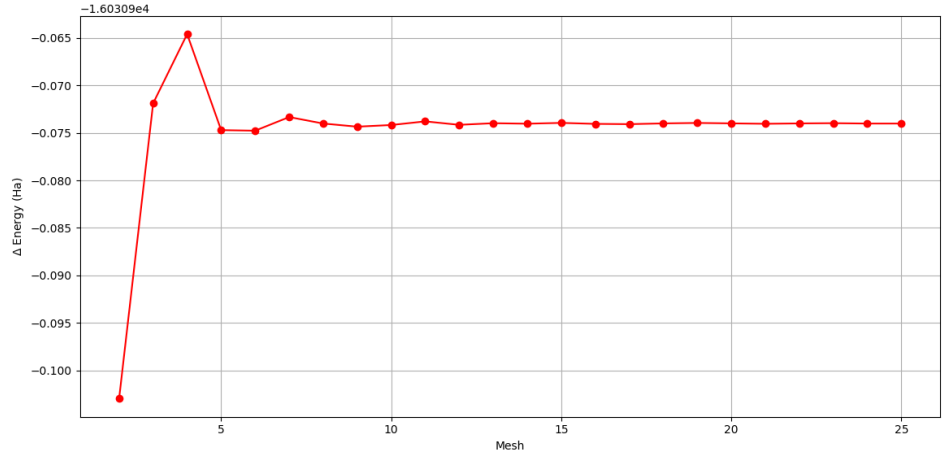

(b) SmCd with so

Figure 48 – k-points variations in function of energies differences of SmCd with spin polarization (sp) and spin polarization plus spin orbit (so) the x-axis represents points in x, y and z direction. Source: the Author.

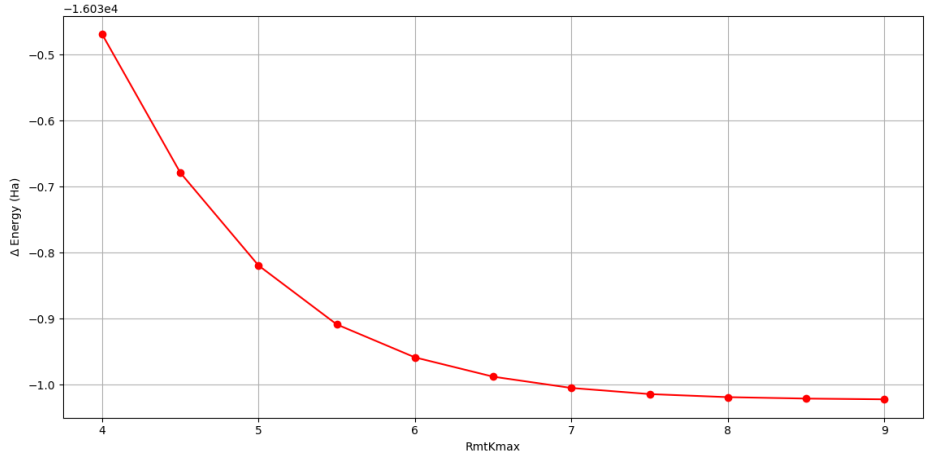

(a) SmCd with sp

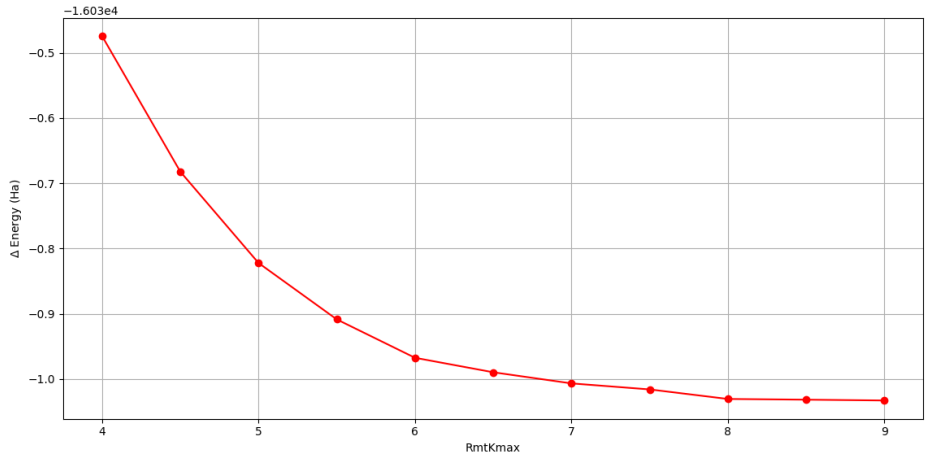

(b) SmCd with so

Figure 49 – $R_{mt}K_{max}$ variations in function of energies differences of SmCd with spin polarization (sp) and spin polarization plus spin orbit (so). Source: the Author.

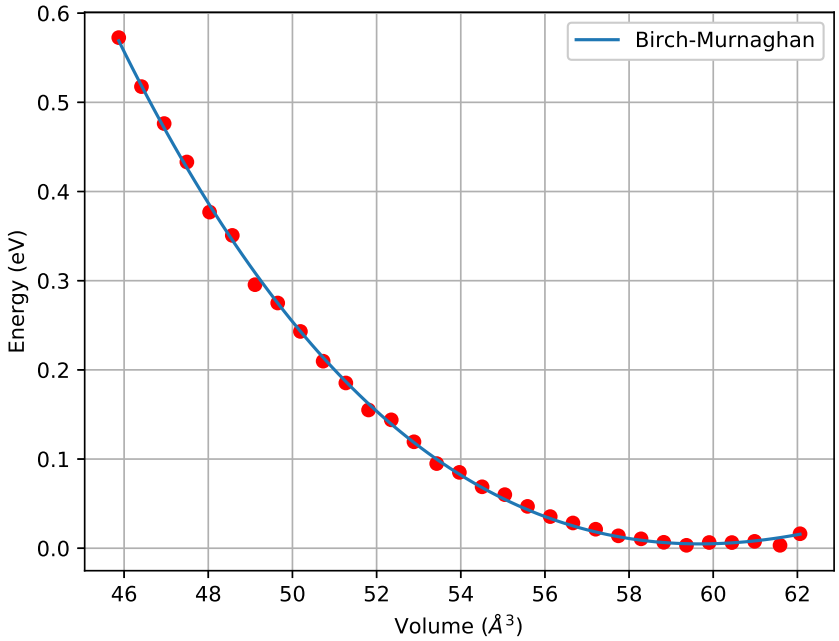

(a) SmCd with sp

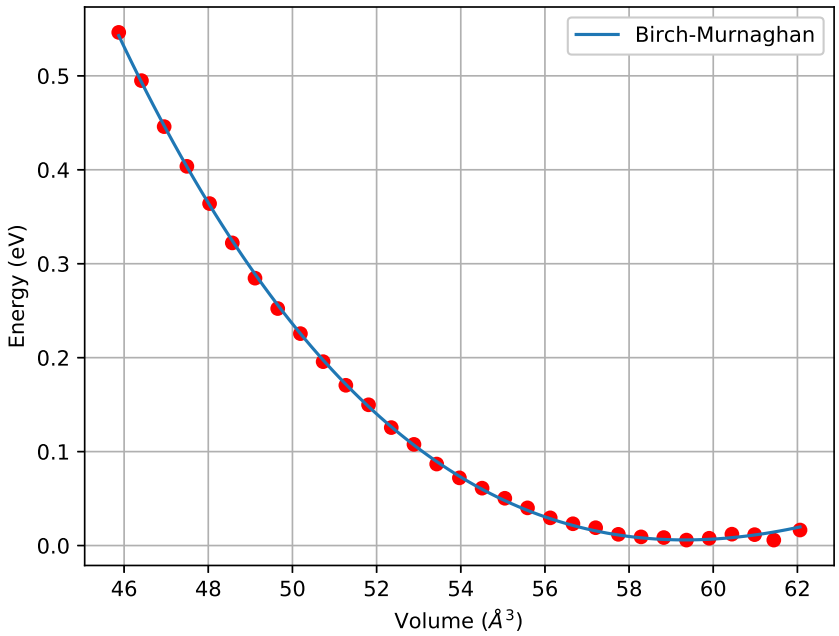

(b) SmCd with so

Figure 50 – Volume variations in function of energies differencies of SmCd with spin polarization (sp) and spin polarization plus spin orbit (so). Source: the Author.

D.0.4 TbCd

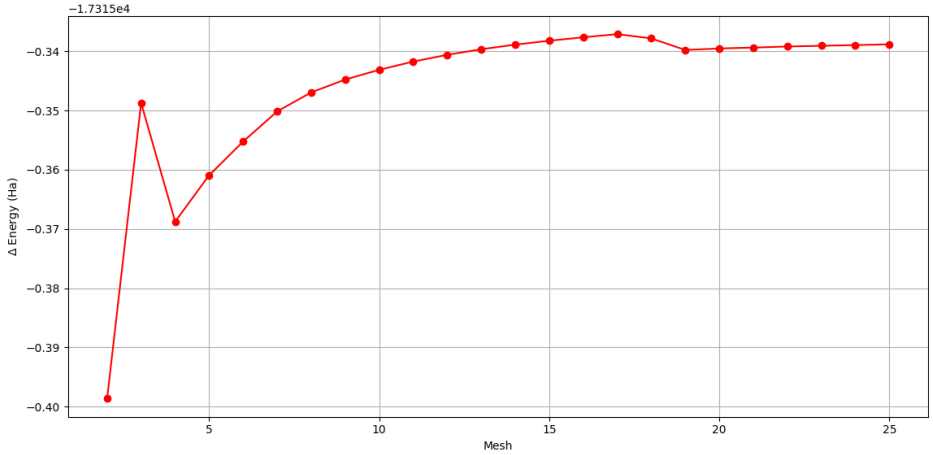

(a) TbCd with sp

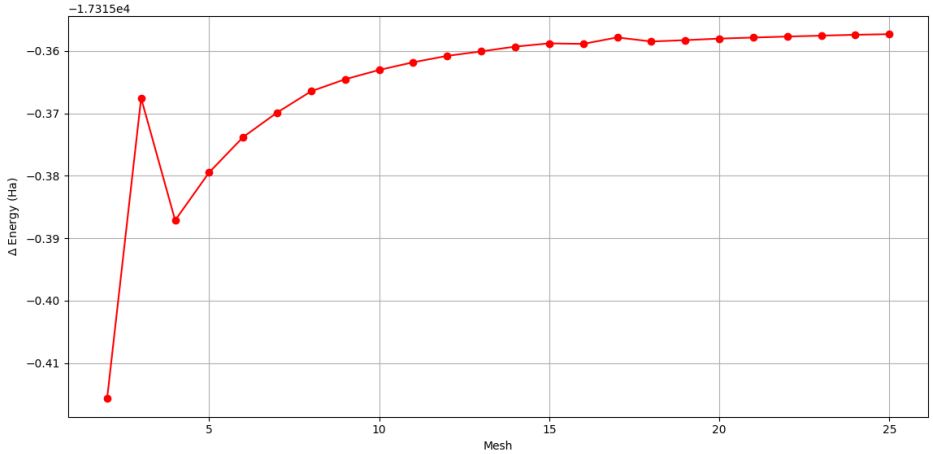

(b) TbCd with so

Figure 51 – k-points variations in function of energies differences of TbCd with spin polarization (sp) and spin polarization plus spin orbit (so) the x-axis represents points in x, y and z direction. Source: the Author.

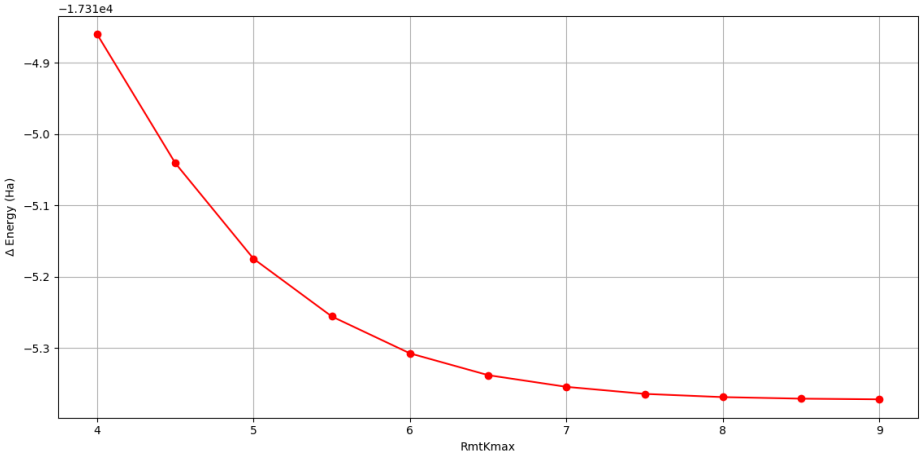

(a) TbCd with sp

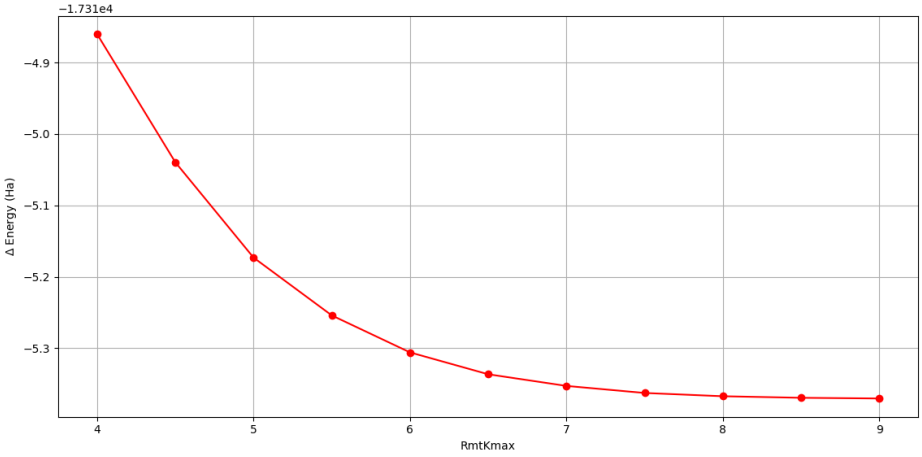

(b) TbCd with so

Figure 52 – $R_{mt}K_{max}$ variations in function of energies differences of TbCd with spin polarization (sp) and spin polarization plus spin orbit (so). Source: the Author.

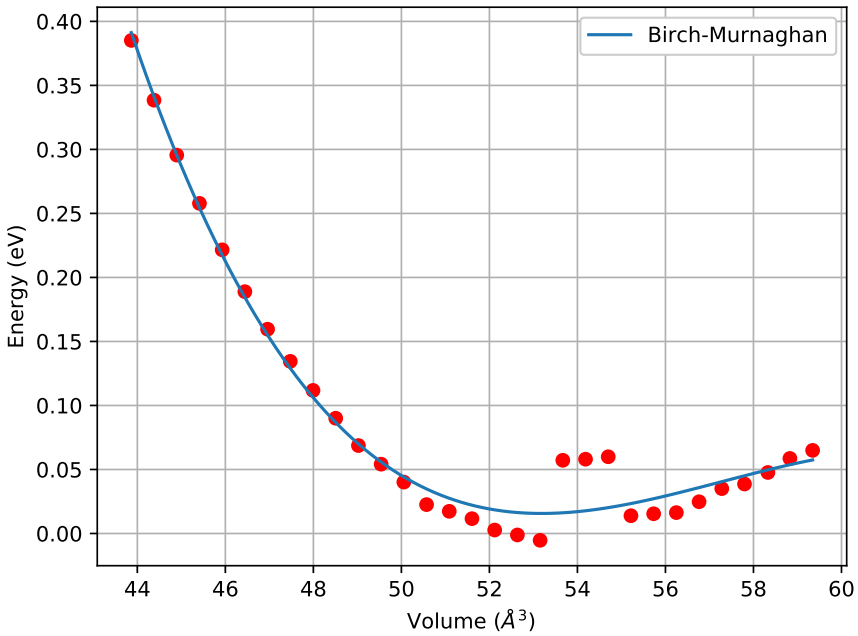

(a) TbCd with sp

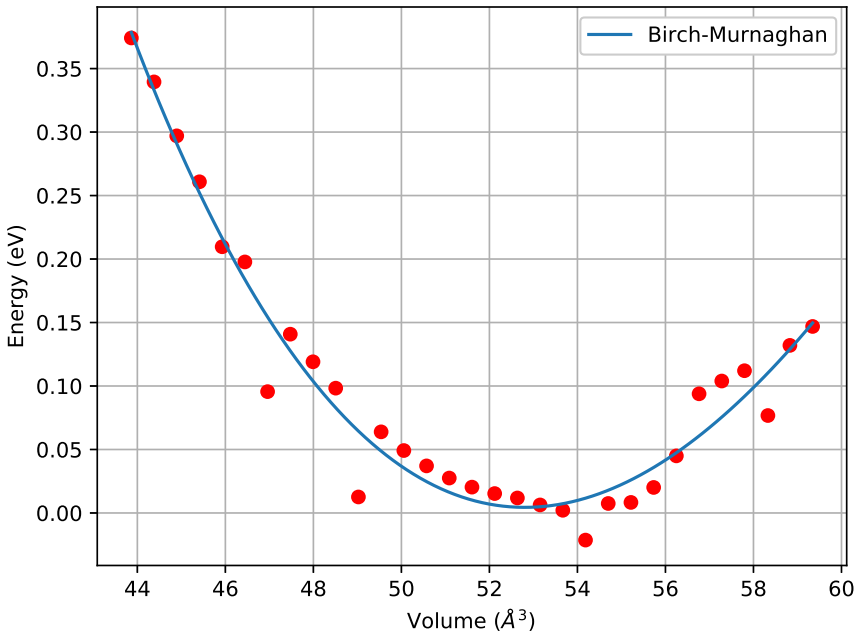

(b) TbCd with so

Figure 53 – Volume variations in function of energies differencies of TbCd with spin polarization (sp) and spin polarization plus spin orbit (so). Source: the Author.

D.0.5 DyCd

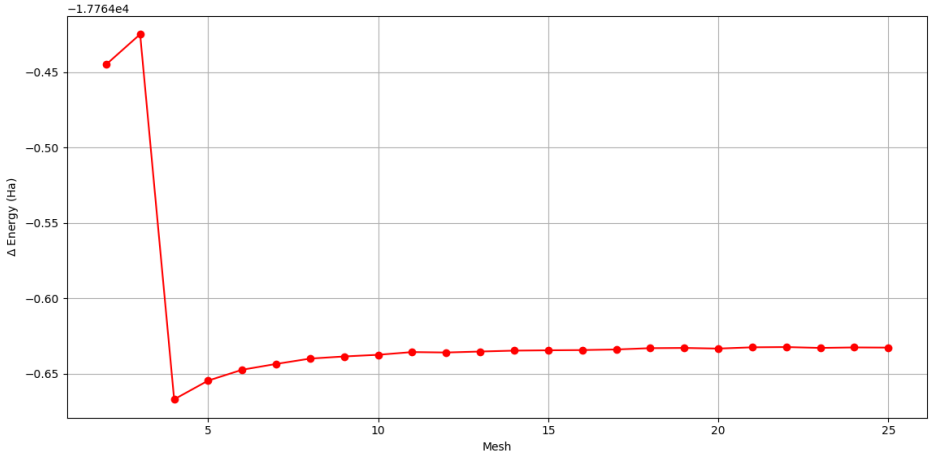

(a) DyCd with sp

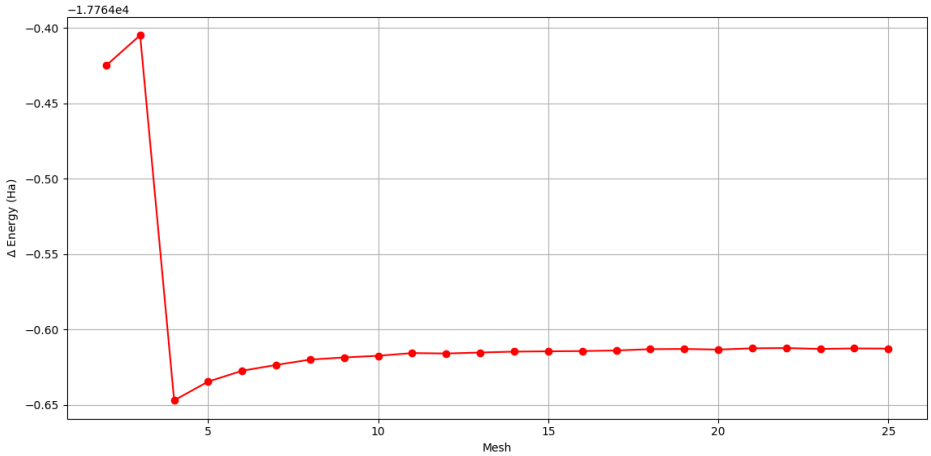

(b) DyCd with so

Figure 54 – k-points variations in function of energies differences of DyCd with spin polarization (sp) and spin polarization plus spin orbit (so) the x-axis represents points in x, y and z direction. Source: the Author.

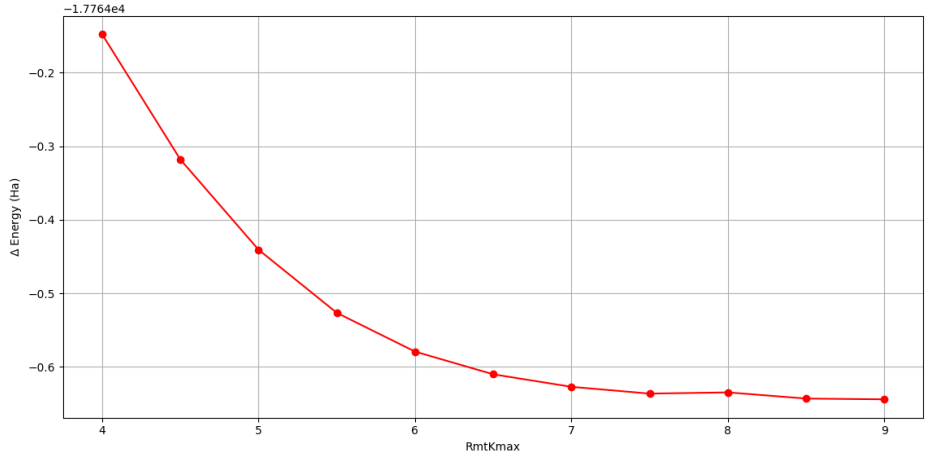

(a) DyCd with sp

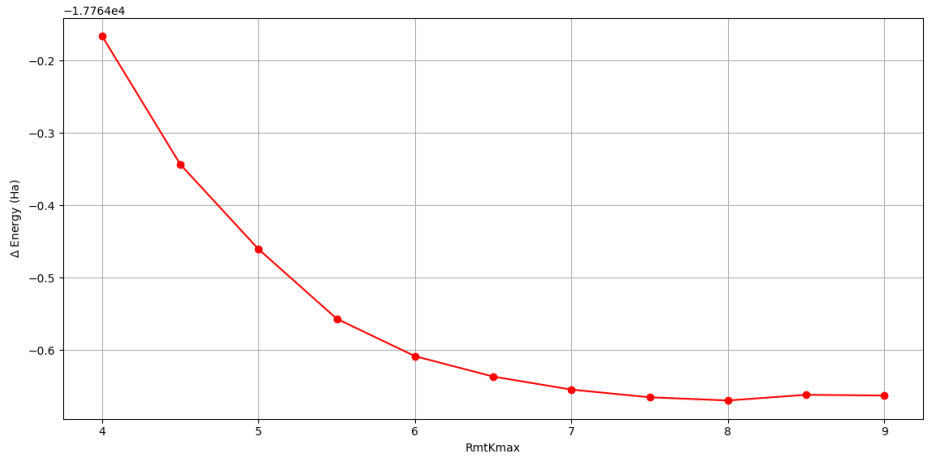

(b) DyCd with so

Figure 55 – $R_{mt}K_{max}$ variations in function of energies differences of DyCd with spin polarization (sp) and spin polarization plus spin orbit (so). Source: the Author.

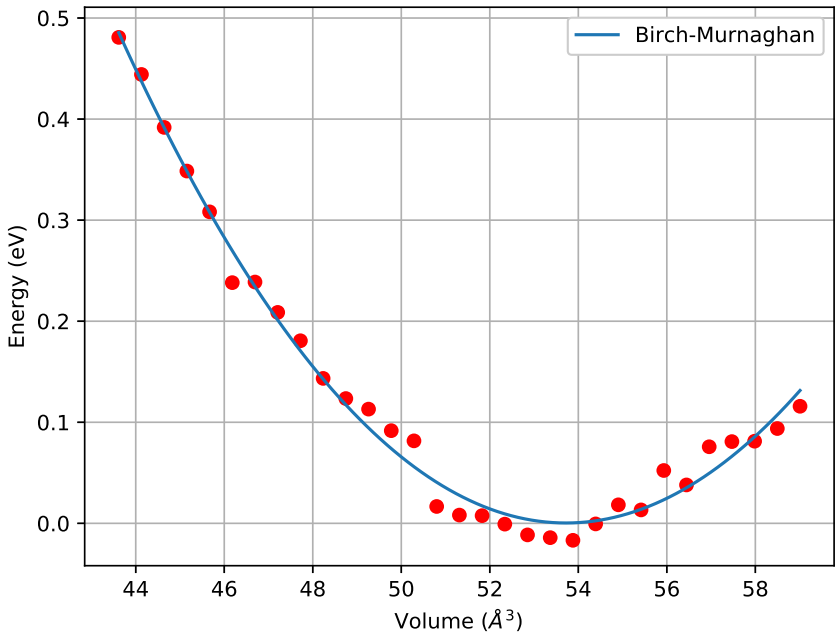

(a) DyCd with sp

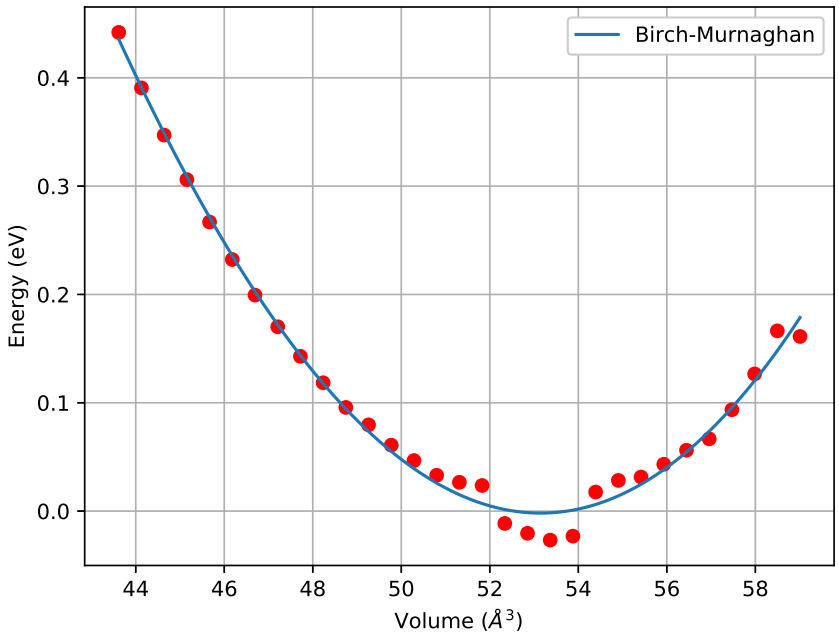

(b) DyCd with so

Figure 56 – Volume variations in function of energies differencies of DyCd with spin polarization (sp) and spin polarization plus spin orbit (so). Source: the Author.

D.0.6 HoCd

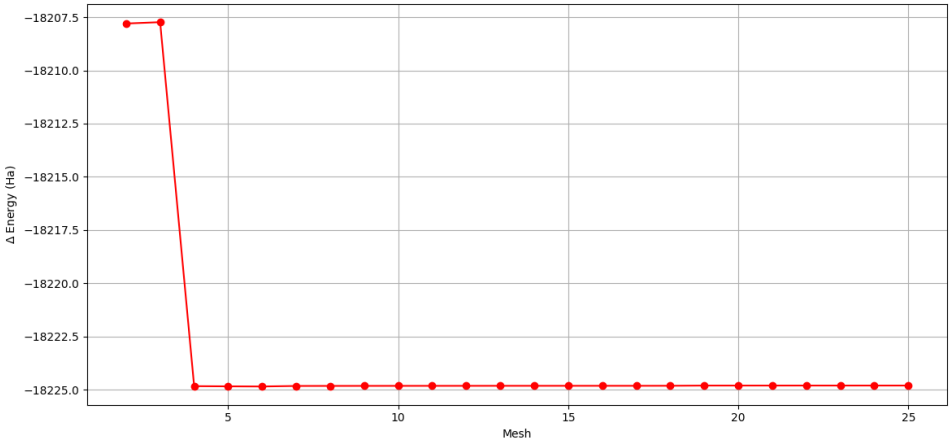

(a) HoCd with sp

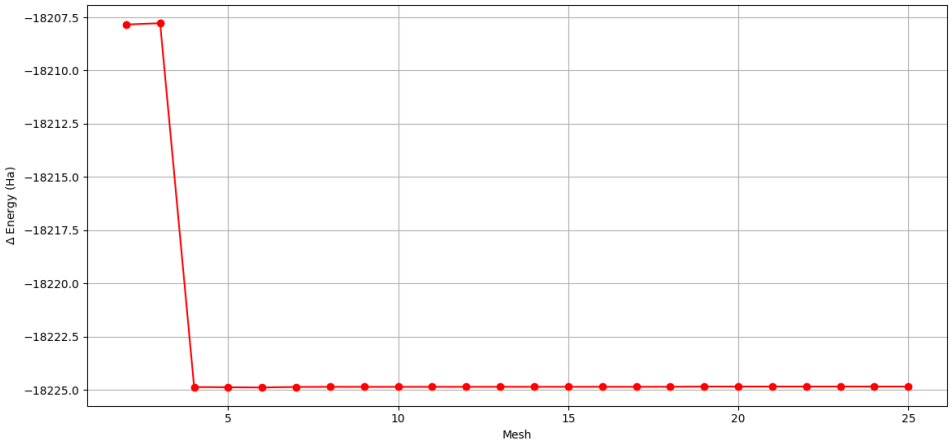

(b) HoCd with so

Figure 57 – k-points variations in function of energies differences of HoCd with spin polarization (sp) and spin polarization plus spin orbit (so) the x-axis represents points in x, y and z direction. Source: the Author.

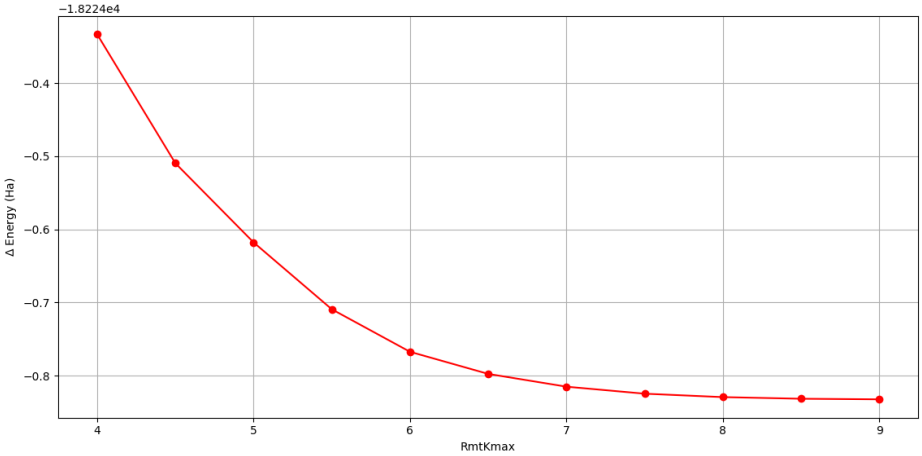

(a) HoCd with sp

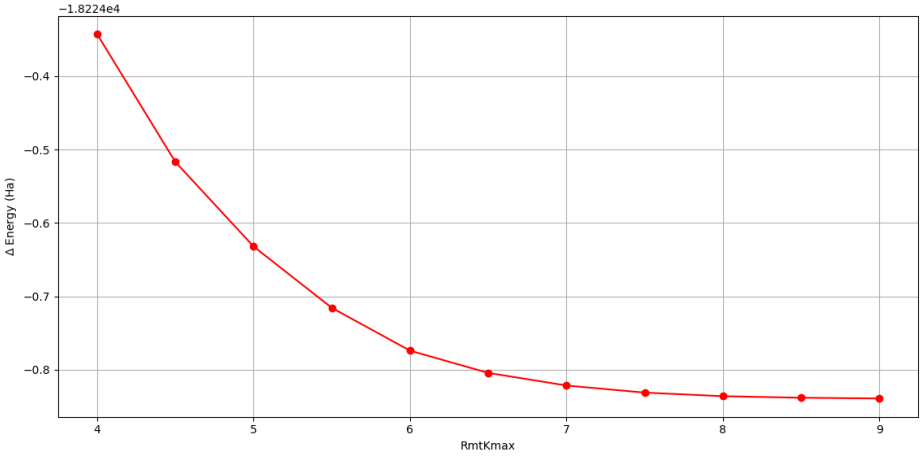

(b) HoCd with so

Figure 58 – $R_{mt}K_{max}$ variations in function of energies differences of HoCd with spin polarization (sp) and spin polarization plus spin orbit (so). Source: the Author.

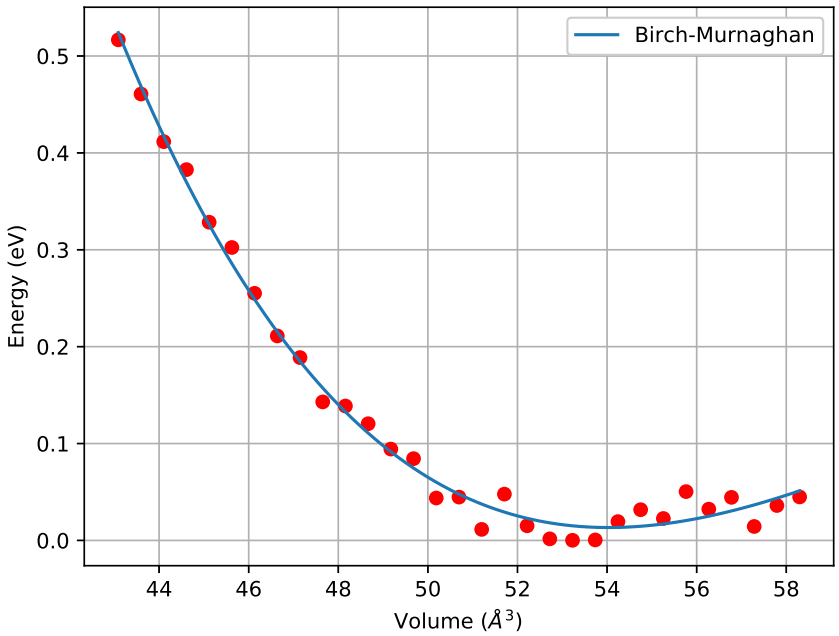

(a) HoCd with sp

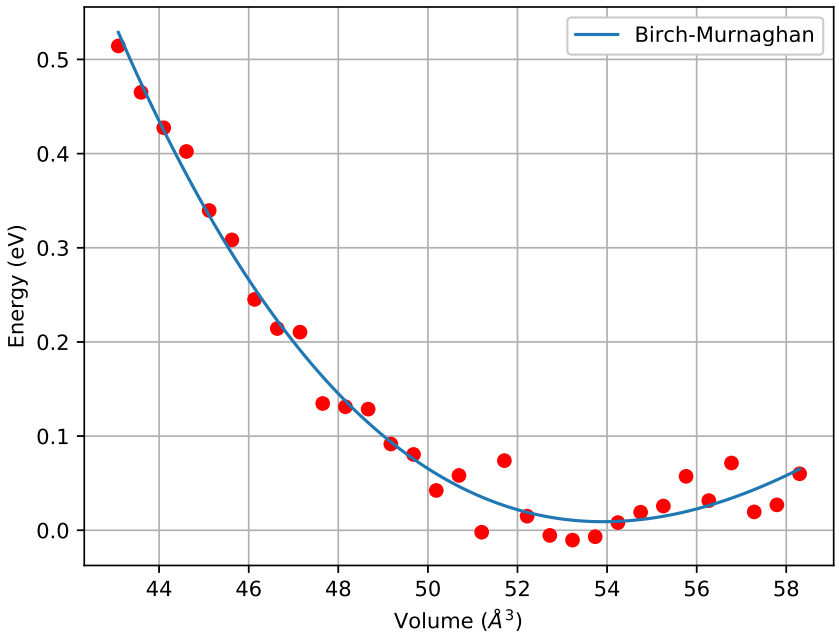

(b) HoCd with so

Figure 59 – Volume variations in function of energies differencies of HoCd with spin polarization (sp) and spin polarization plus spin orbit (so). Source: the Author.

D.0.7 EuCd

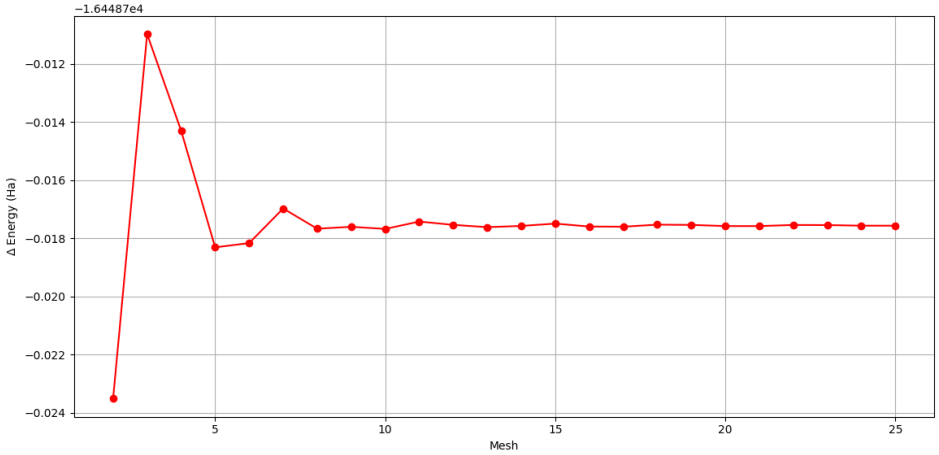

(a) EuCd with sp

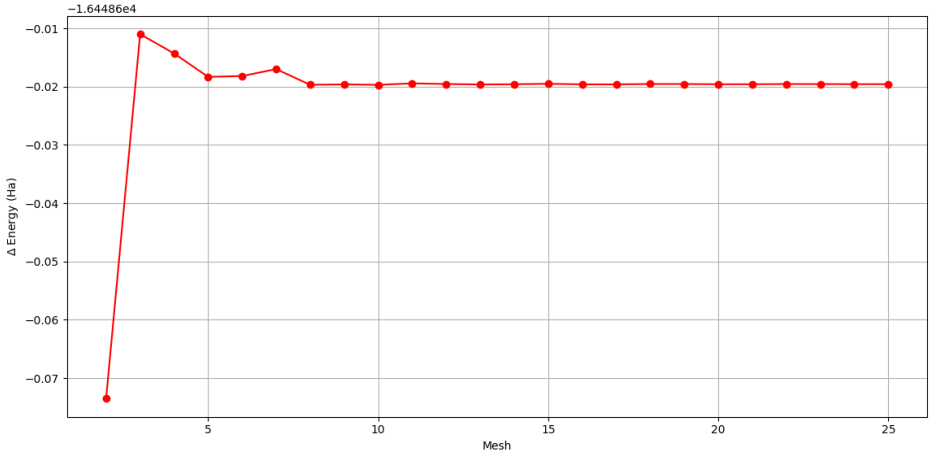

(b) EuCd with so

Figure 60 – k-points variations in function of energies differences of EuCd with spin polarization (sp) and spin polarization plus spin orbit (so) the x-axis represents points in x, y and z direction. Source: the Author.

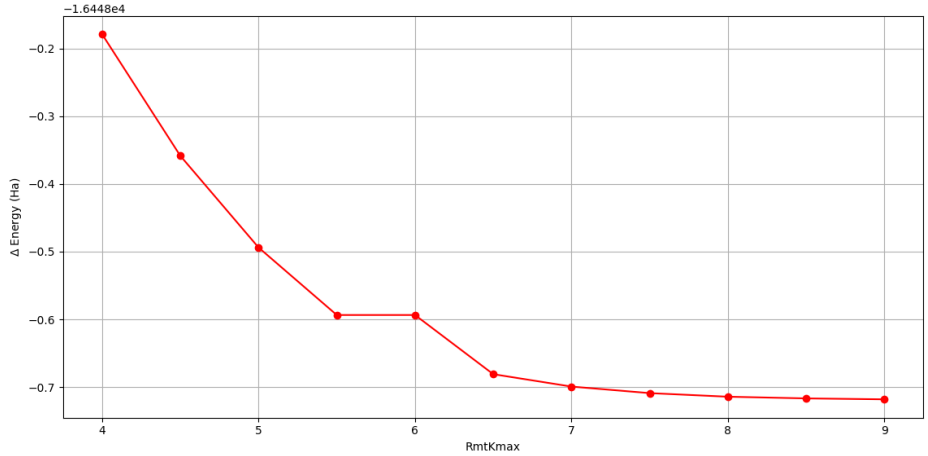

(a) EuCd with sp

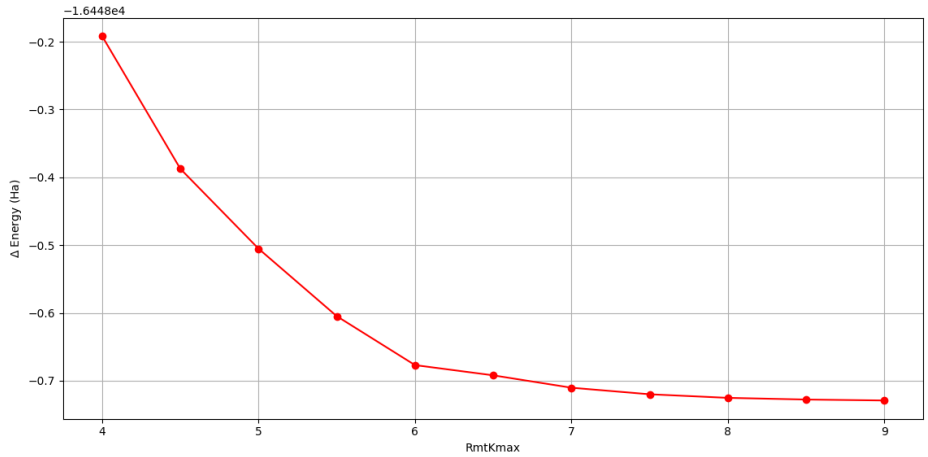

(b) EuCd with so

Figure 61 – $R_{mt}K_{max}$ variations in function of energies differences of EuCd with spin polarization (sp) and spin polarization plus spin orbit (so). Source: the Author.

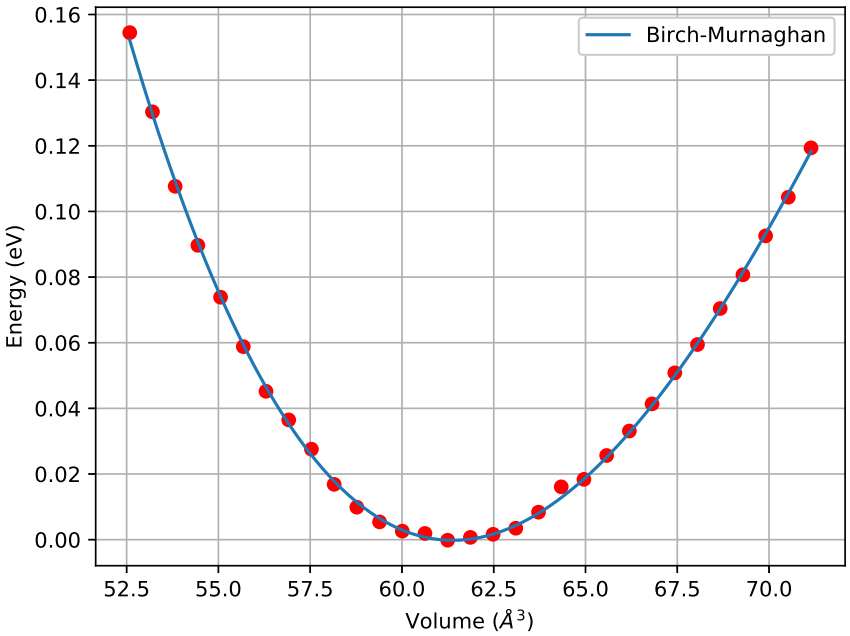

(a) EuCd with sp

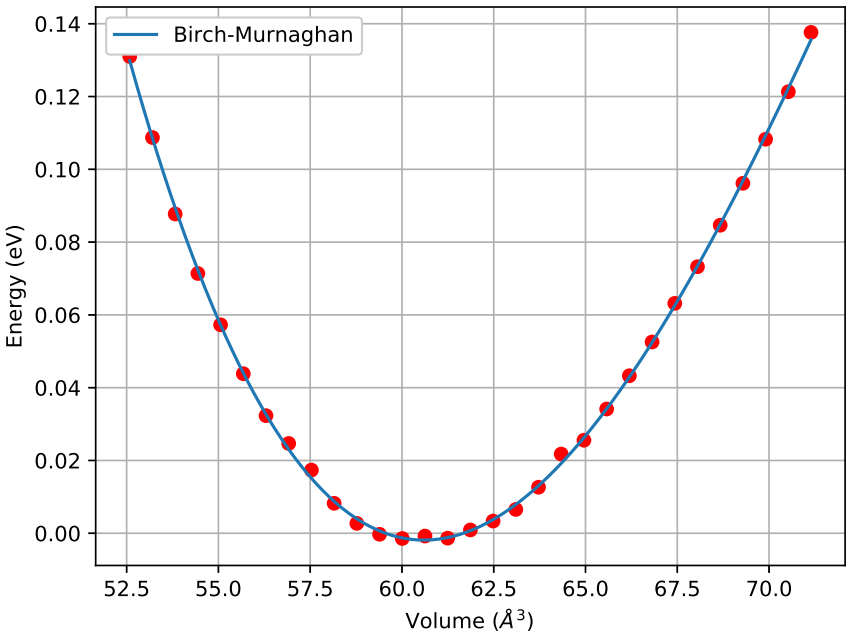

(b) EuCd with so

Figure 62 – Volume variations in function of energies differencies of EuCd with spin polarization (sp) and spin polarization plus spin orbit (so). Source: the Author.

D.0.8 TmCd

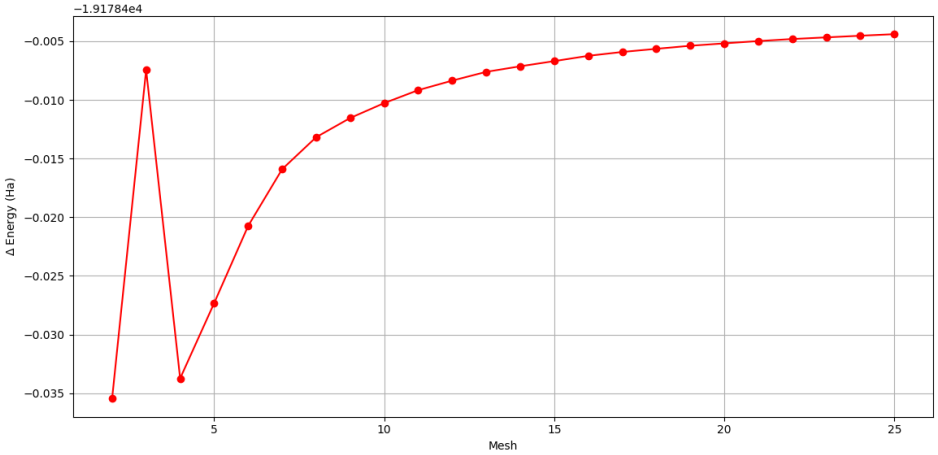

(a) TmCd with sp

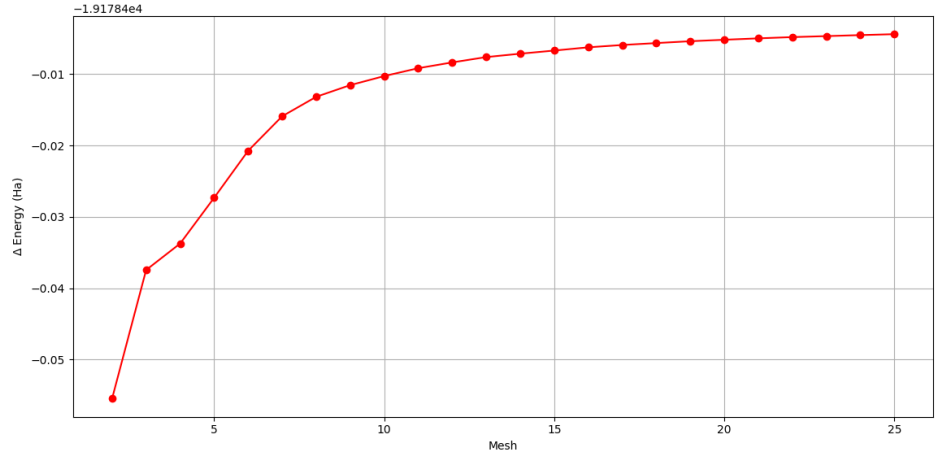

(b) TmCd with so

Figure 63 – k-points variations in function of energies differences of TmCd with spin polarization (sp) and spin polarization plus spin orbit (so) the x-axis represents points in x, y and z direction. Source: the Author.

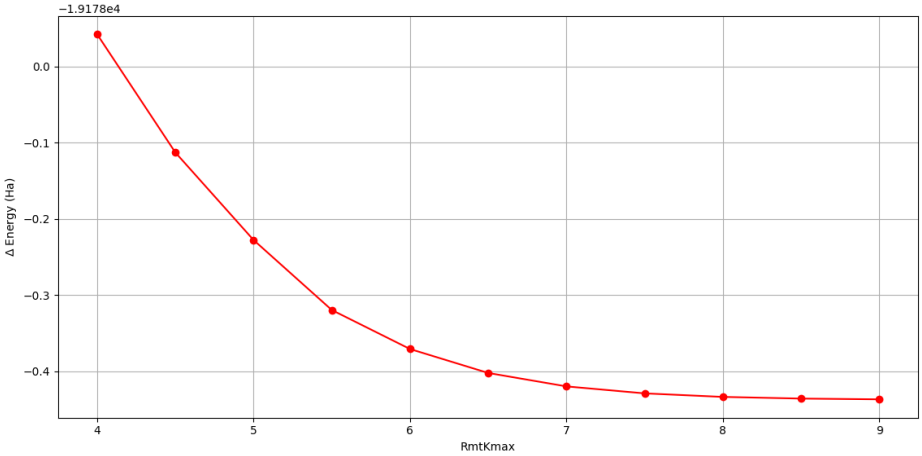

(a) TmCd with sp

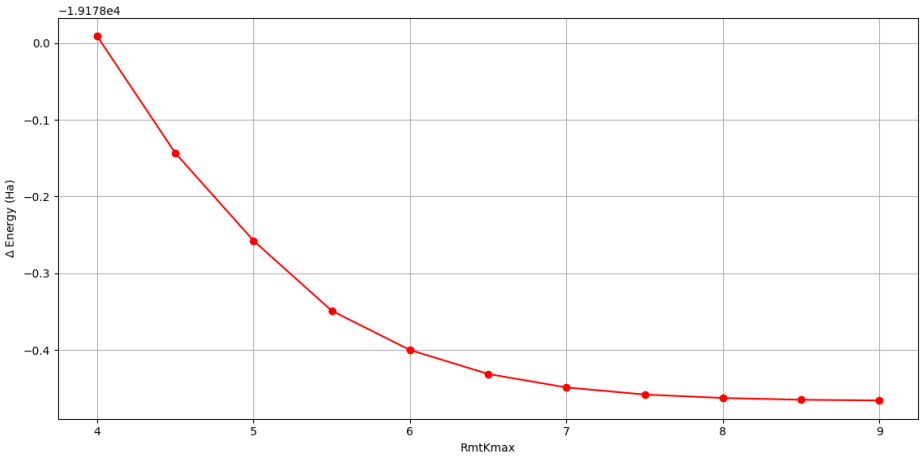

(b) TmCd with so

Figure 64 – $R_{mt}K_{max}$ variations in function of energies differences of TmCd with spin polarization (sp) and spin polarization plus spin orbit (so). Source: the Author.

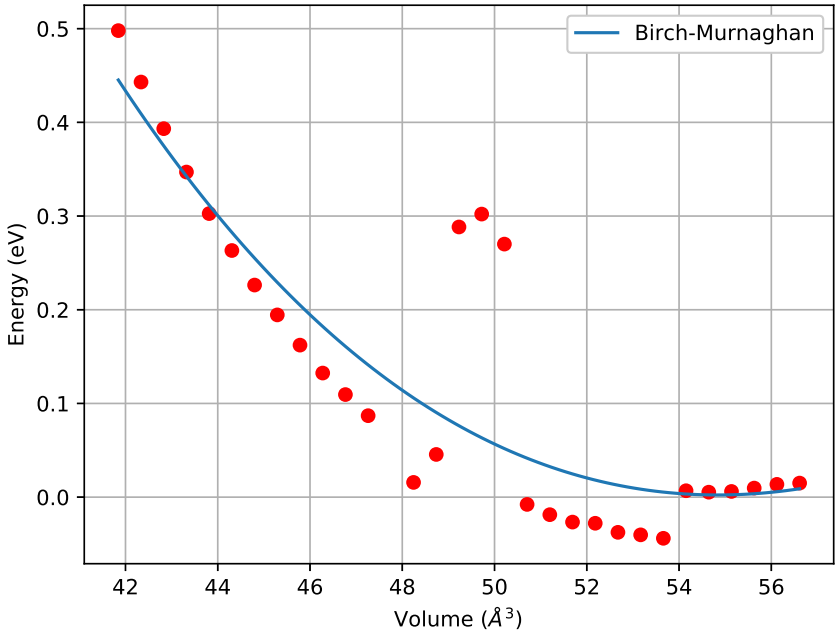

(a) TmCd with sp

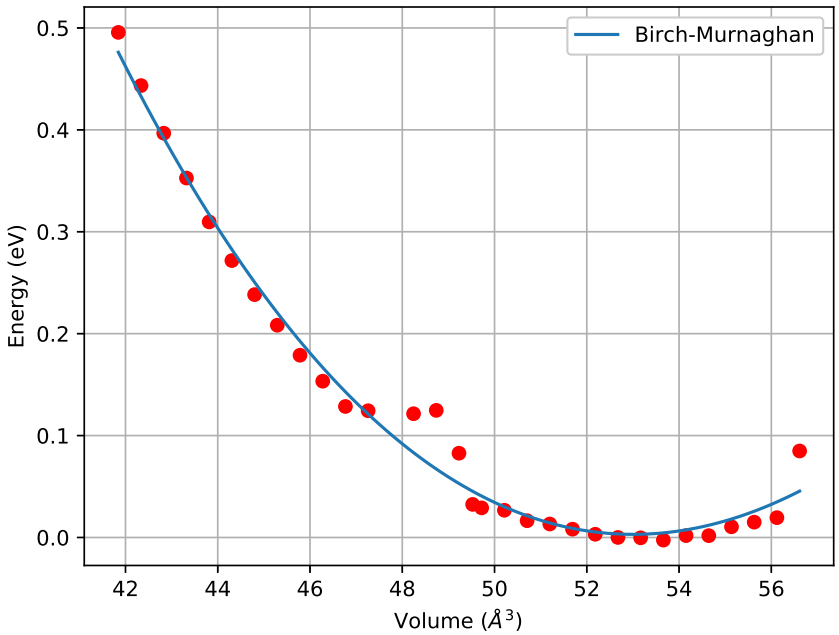

(b) TmCd with so

Figure 65 – Volume variations in function of energies differencies of TmCd with spin polarization (sp) and spin polarization plus spin orbit (so). Source: the Author.

D.0.9 YbCd

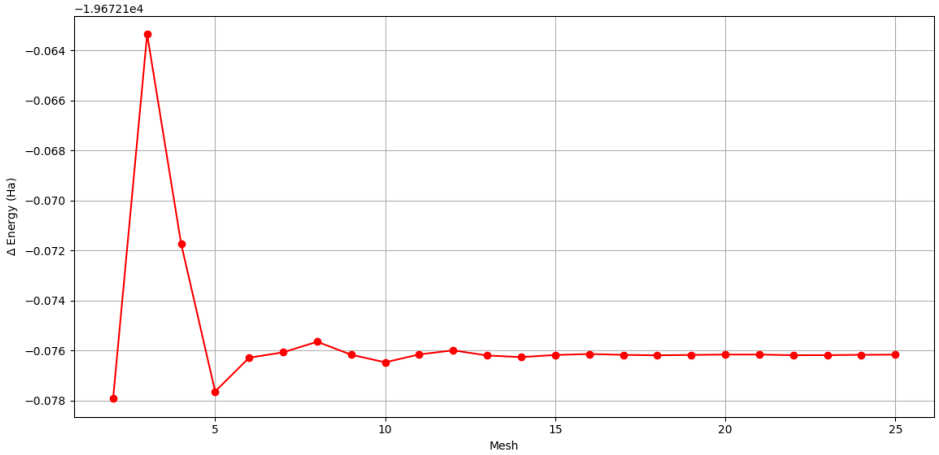

(a) YbCd with sp

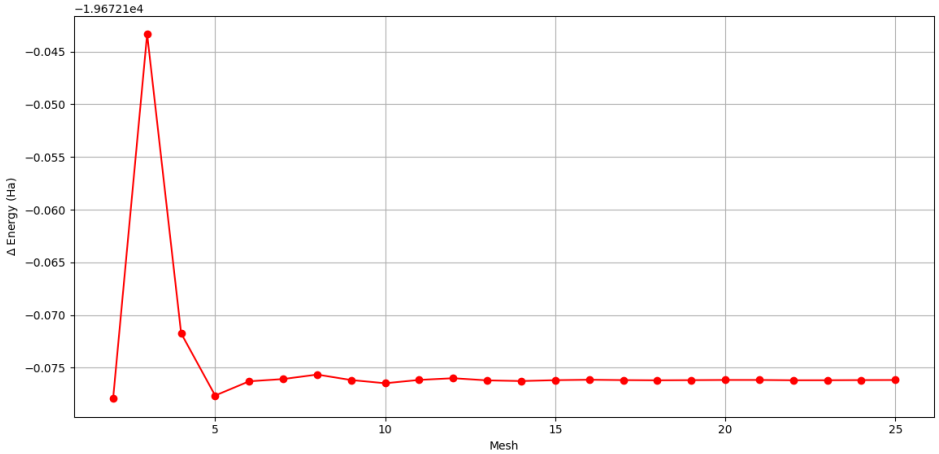

(b) YbCd with so

Figure 66 – k-points variations in function of energies differences of YbCd with spin polarization (sp) and spin polarization plus spin orbit (so) the x-axis represents points in x, y and z direction. Source: the Author.

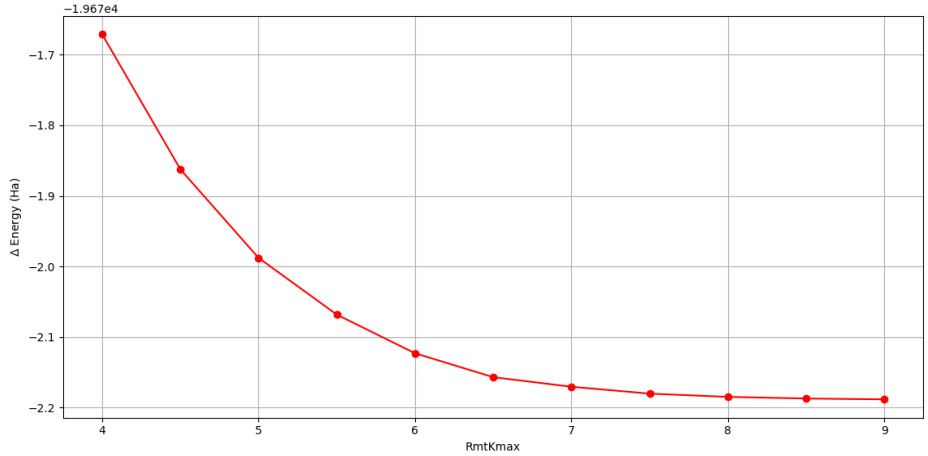

(a) YbCd with sp

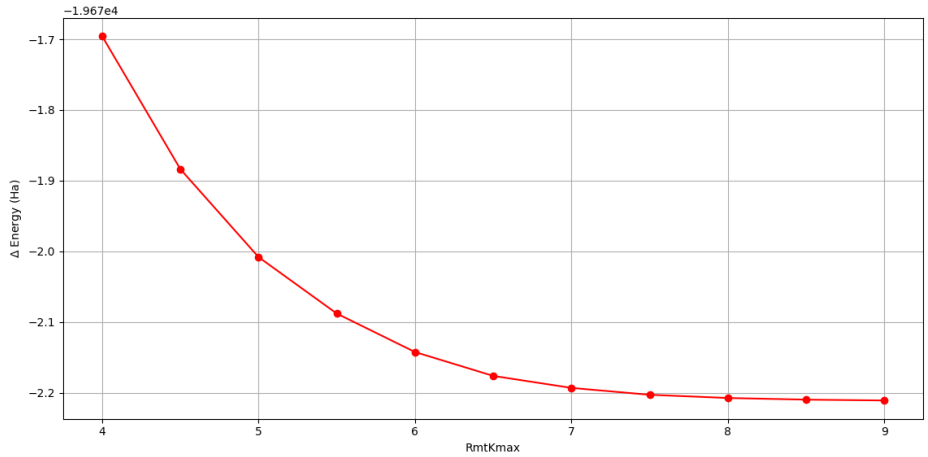

(b) YbCd with so

Figure 67 – $R_{mt}K_{max}$ variations in function of energies differences of YbCd with spin polarization (sp) and spin polarization plus spin orbit (so). Source: the Author.

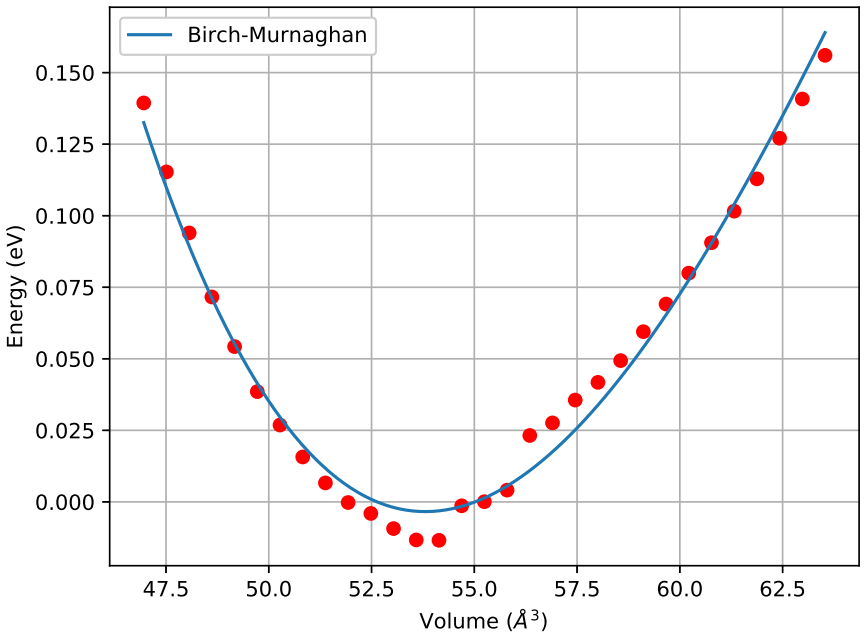

(a) YbCd with sp

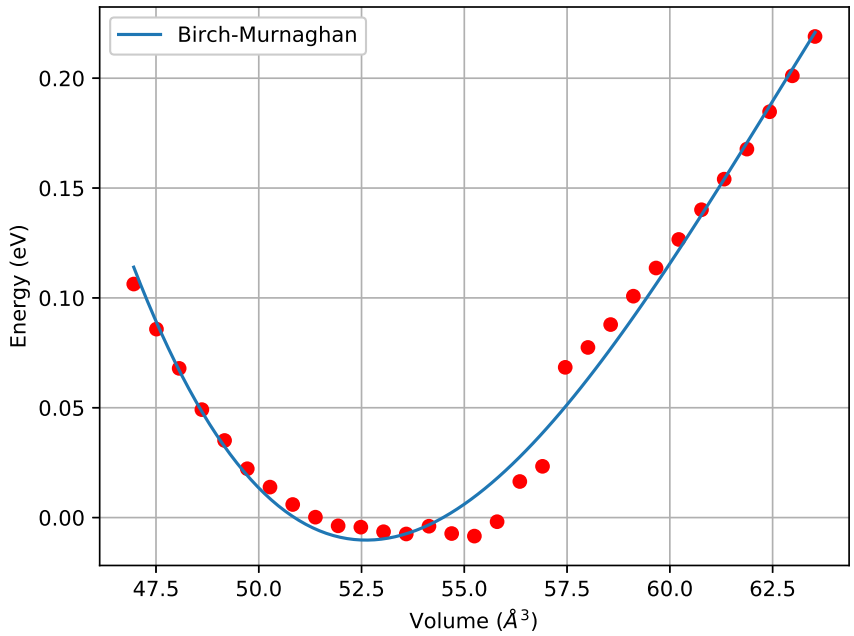

(b) YbCd with so

Figure 68 – Volume variations in function of energies differencies of YbCd with spin polarization (sp) and spin polarization plus spin orbit (so). Source: the Author.

INSTITUTO DE PESQUISAS ENERGÉTICAS E NUCLEARES
Diretoria de Pesquisa, Desenvolvimento e Ensino
Av. Prof. Lineu Prestes, 2242 – Cidade Universitária CEP: 05508-000
Fone/Fax(0XX11) 3133-8908
SÃO PAULO – São Paulo – Brasil
http://www.ipen.br

O IPEN é uma Autarquia vinculada à Secretaria de Desenvolvimento, associada à Universidade de São Paulo e gerida técnica e administrativamente pela Comissão Nacional de Energia Nuclear, órgão do Ministério da Ciência, Tecnologia, Inovações e Comunicações.